SLOPE STABILITY ANALYSIS USING THE KINEMATIC ELEMENT METHOD

SLOPE STABILITY ANALYSIS USING THE KINEMATIC ELEMENT METHOD

By ADNAN A. KADER, B.A.Sc.

A Thesis Submitted to the School of Graduate Studies in Partial Fulfilment of the Requirements for the Degree Master of Applied Science

McMaster University MASTER OF APPLIED SCIENCE (2019) Hamilton, Ontario

(Civil Engineering)

TITLE: Slope Stability Analysis Using the Kinematic Element Method

AUTHOR: Adnan A. Kader, B.A.Sc. (University of Toronto)

SUPERVISOR: Professor Dieter F. E. Stolle

NUMBER OF PAGES: xvi, 121

Lay Abstract

The stability of slopes is a challenging subject in geotechnical engineering. Geotechnical engineers are often interested in the factor of safety (FS), which is a quantitative measure of the stability of a slope. In this thesis, the effectiveness of the Kinematic Element Method (KEM) is evaluated by comparing its solutions to the Limit Equilibrium Method (LEM). The KEM was shown to predict similar potential failure mechanisms and values for the factor of safety. A simplified version of the KEM (KEMv) was developed based on LEM formulations. In KEMv, an alternate iterative scheme to determine the FS is proposed, in which the boundaries between elements are vertical. The KEMv provided similar values for the factor of safety and element forces as Gussmann's KEM for vertical interelement boundaries. In a parametric study, KEM displayed similar trends in the change in FS and critical slip surface as the LEM.

Abstract

In this thesis, the effectiveness of the Kinematic Element Method (KEM), developed by Dr. Gussmann at the University of Stuttgart, was evaluated by comparing the solutions with the Limit Equilibrium Method (LEM), specifically the Morgenstern-Price method. The KEM was evaluated using a variety of problems, ranging from homogeneous slopes to retaining walls. The KEM was shown to predict similar potential failure mechanisms and values for the factor of safety (FS) as the Morgenstern-Price method. The FS were generally within the ±6% which is the range of variance for rigorous limit equilibrium methods. A simplified version of KEM (KEMv) was developed based on limit equilibrium formulations. In KEMv, an alternate iterative scheme to determine the FS is proposed, in which boundaries between elements are vertical. The KEMv provided similar values for the factor of safety and interelement forces as Gussmann's KEM for vertical interelement boundaries given similar element locations. The KEM was assumed by Gussmann to be an upper bound solution. However, given the similarities in the solutions between KEM and KEMv, it may be a limit equilibrium method. The interelement forces from the KEM and KEMv were found to be sensitive to the location of the elements. Elements in the upper part of the slope often had small normal forces relative to shear forces, possibly being negative as well. Sensitivity analysis regarding the number of elements showed that a 5-element solution predicts the appropriate failure mechanism and provides a reasonably accurate FS. In a parametric study, slope geometry and soil properties were varied and comparisons were made between KEM and the Morgenstern-Price method. The KEM

displayed similar trends in factor of safety as the Morgenstern-Price method but predicted slightly larger values. The change in KEM critical slip surfaces with soil properties was consistent with trends predicted by Janbu's dimensionless parameter.

Acknowledgements

In presenting this thesis, the author would like to express his gratitude to the following:

- My family for their support
- My supervisor, Dr. Stolle, for his guidance, support, and patience
- Dr. Gussmann, for allowing my supervisor the use of his Kinematic Element Method program
- McMaster University and the supervisor's NSERC Discovery grant for providing the funding that made this possible

Table of Contents

List of Figures

List of Tables

List of Abbreviations and Symbols

Abbreviations

FEM	Finite Element Method
FS	Factor of Safety
GKEMv	Gussmann's Kinematic Element Method- Vertical
KEM	Kinematic Element Method
KEMv	Vertical Kinematic Element Method- Vertical
LEM	Limit Equilibrium Method
M-P	Morgenstern-Price
OMS	Ordinary Method of Slices
PSO	Particle Swarm Optimization
RFEM	Rigid Finite Element Method
SRM	Strength Reduction Method
SSP	Slope Stability Program

Symbols

Notation

$\boldsymbol{b}$	width of a slice
$\boldsymbol{c}$	cohesion
$\boldsymbol{c'}$	effective cohesion
$\boldsymbol{c_m}$	mobilized cohesion
$\boldsymbol{c'_m}$	effective mobilized cohesion
$\boldsymbol{C^h_{i,m}}$	mobilized cohesive resistance along an interelement boundary
$\boldsymbol{C^l_{i,m}}$	mobilized cohesive resistance along slip surface of an element
$\boldsymbol{E}$	interslice or interelement normal force corresponding to the limit equilibrium method and kinematic element method, respectively

$\boldsymbol{F_h}$	forces acting in the horizontal direction
$\boldsymbol{FS}$	factor of safety
$\boldsymbol{FS'}$	updated value for the factor of safety
$\boldsymbol{FS_0}$	initial assumption for the factor of safety
$\boldsymbol{FS_f}$	factor of safety corresponding to global horizontal force equilibrium
$\boldsymbol{FS_m}$	factor of safety corresponding to global moment equilibrium
$\boldsymbol{F_v}$	forces acting in the vertical direction
$\boldsymbol{f(x)}$	interslice force function for the Morgenstern-Price method or General Limit Equilibrium formulation
$\boldsymbol{h}$	height of a slice or interelement boundary
$\boldsymbol{H}$	height of the slope from its crest to its toe
$\boldsymbol{l}$	length of a slice or element base
$\boldsymbol{L}$	horizontal distance from the crest of the slope to the toe
$\boldsymbol{m_\alpha}$	term used to simplify calculations for some method of slices
$\boldsymbol{n}$	unit vector of the normal to the slip surface
$\boldsymbol{N}$	basal normal force
$\boldsymbol{N'}$	basal effective normal force
$\boldsymbol{O}$	point about which the critical failure surface originates and moment equilibrium is taken in methods of slices
$\boldsymbol{P}$	normal force acting on the surface of a slope in the kinematic element method
$\boldsymbol{P_b}$	external load for KEM computations
$\boldsymbol{q}$	load acting on a foundation in a bearing capacity problem
$\boldsymbol{q_{ult}}$	ultimate bearing capacity of a foundation
$\boldsymbol{Q}$	normal force acting on the surface of a slope in the kinematic element method
$\boldsymbol{R}$	moment arm associated with S_m
$\boldsymbol{S}$	actual shear strength in a slope
$\boldsymbol{S_m}$	mobilized basal shear force for methods of slices
$\boldsymbol{S_u}$	undrained shear strength
$\boldsymbol{t}$	unit vector of the tangent to the slip surface
$\boldsymbol{T}$	basal shear force for KEM elements
$\boldsymbol{T_m}$	mobilized basal shear force for KEM elements
$\boldsymbol{u}$	pore water pressure
$\boldsymbol{U}$	force due to pore water pressure
$\boldsymbol{v}$	velocity of a KEM boundary
$\boldsymbol{W}$	weight of a slice or element

$\boldsymbol{X}$	interslice or interelement shear force corresponding to the limit equilibrium method and kinematic element method, respectively
$\boldsymbol{Z}$	interslice force for Spencer's method

Greek

$\boldsymbol{\alpha}$	inclination of the base of a slice or element with respect to the horizontal
$\boldsymbol{\beta}$	inclination of the slope with respect to the horizontal
$\boldsymbol{\gamma}$	unit weight of the soil
$\boldsymbol{\Delta\ x}$	distance from the midpoint of a slice to the origin (O) in methods of slices procedures
$\Delta\boldsymbol{T}$	imbalanced basal shear force
$\boldsymbol{\theta}$	angle of the interslice force with respect to the horizontal in Spencer's method
$\boldsymbol{\lambda}$	scaling factor for the Morgenstern-Price method or General Limit Equilibrium formulation interslice force function
$\boldsymbol{\lambda_{\phi c}}$	Janbu's dimensionless parameter
$\boldsymbol{\sigma}$	normal stress or total stress
$\boldsymbol{\sigma'}$	effective stress
$\boldsymbol{\tau}$	mobilized shear strength in a slope
$\boldsymbol{\phi}$	friction angle
$\boldsymbol{\phi'}$	effective friction angle
$\boldsymbol{\phi_m}$	mobilized friction angle
$\boldsymbol{\phi'_m}$	effective mobilized friction angle
$\boldsymbol{\psi}$	dilation angle

Declaration of Academic Achievement

All of the work contained in this thesis was carried out by the student. The thesis was written by the student with editing done by the supervisor, Dr. Stolle. The slope stability analyses using the KEM and Morgenstern-Price method were carried out by the student with some suggestions from the supervisor regarding possible problems. The development of the thesis, including the organization of the chapters, was carried out by the student with some input from the supervisor. The KEMv formulation along with its MATLAB code for 5 and 3-element solutions were developed in collaboration with the supervisor.

Chapter 1 Introduction

Slope stability analysis in geotechnical engineering is a complex and challenging problem. It is a necessary step for the design of potentially unstable soil masses formed through human activity or natural processes (Knappett & Craig, 2012). Slopes can fail due to multiple factors, including: geometry of the slope, geological conditions, groundwater conditions, soil strength and loading (Kassim et al., 2012). Currently, the two most popular methods of analyzing the stability of slopes are the Limit Equilibrium Method (LEM) and the Finite Element Method (FEM).

The limit equilibrium method assumes that the slope fails along a pre-determined surface and the equations of equilibrium are applied to obtain a factor of safety (Stolle & Guo, 2008). The finite element method discretizes the slope into small elements and calculates displacements, strains and stresses for a given loading (Ahmed, 2017). For both cases, an appropriate constitutive law must be introduced, which relates the stresses to failure parameters. The Kinematic Element Method (KEM) is a compromise between the aforementioned methods where deformation and static equilibrium are separated (Stolle & Guo, 2008).

The primary objective of this thesis is to assess the effectiveness of the KEM in slope stability analysis. The KEM solutions are compared to those obtained via Morgenstern-Price method. In the analysis, the minimum factors of safety and corresponding failure surfaces, also known as critical failure surfaces or critical slip surfaces, are compared. Various problems ranging from simple homogeneous slopes to slopes with weak layers will be utilized. Of interest is the ability of the KEM to locate the appropriate failure mechanism for each problem. To demonstrate the KEM solution methodology, a simplified version with vertical interelement boundaries is presented by the author.

This thesis consists of 10 chapters. Chapter 2 presents a literature review of the limit equilibrium method, finite element method and kinematic element method in regard to slope stability analysis. Chapter 3 contains various example problems where the KEM and Morgenstern-Price method solutions are compared. Chapter 4 displays the kinematics of slope failures of varying complexity in the KEM, with Chapter 5 presenting the derivation of the simplified version of the KEM with vertical boundaries. Chapter 6 explores the effect of forcing vertical interelement boundaries on KEM solutions, with Chapter 7 examining the computed interelement shear and normal forces in the KEM with vertical boundaries. Chapter 8 contains a sensitivity analysis regarding the number of elements in a KEM solution and a parametric study where the slope geometry and soil properties are varied to observe their effects on factors of safety and critical slip surfaces. Chapter 9 applies the KEM to a case study regarding the mitigation of a potential embankment failure. Finally, Chapter 10 presents the concluding remarks and recommendations for further study.

Chapter 2 Literature Review

In this literature review, the application of the limit equilibrium method, finite element method and kinematic element method to slope stability analysis is discussed. Also, some cases where conventional methods of slope stability analysis are insufficient, are briefly addressed.

2.1 Limit Equilibrium Method

In the limit equilibrium method, equations of statics are applied to assumed failure surfaces and the factor of safety, a measure of the stability of the slope, is determined. The factor of safety (FS) is defined as the ratio of the shear strength in the slope (S) to the mobilized shear strength (τ) of the slope (Fang & Mikroudis, 1991):

$$FS = S/\tau \tag{2.1}$$

Essentially, the factor of safety is the value by which the shear strength in the soil must be reduced in order to bring the slope to a state of limiting equilibrium. Alternatively, it may be viewed as the ratio of stabilizing forces with respect to forces driving instability. In the limit equilibrium method, the Mohr-Coulomb equation is used to express the shear strength of the soil, with c being the cohesion of the soil, ϕ representing the internal friction angle of the soil and σ denoting the normal stress acting along the failure surface. In general, the mobilized shear strength can be represented by

$$\tau = \frac{c}{FS} + \frac{\sigma tan\phi_m}{FS} \rightarrow c_m + \sigma \tan \phi_m \tag{2.2}$$

where c_m and ϕ_m correspond to the mobilized cohesion and friction angle acting along the failure surface, respectively.

$$\phi_m = \tan^{-1}\left(\frac{\tan \phi}{FS}\right) \quad c_m = \frac{c}{FS} \tag{2.3}$$

For soils, eq. (2.2) should be written in terms of effectives stress, where c'_m and ϕ'_m represent cohesion and friction angle for drained conditions, respectively, and u is the pore water pressure. Given the definition of effective stress, $\sigma' = \sigma - u$:

$$\tau = c'_m + \sigma' \tan \phi'_m \rightarrow \tau = c'_m + (\sigma - u) \tan \phi'_m \tag{2.4}$$

For many of the formulations that follow, the equations are presented in terms of total stress with the understanding that they must be modified when pore water pressure is important. The equations of statics are applied to an assumed failure surface or mechanism to write the conditions for horizontal force, vertical force and moment equilibrium. The equilibrium conditions satisfied can vary between limit equilibrium procedures.

There are two types of limit equilibrium methods: single free-body procedures and the methods of slices. In single free-body procedures, the equations of equilibrium are written for the entire failure surface and solved while for the methods of slices, the failure domain is divided into vertical sections, “slices”, and the equations of equilibrium are written and solved. For both types of procedures, multiple potential failure surfaces must be evaluated with the failure surface corresponding to the minimum factor of safety being considered the critical failure surface. The minimum acceptable value for the factor of safety varies with the uncertainty in the design and the consequences of failure (Duncan, 1996).

2.1.1 Single Free-Body Methods

Single free-body methods are simple procedures that are limited in applicability and unlike the methods of slices do not require an iterative solution. Also, these methods satisfy all conditions of equilibrium. Two such procedures are:

- Infinite slope method- The failure surface is assumed to be a sliding block parallel to the slope face, see Figure 2.1. It explicitly satisfices force equilibrium and implicitly satisfies moment equilibrium (Duncan et al., 2014).
- Swedish circle method- The failure surface is assumed to be circular, see Figure 2.2. It is limited to cohesive soils. Moment equilibrium is satisfied explicitly and force equilibrium is satisfied implicitly (Duncan et al., 2014).

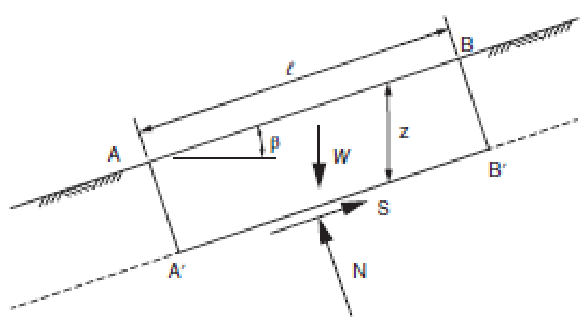

Figure 2.1. Infinite slope procedure (Duncan et al., 2014)

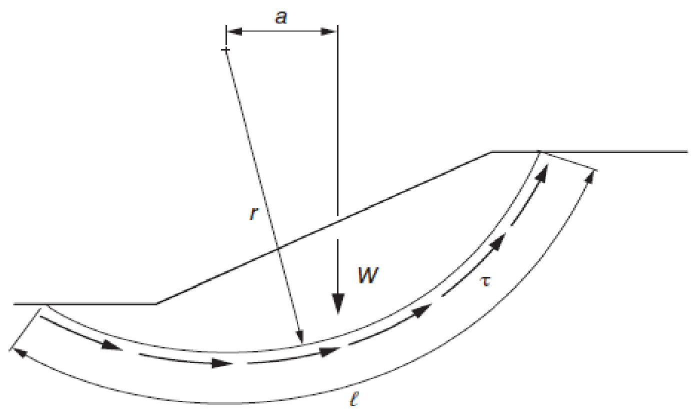

Figure 2.2. Swedish method (Duncan et al., 2014)

2.1.2 Method of Slices

As previously mentioned, for the method of slices, a potential failure domain is divided into vertical slices and the equations of equilibrium are applied at the slice level. The method of slices is a statically indeterminate problem, so assumptions must be made regarding the interslice forces (Zhu et al., 2003). A schematic of the failure surface along with forces acting on each slice is presented in Figure 2.3, where:

- O is the point about which the critical failure surface originates and moment equilibrium is taken
- b is the width of a slice
- $\Delta\, x$ is the distance from the midpoint of a slice to the origin (O)
- S_m is the mobilized shear force along the base of a slice
- R is the moment arm associated with S_m
- L is the length of the slope from crest to toe
- H is the height of the slope from crest to toe
- α is the inclination of the base of a slice with respect to the horizontal
- β is the inclination of the slope with respect to the horizontal
- γ is the unit weight of the soil
- E is the interslice normal force

- X is the interslice shear force
- W is the weight of a slice
- l is the length of a slice
- h is the height of a slice
- N' is the effective normal force acting on the base of the slice
- U is the force due to pore pressure corresponding to ul

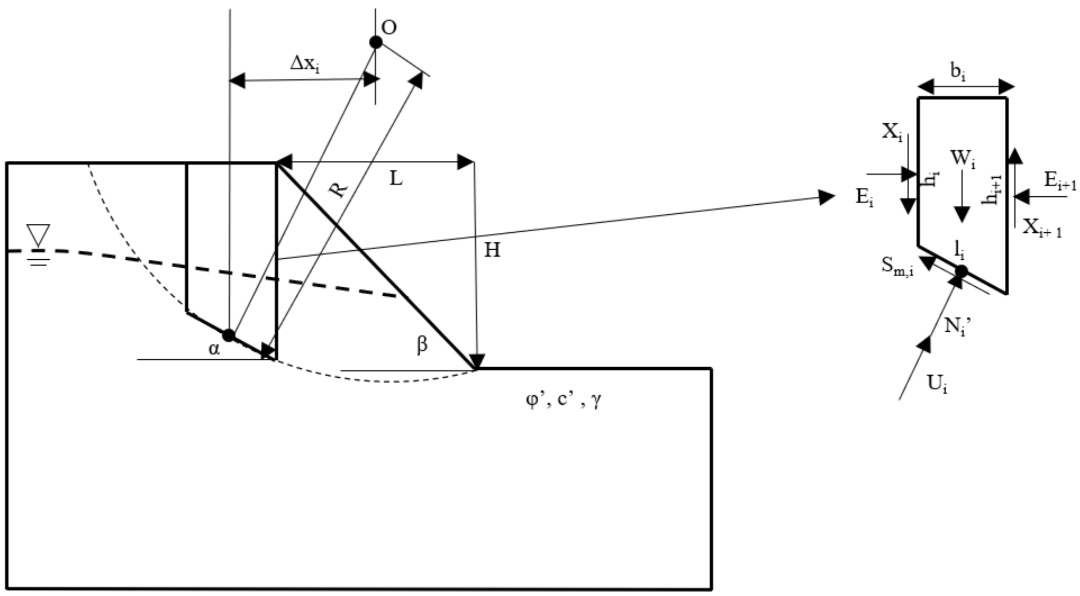

Figure 2.3. Method of slices failure surface with forces. Adapted from Fredlund et al. (1981)

Assuming that the normal stress acting on the base of a slice is consant, the normal force, N, can be written as $N = \sigma l$. So the mobilized shear force along the base of the slice is

$$S_m = \frac{l}{FS}\{c'l + (N - ul)\tan\phi'\} \tag{2.5}$$

The factor of safety is obtained from the equations of equilibrium and is assumed to be constant along the failure surface. The various methods of slices differ in terms of the assumptions regarding the interslice forces and the conditions of equilibrium that are satisfied. When written in terms of total stresses

$$S_m = \frac{l}{FS}(cl + N\tan\phi) \tag{2.6}$$

2.1.2.1 Ordinary Method of Slices

The Ordinary Method of Slices (OMS), also known as the Swedish method or the Fellenius method, is one of the earliest method of slices procedure. In this method, the interslice shear and normal forces are assumed to be zero, see Figure 2.4. One possible interpretation of this method is that for thin slices, the changes in interslice forces are much smaller than the corresponding basal shear (S_m) and normal forces (N).

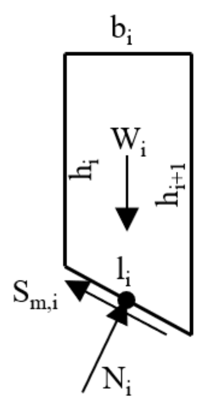

Figure 2.4. Slice with forces considered in the Ordinary Method of Slices. Adapted from Duncan et al. (2014)

The forces perpendicular to the base of the slice can be resolved to determine the normal force.

$$N = W \cos \alpha \tag{2.7}$$

Taking moment equilibrium about the origin (O) and substituting in the expression for the mobilized shear, S_m, using eq. (2.6), an expression for the factor of safety is developed:

$$FS = \frac{\sum(cl + W \cos \alpha \tan \phi)}{\sum W \sin \alpha} \tag{2.8}$$

The Swedish method provides more conservative results for the factor of safety compared to those of more general formulations and depending on the pore pressure conditions, can underestimate the factor of safety by 50-60% (Lei et al., 2011). Owing to these concerns, the use of the Swedish method is not recommended (Knappett & Craig, 2012).

2.1.2.2 Bishop's Method

Bishop (1955) developed a method of slice where the interslice shear forces are neglected, with moment equilibrium being satisfied, see Figure 2.5.

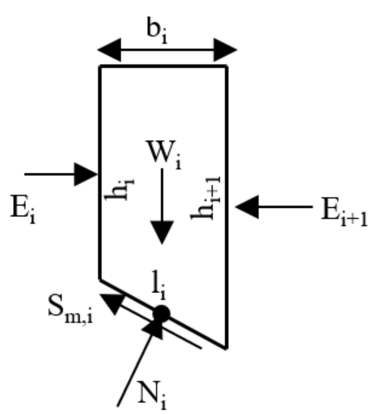

Figure 2.5. Slice with forces considered in Bishop's method

Using vertical force equilibrium, the normal force can be determined.

$$N = \frac{W - \frac{cl \sin \alpha}{FS}}{m_\alpha} \tag{2.9}$$

$$m_\alpha = \cos \alpha + \frac{\sin \alpha \tan \phi}{FS} \tag{2.10}$$

Taking moments about the origin, the factor of safety is calculated.

$$FS = \frac{\sum [cl + N \tan \phi] R}{\sum W \Delta x} \tag{2.11}$$

The equations for the factor of safety for Bishop's method and the OMS are identical (Fredlund & Krahn, 1977). However, the two methods differ in the definition of the normal force.

2.1.2.3 Janbu's Simplified Method

Janbu's simplified method assumes that the interslice forces are horizontal (i.e. interslice shear forces are neglected), with horizontal and vertical force equilibrium being satisfied (Duncan et al., 2014). The interslice force assumption is identical to Bishop's method. The reader is referred to Figure 2.5. As the interslice force assumption is identical and the normal force is determined through vertical force equilibrium, the same equation for the normal force (N) is obtained as for the Bishop method, see eq. (2.9). The factor of safety is effected through global horizontal force equilibrium to yield (Fredlund & Krahn, 1977)

$$FS_0 = \frac{\sum \{cl + N \tan \phi\} \cos \alpha}{\sum N \sin \alpha} \tag{2.12}$$

$$FS = FS_0 f_0 \tag{2.13}$$

FS_0 is underestimated compared to methods that satisfy all conditions of equilibrium. This led Janbu et al. (1956) to develop correction factors (f_0). The correction factor is a function of the soil type (cohesive, cohesionless or mixed) and the ratio of the depth of the failure to its length, see Figure 2.6.

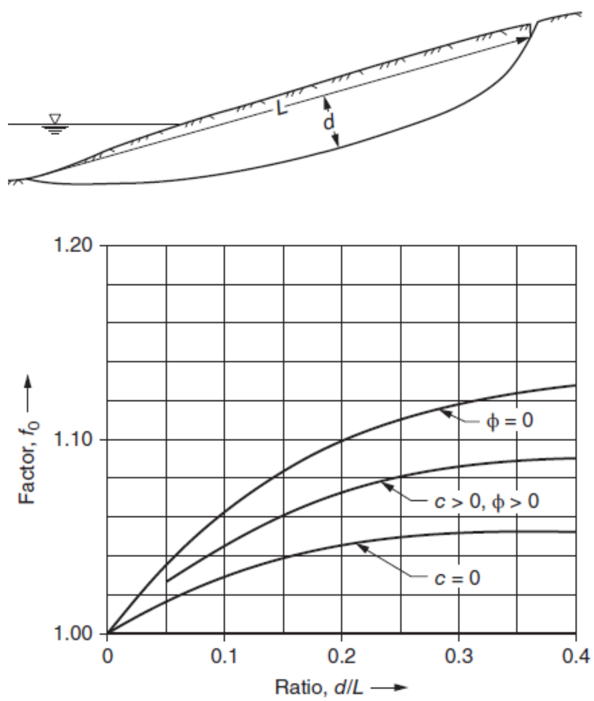

Figure 2.6. Janbu's method correction factors (Duncan et al., 2014)

2.1.2.4 Spencer's Method

Spencer (1967) developed a method where the relation between the interslice shear and normal forces is constant. This method satisfies all conditions of equilibrium. The interslice force (Z) is assumed to act at an angle (θ) with respect to the horizontal, see Figure 2.7.

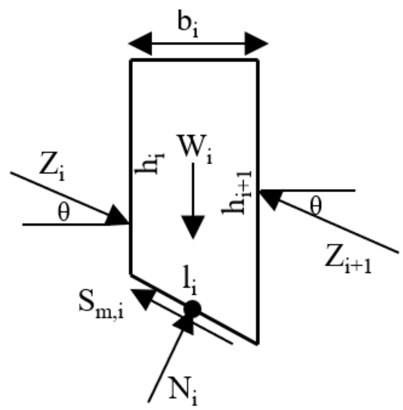

Figure 2.7. Slice with forces considered in Spencer's method. Adapted from Spencer (1967)

The relation between the interslice force components are shown in eq. (2.14).

$$\frac{E_i}{Z_i} = \frac{E_{i+1}}{Z_{i+1}} = \cos\theta \qquad \frac{X_i}{Z_i} = \frac{X_{i+1}}{Z_{i+1}} = \sin\theta \qquad \frac{X_i}{E_i} = \frac{X_{i+1}}{E_{i+1}} = \tan\theta \tag{2.14}$$

With Spencer’s method, two factors of safety are introduced, one corresponding to moment and the other to horizontal force equilibrium. There exists a certain θ value where the factors of safety from moment and horizontal force equilibrium are identical, which is assumed to correspond to the sought solution. The normal force can be obtained at the slice-level by summing forces perpendicular to the interslice force (Fredlund & Krahn, 1977).

$$N = \frac{W - (E_{i+1} - E_i)\tan\theta - \frac{cl\sin\alpha}{FS}}{m_\alpha} \tag{2.15}$$

Following the calculation of the normal force, the horizontal interslice shear force, E_i, can be calculated by taking horizontal force equilibrium (Fredlund & Krahn, 1977).

$$\sum F_h = 0 \;\; \rightarrow \;\; -(E_{i+1} - E_i) + N \sin\alpha - S_m \cos\alpha = 0 \tag{2.16}$$

As the interslice forces cancel out, the factor of safety for moment equilibrium, FS_m, is identical to that for Bishop's method (Fredlund & Krahn, 1977).

$$FS_m = \frac{\sum[cl + N \tan\phi]R}{\sum W\Delta x} \tag{2.17}$$

The equation for the factor of safety for horizontal force equilibrium (FS_f) can be determined using the following equation (Fredlund & Krahn, 1977).

$$FS_f = \frac{\sum\{cl \cos\alpha + N \tan\phi \cos\alpha\}}{\sum N \sin\alpha} \tag{2.18}$$

2.1.2.5 Morgenstern-Price Method

Morgenstern & Price (1965) developed a method where a relation between the interslice normal and shear forces is assumed, see Figure 2.8.

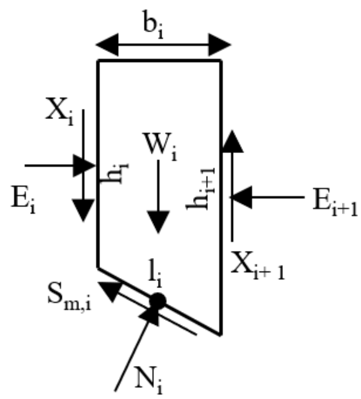

Figure 2.8. Slice with forces considered in the Morgenstern-Price method

Similar to Spencer's method, this procedure satisfies all conditions of equilibrium. The interslice shear and normal forces are related by the following equation where $f(x)$ is an interslice force function and λ is a scaling factor (Morgenstern & Price, 1965).

$$X = \lambda f(x)E \tag{2.19}$$

Factors of safety are obtained for both horizontal force equilibrium and moment equilibrium and there exists a unique λ value such that both are identical. The function can be determined from elastic theory, field measurements or assumed (Morgenstern & Price, 1965). Fan et al. (1986) carried out finite element analyses to calculate stresses in homogeneous soil to determine force functions. The authors discovered that homogeneous slopes generally have a bell-shaped interslice force function. According to Morgenstern & Price (1965), the factor of safety is relatively insensitive to the assumed interslice force function. The normal force at the base is derived from vertical force equilibrium (Fredlund & Krahn, 1977)

$$N = \frac{\{W - \left(X_{(i+1)} - X_i\right) - \frac{cl \sin \alpha}{FS}\}}{m_\alpha} \tag{2.20}$$

The factor of safety from moment equilibrium is identical to that for Bishop's method (Fredlund & Krahn, 1977).

$$FS_m = \frac{\sum(cl + N \tan \phi)R}{\sum W \Delta x} \tag{2.21}$$

The horizontal interslice forces are obtained via vertical and horizontal force equilibrium.

$$(E_{i+1} - E_i) = \{W - (X_{i+1} - X_i)\}\tan\alpha - \frac{S_m}{\cos \alpha} \tag{2.22}$$

The equation for the factor of safety for horizontal force equilibrium is identical to that of Spencer's method (Fredlund & Krahn, 1977).

$$FS_f = \frac{\sum(cl + N \tan \phi) \cos \alpha}{\sum N \sin \alpha} \tag{2.23}$$

2.1.2.6 General Limit Equilibrium (GLE)

Fredlund et al. (1981) developed a General Limit Equilibrium (GLE) formulation for the method of slices that builds on the formulation derived by Morgenstern & Price (1965).

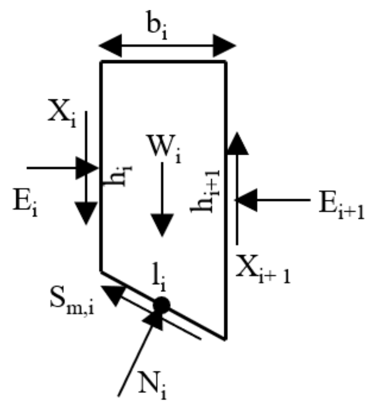

Figure 2.9. Slice with forces considered in the GLE formulation

The GLE assumes that the interslice shear and normal forces are related once again by the equation $X = \lambda f(x)E$. The GLE was developed in a manner such that all methods of slices, except for the Fellenius method, can be incorporated as special cases of the GLE. For example, Spencer's method can be considered for the case where $f(x) = 1$ and $\lambda = \tan\theta$ where θ is the inclination of the interslice force, Z (Fredlund et al., 1981).

2.2 Limitations of the Limit Equilibrium Method

One of the limitations of the limit equilibrium methods is that there is "missing physics" in the limit equilibrium method (Krahn, 2003). There is a lack of knowledge regarding the strains and displacements in the slope (Krahn, 2003). The factor of safety in the slope is assumed to be constant throughout. According to Krahn (2003), this assumption is known to be untrue but is still applied as it ensures that the unrealistic forces/stresses calculated using these methods provide a realistic "average" factor of safety. Krahn (2003) calculated stresses using the finite element method and imported the results into a limit equilibrium program to solve for the factor of safety. He presented the variation of the factor of safety along the failure surface for both toe and deep-seated failures. Stolle & Guo (2008) applied the Rigid Finite Element Method (RFEM) to the method of slices. They assumed that the slices are rigid and a non-linear failure criterion relates the stresses and displacements along the interslice boundaries. The local factors of safety, which are determined from the displacements, were shown to vary along the failure surface.

2.3 Accuracy of the Limit Equilibrium Method

The factors of safety calculated using methods which satisfy all conditions of equilibrium are considered to be within ±6% of the "correct" answer (Duncan, 1996). He states that it is difficult to know what the absolute "correct" answer is, but it can be determined with sufficient accuracy for practical applications. This was concluded based on the observation that various methods of slices, finite element methods and the log-spiral method, which are different approaches, give similar values for the factor of safety. Uzielli et al. (2006) presented typical values of variance for various geotechnical parameters. For example, they found that drained friction angle of soils and undrained shear strength of clays can vary by 5-15% and 10-30%, respectively. Considering the greater possible variance in the parameters involved in the analysis, the accuracy of ±6% can be considered to be quite good (Duncan, 1996).

2.4 Methods for Locating Critical Failure Surface

Originally, grid-and-radius methods were utilized to locate the critical circular failure surface (Duncan, 1996). In this procedure, a grid is created with multiple origins (O) and the radius of the circle is varied to delineate potential failure surfaces to calculate factors of safety (McCarthy, 1982). The objective is to locate the origin (O) and the corresponding radius (R) that provides the minimum factor of safety.

Often, critical failure surfaces may not be circular and algorithms using optimization techniques were developed to identify the critical failure surfaces (Duncan, 1996). Nguyen (1984) applied the simplex reflection method to determine the minimum global factor of safety, as well as the critical failure surface. Cheng et al. (2007) applied particle swarm optimization (PSO) in combination with Spencer's method. The procedure mimics social models, such as bird flocking, to locate the critical failure surface. Karchewski et al. (2011) and Zolfaghari et al. (2005) optimized the critical failure surface obtained from the Morgenstern-Price method using genetic algorithms that mimic the production of chromosomes in genetics. The reader is referred to these papers for further details.

2.5 Three-Dimensional Limit Equilibrium Methods

Three-dimensional limit equilibrium is more useful for slopes with more complex geometries or are highly inhomogeneous or anisotropic (Naderi, 2013). These limit equilibrium methods often utilize the method of columns which is an extension of the method of slices used in two-dimensional analysis (Hungr et al., 1989). Xing (1988) developed a three-dimensional limit equilibrium method for concave slopes and Hungr et al. (1989) extended Bishop's and Janbu's methods to three-dimensional columns. As these limit equilibrium methods are beyond the scope of this thesis, the reader is referred to a comprehensive list presented in a paper by Duncan (1996).

2.6 Finite Element Method

In the finite element method, the slope is discretized into elements and the virtual work method is applied to effect the global equilibrium equation of a domain to determine the displacements at the nodes as well as the distribution of strains and stresses within the domain (Stolle et al. 2004).

When applying virtual work, assumptions must be made with respect to the variation of displacements within each element. Also, appropriate constitutive laws expressing the relation between stress and strain, as well as failure, must be included. Given the nonlinear nature of the equilibrium equation, an iterative algorithm is required to develop a solution. This procedure attempts to take into account all the physics associated with the boundary value problem. The reader is referred to Zienkiewicz & Taylor (2000) or Logan (2012) for further details on finite element methodology.

The Strength Reduction Method (SRM) is currently the most commonly used algorithm for the finite element method to determine the factor of safety of a slope. In the SRM, the failure properties c and $tan\phi$ of the soil are reduced until a failure mechanism develops (Matsui & San, 1992). The definition of the factor of safety is similar to that used in the LEM. In the strength reduction method, a shear strain failure criterion is often utilized to delineate the critical failure surface (Matsui & San, 1992). Cheng et al. (2013) used maximum shear strains and maximum shear strain increment to locate critical failure surfaces.

In the finite element method, the stresses and strains are computed in the domain and transferred to the nodes via a smoothening algorithm. Thereafter, the stresses are inserted into the Mohr-Coulomb failure criterion to identify which points in space correspond to failure, see e.g. Griffiths & Lane (1999). Cheng et al. (2007), Lui et al. (2015) and Griffiths & Lane (1999) applied the Mohr-Coulomb failure criterion in the SRM. They assumed the soil to be linear elastic-perfectly plastic. The adopted stress-strain relation was found to provide reasonable results for stresses and factors of safety. For the accurate prediction of deformation, it is recommended to utilize correct values for the Poisson ratio and the elastic modulus (Duncan, 1996). According to Griffiths & Lane (1999), failure of the slope numerically occurs where there is non-convergence in the solution which is accompanied by massive increases in nodal displacements.

2.6.1 Comparison of LEM and FEM

Cheng et al. (2007), Lui et al. (2015) and Griffiths & Lane (1999) compared the results of the FEM to the LEM and found that generally both methods provided similar values for the factor of safety and similar failure surfaces.

The FEM has some advantages compared to the LEM (Griffiths & Lane, 1999):

- There is no need to assume the failure surface and interslice force functions.
- The FEM more accurately predicts the stresses in the slope and if correct values for compressibility (Poisson’s ratio and modulus) are provided, deformation as well.
- The finite element method is also capable of modeling progressive failure of the slope.

The following are some disadvantages of using the FEM compared to the LEM:

- The criteria of non-convergence is used to determine when failure occurs, but this may be caused by other factors, such as initial stresses in the slope, gravity loading procedures, and the incremental load step-size (Krahn, 2003).
- The FEM is more challenging to apply as it requires more time to learn and more effort and cost (Duncan, 1996). Also, the choice of the correct constitutive model and parameters can be challenging (Cheng et al., 2007).

2.7 Kinematic Element Method

In the kinematic element method, virtual displacements are determined to identify potential failure mechanisms and equations of equilibrium are applied to calculate the factor of safety. According to Stolle et al. (2004), the kinematic element method developed by Gussmann (1982), is a compromise between finite element methods and limit equilibrium methods. Gussmann (1982) suggests that the KEM provides an upper bound solution in plasticity theory, so the computed loads are on the unsafe side. Similar to the limit equilibrium method, the failure domain is assumed. It is generally discretized into rigid triangular and quadrilateral elements, see Figure 2.10.

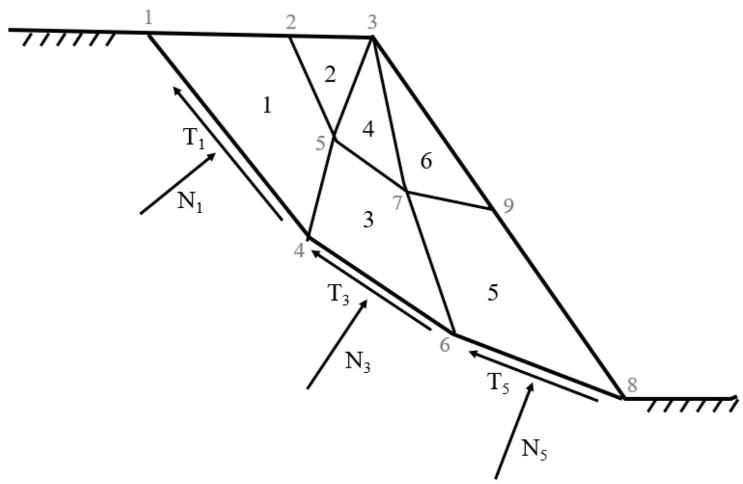

Figure 2.10. Assumed failure domain discretized with a KEM mesh

The method only allows for interelement sliding to occur (i.e. the relative normal displacements between elements is 0) and failure is governed by the Mohr-Coulomb failure criterion where τ is the mobilized shear stress.

To simplify the presentation in this section, equations are written in terms of total stress. Effective stress analysis can be carried out by also taking into account the forces due to pore water pressure (u) perpendicular to the failure surface at the same point as the normal force. As before, the mobilized shear stress

$$\tau = c_m + \sigma \tan \phi_m \tag{2.24}$$

Virtual displacements along the element boundaries are calculated based on the assumption of non-associated flow with the dilatancy angle $\psi = 0$ so velocity jumps between elements must be parallel to the interelement boundary (Linnweber et al., 2002). For the sake of simplicity, the details of the KEM will be discussed using only 1 row of elements. Also, based on experience, the use of 1 row of elements usually provides reasonable results for the factor of safety for slope stability problems (Gussmann, 2000).

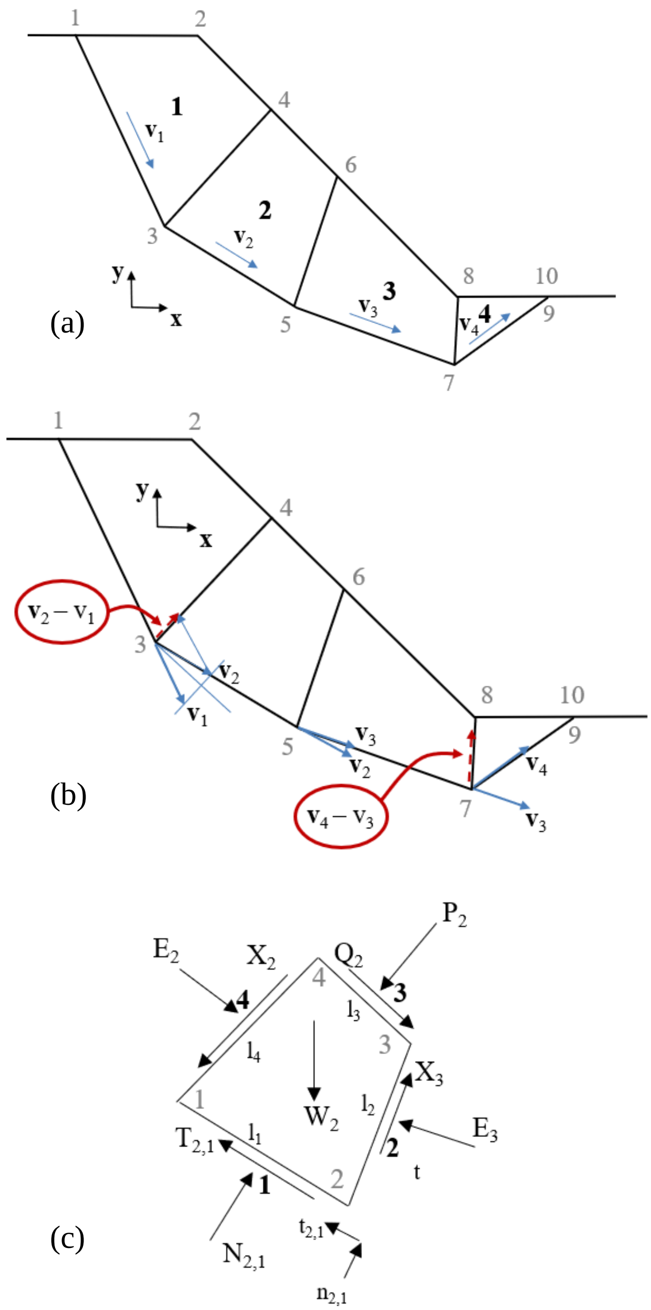

Figure 2.11. Definition of the problem for a simplified mesh: a) Geometry and element numbering, b) Kinematics and c) Statics for element 2

2.7.1 Kinematics

The kinematics are required to determine in which direction the shear forces act along an interface. The velocities can also be used to compare the energy dissipated to the work rate of external forces. For slope stability problems in KEM, the failure mechanism is discretized as shown in Figure 2.11(a) where the velocities along the failure surface for the i^{th} element is $\boldsymbol{v}_i$. As the flow rule is non-associated, only shear velocities parallel to the failure surface along the boundary 1-3-5-7-9 occur. The material outside of the failure surface is perfectly rigid (i.e. velocity vanishes). As stated previously, the normal velocity jumps between elements (perpendicular to the interelement boundary) is zero. So, between elements i and $i+1$, $v_{n,i} - v_{n,i+1} = 0$. This constraint allows for the kinematics to be solved.

Gussmann (1982) solved the kinematics using a linear system of equations containing the direction cosines and Linnweber et al. (2002) solved the kinematics using hodographs. For example, assuming element 1 has a velocity parallel, to the failure surface with the magnitude, $|v_1| = 1$, and knowing that the normal velocity difference is 0, the orientation of v_2 and its magnitude can be calculated. Once v_2 is known, this procedure can be repeated for the elements that follow. For details regarding the original formulation of the KEM, the reader is referred to Gussmann (1982) and Gussmann (1988).

2.7.2 Statics

The kinematic element method satisfies horizontal and vertical force equilibrium explicitly and moment implicitly. As the equations only satisfy force equilibrium, the forces acting on the element boundaries can act at any point and thus at infinite locations. There exists a certain set of locations for the forces where moment equilibrium is satisfied for each element. A similar assumption is also made for the Swedish method, except for force equilibrium. The statics for element 2 are observed in Figure 2.11(c), where T and N are the shear force and normal force along the failure surface, X and E are the shear and normal forces between elements, P and Q are shear and normal forces acting on the surface of the slope, the light numbers are the local node numbers, and the bolded numbers represent the local boundary numbers, i where $i = 1$ to 4.

Failure along the failure surface and interelement boundaries is according to the Mohr-Coulomb criterion, see eq. (2.24). Assuming that the stresses are constant along the boundaries; eq. (2.25) provides the relation between shear and normal force along the basal boundary for the i^{th} element. It is understood that these forces correspond to mobilized values.

$$T_i = N_i \tan\phi + cl_i \tag{2.25}$$

This process can be repeated for the interelement boundaries as well. The only information from the kinematics utilized in the static analysis of the problem is to identify the direction of the boundary shear forces. For example, referring to Figure 2.11(b), we observe that while element 1 moves down, element 2 moves upwards relative to it. Thus, the shear force of element 2 acting on 1 is upward, with the opposite being true for 1 acting on 2. Assuming that there are no external loads where $P_2 = Q_2 = 0$, the following is the vector equation for force equilibrium for element 2

$$-N_2\boldsymbol{n}_2 - T_2\boldsymbol{t}_{2,1} - E_3\boldsymbol{n}_{2,2} + X_3\boldsymbol{t}_{2,2} - E_2\boldsymbol{n}_{2,4} + X_2\boldsymbol{t}_{2,4} + W_2(0,-1) = 0 \qquad (2.26)$$

where $\boldsymbol{n}_{2,1}$ and $\boldsymbol{t}_{2,1}$ are the normal and tangential unit vectors for boundary 1 for element 2, respectively. This procedure can be repeated for all elements and a system of linear equations can be assembled.

2.7.3 Numerical Solution for Slope Stability Analysis

The procedures given in the previous sections can be applied to general kinematic element problems. To apply the kinematic element method for slope stability analysis, an objective function is required. In the case of slope stability analysis, the Fellenius definition of the Factor of Safety (used in the limit equilibrium method) is applied to the problem, where ϕ_m and c_m are the mobilized friction angle and cohesion, respectively. Gussmann (2000) developed a matrix solution procedure to the slope stability problem analogous to the finite element method. As the procedure is non-linear similar to what we have for general limit equilibrium methods, an iterative procedure is required. There are two levels of nonlinear analysis in the KEM:

1. Identify the factor of safety for a given failure mechanism
2. Identify the mechanism leading to the minimum factor of safety

One way to identify the factor of safety for a given mechanism is to introduce a fictitious force ($P_{b,1}$) acting at the crest of the slope which drives instability. The objective function then is to find the factor of safety consistent with $P_{b,1}$= 0. Engel & Lauer (2017) presented a similar procedure where a fictitious force (ΔT) acts along the failure plane of the largest element (often the middle) that drives failure. The factor of safety is derived in terms of the fictitious force and the value where $\Delta T = 0$ corresponds to the solution. The reader is referred to articles by Gussmann (2000) and Engel & Lauer (2017) for details.

Gussmann (2000) presented a limited number of example problems wherein the method was shown to be quite effective for a small number of elements. He calculated the factor of safety of slope with a mixed soil using 2 and 8 elements. An increase in the number of elements from 2 to 8 only improved the factor of safety by 4%. In a more recent version of his program, 4 points are required to start an analysis for a given slope geometry: the minimum entry point of the failure surface (laterally), the maximum exit point of the failure surface (laterally), the crest of the slope, and the lowest point of the failure surface. Particle swarm optimization is utilized to locate the critical failure surface and the associated minimum factor of safety. The reader is referred to Cheng et al. (2007) for the description of a PSO algorithm.

2.7.4 Comparison of KEM Solutions with LEM and FEM

There is a little literature available on the comparison of the kinematic element method to more established methods, such as the limit equilibrium method and the finite element method. Nevertheless, Stolle et al. (2004) compared the results of a finite element program, Spencer's method and the KEM in the analysis of a slope with a weak clay layer. They obtained factors of safety similar to Spencer's method and the finite element program, however the failure surface obtained using the KEM did not pass through the weak layer.

Upon forcing the failure surface through the weak layer, they obtained a significantly higher factor of safety that was in agreement with classical wedge analysis. This demonstrates the non-uniqueness of solutions and the dependence on the method of analysis.

2.8 Specialized Modes of Slope Failure

In the previous sections, the slope stability analyses considered the shear failure of soil slopes associated with gravitational loading. There are other non-traditional modes and mechanisms of failure that cannot fully be explained using these types of models. In this section, situations where simply considering the shear strength of the slope may be insufficient in design and analysis are briefly addressed.

2.8.1 Landslides

A landslide is defined as the downward movement of soil and rock along a slope until equilibrium with shear strength and or gravity is reached (Toprak & Korkmaz, 2017). Cruden & Krahn (1973) investigated a landslide consisting of 90 million tons of rock and soil in the town of Frank in southwestern Alberta. Their investigation concluded that the failure was caused by joint sets in the rock mass perpendicular to the bedding plane and slip along the planes. Numerous landslides in marine clays have occurred in Eastern Canada, see e.g. La Rochelle et al. (1970). One of the contributing factors was the leaching of salt from the marine clays. A reduction in the salt content in marine clays decreased the shear strength of the marine clay and caused it to become more sensitive (La Rochelle et al., 1970). Panthi & Nilsen (2006) modeled the rockslide in the village of Tafjord in Norway using the finite element method. They determined that high stress anisotropy caused displacement in the slope that led to the creation of joints and a reduction in the shear strength of the soil. An additional mode of failure is associated with slope creep. Slope creep is the slow slow, continuous flow or deformation of slopes over time (Emery, 1978). With regard to this form of failure, the undrained shear strength appears to decrease with time. More sophisticated analysis indicates the effective stress in soil decreases due to a deformation-dependent increase in excess pore pressure (Vermeer et al., 1997). These are a few examples where the geology and fabric of the soil had greater impact on the stability of slopes than the shear strength in the classical sense.

2.8.2 Progressive failure

In all limit equilibrium methods, the shear strength of the soil is assumed to be mobilized simultaneously along the failure surface. However, this assumption does not hold true when progressive failure takes place. In progressive failure, the slope may fail at a certain location and the shear strength may decline below its peak value (Duncan et al., 2014). This causes the local unbalanced load to be transferred to other areas of the slope leading to the zone of failure spreading. According to Duncan et al. (2014), progressive failure is common in brittle soils with high horizontal stresses, such as stiff fissured clay. Progressive failure can be modelled using the FEM, but few LEM models exist to capture this behaviour. Law & Lumb (1978) developed a model for progressive failure that required two processes: local failure and propagation of local failure. In local failure, the slice is in limiting equilibrium with the post-peak strength being mobilized. After local failure of an individual slice, its strength decreases to a lower post-peak strength and neighbouring slices are subject to an increase in loading resulting in local failure propagation. The reader is referred to their paper for further details.

Chapter 3 Slope Stability Example Problems

This chapter evaluates the effectiveness of the kinematic element method for slope stability analysis. Various slope conditions are tested, ranging from basic homogeneous slopes to retaining walls. The critical failure surfaces and associated minimum factors of safety obtained using the KEM are compared to those predicted by the Morgenstern-Price method. A summary of the two programs is provided below:

- The Slope Stability Program (SSP) developed by Karchewski (2012) employs the Morgenstern-Price (M-P) method and a genetic algorithm to locate the critical failure surface and the corresponding factor of safety. The SSP generates critical slip surfaces without user input regarding the required number of slices. However, the number of slices has been observed to vary from 30 to 40, based on experience. According to Spencer (1967), there is minimal improvement in the factor of safety beyond 32 slices. Thus, the number of slices used in SSP seems to be sufficient.
- The Kinematic Element Method (KEM) developed by Gussmann (2017), uses rigid body elements to predict a critical failure mechanism and the corresponding factor of safety. The solutions presented in this section are for 5 elements, unless otherwise stated. The KEM program allows for the mesh to be refined vertically or horizontally. To demonstrate this, the division of a single element vertically and horizontally is shown in Figure 3.1.

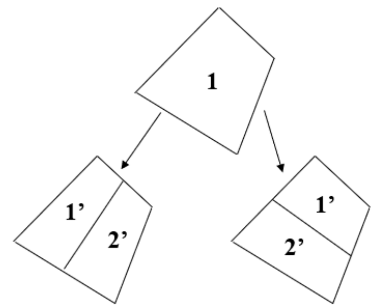

Figure 3.1. Possible KEM mesh refinements

A subdivision both vertically and horizontally produces 2 elements each. It is possible for the subdivided elements to differ in size. The most significant difference is in the interelement boundaries. Thus, the computed interelement shear and normal forces will differ depending on the type of mesh refinement.

In the following examples, the factors of safety and critical failure surfaces obtained from the SSP and KEM are compared as well as to solutions presented in literature. Ideally, the difference in the factors of safety between the KEM and the SSP are within ±6% of solutions observed for limit equilibrium solutions that satisfy all conditions of equilibrium. It is assumed that if the KEM factors of safety are within the expected range of variance, a reasonably accurate solution has been found.

3.1 Homogeneous Slope

In this first example, the stability of a homogeneous slope with a height of 20 m and length of 30 m is analyzed. This problem is presented in a paper by Arai & Tagyo (1985). The soil has a friction angle $\phi = 15°$, cohesion $c = 41.65\ kPa$ and unit weight $\gamma =$

18.82 kN/m^3. Janbu (1954) carried out dimensionless analysis to create stability charts for homogeneous slopes and defined a dimensionless parameter, $\lambda_{\phi c}$:

$$\lambda_{\phi c} = \frac{\gamma H(\tan\phi)}{c} \tag{3.1}$$

The value of $\lambda_{\phi c}$ can be used to predict the failure mechanism of the slope. A value greater than 2 indicates a toe failure (Duncan & Wright, 1980). The $\lambda_{\phi c}$ value for this slope is 2.42, indicating a toe failure, as observed in Figure 3.2.

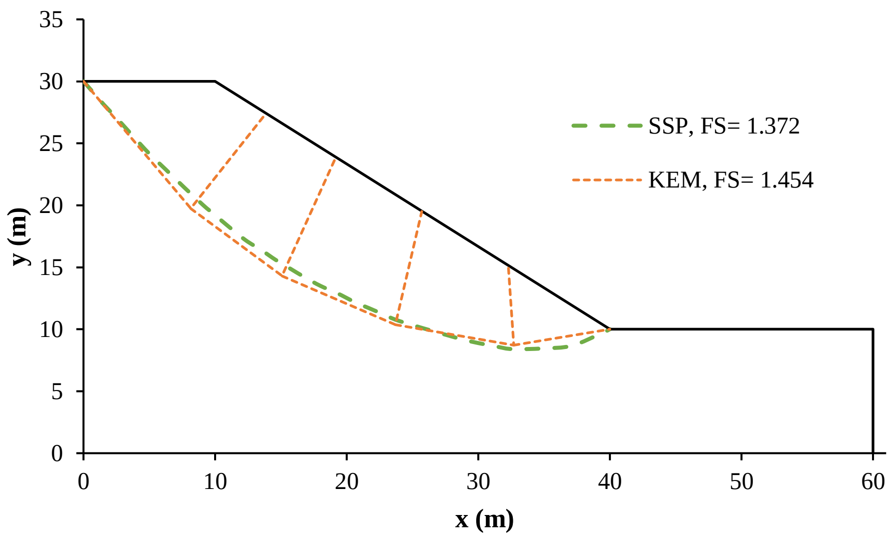

Figure 3.2. Critical failure surfaces of the homogeneous slope

The critical failure surfaces obtained from the SSP and the KEM are observed to be nearly identical. The factor of safety obtained using the KEM is 6% greater than that determined by SSP. This is not unexpected as KEM is said to provide an upper bound solution. We observe, unlike the method of slices, that the transverse optimum interfaces are not necessarily vertical. The orientations of the interfaces are determined as part of the solution. The factor of safety obtained using the SSP, which is based on the Morgenstern-Price method, is approximately 4% less than the reference value presented by Deng et al. (2014). Reference factors of safety presented by Deng et al. (2014) are summarized in Table 3-1.

Table 3-1. Reference factors of safety (Deng et al., 2014)

Method	Circular Slip Surface	Arbitrary Slip Surface
Bishop's	1.415	-----
Spencer's	1.410	1.425
Morgenstern-Price	1.408	1.429

The specific slope stability program, optimization algorithm or relation between interslice forces utilized by Deng et al. (2014) is not stated. Nevertheless, we observe that there can be some difference in the factors of safety obtained using similar LEM formulations. The factor of safety obtained using the KEM is approximately 2% greater than that of the reference values. This is well within the expected variation for the factor of safety for methods that satisfy all conditions of equilibrium. An important observation when referring to Figure 3.2 is that KEM is not restricted to using slices. The element boundaries adopt orientations that contribute to minimizing the factor of safety, as indicated previously.

3.2 Multi-Layered Slope

In this example, the stability of a slope with three distinct soils and complex layering is evaluated. The material properties of the various soil layers are summarized in Table 3-2.

Table 3-2. Slope material properties, (Donald & Giam, 1989)

Material	φ (°)	c (kPa)	γ (kN/m^3)
Layer 1	38	0	19.5
Layer 2	23	5.3	19.5
Layer 3	20	7.2	19.5

KEM and SSP predict similar critical failure surfaces and both indicate a toe failure, see Figure 3.3. The factor of safety obtained using the KEM is 4% higher than that of the SSP. Once again, the SSP provides a more conservative estimate for the factor of safety.

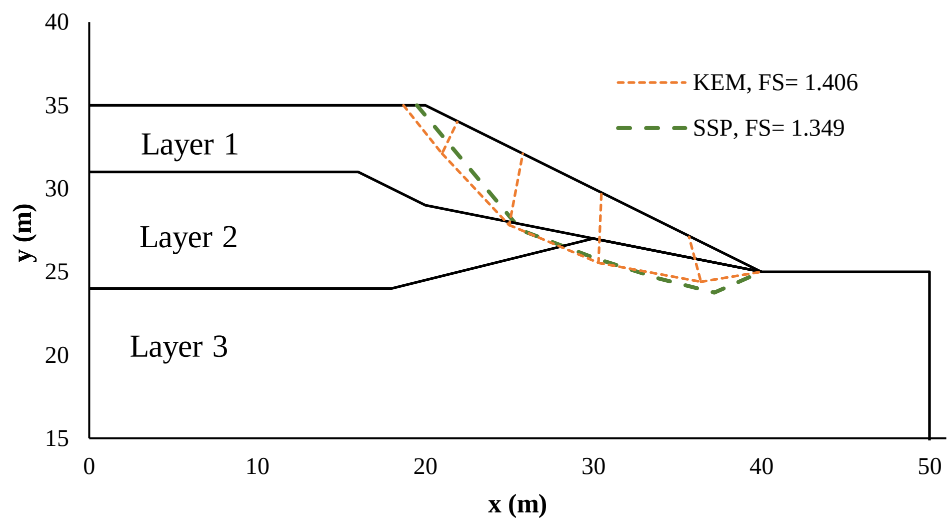

Figure 3.3. Critical failure surfaces of the multi-layered slope

Donald & Giam (1989) presented a factor of safety of 1.39 for this problem. The factors of safety provided by the KEM and SSP deviate from the reference value by 1.2% and 2.5%, respectively. The difference between the reference factor of safety and the KEM is minor, thus the result is considered to be acceptable.

3.3 Slope with a Weak Layer and Water Table

In a classic paper, Fredlund & Krahn (1977) evaluated the change in factor of safety caused by the addition of a weak layer (Soil 2) and pore pressure in the form of a piezometric line. The cross-section of the slope is presented in Figure 3.4.

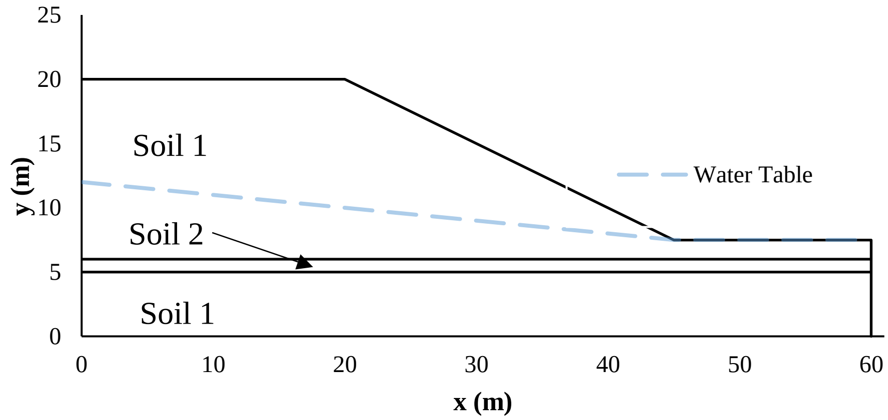

Figure 3.4. Cross-section of the slope with a weak layer and piezometric line. Adapted from Fredlund & Krahn (1977)

The material properties of the soil layers and the various slope conditions are summarized in Table 3-3 and Table 3-4, respectively. The saturated unit weight of Soil 2 is assumed to be equal to the dry unit weight.

Table 3-3. Slope material properties (Fredlund & Krahn, 1977)

Material	φ’ (°)	c’ (kPa)	γ (kN/m^3)
Soil 1	20	28.7	18.85
Soil 2	10	0	18.85

Table 3-4. Summary of slope stability cases

Case no.	Weak Layer	Water Table
1	No	No
2	Yes	No
3	No	Yes

The reference factors of safety given by Fredlund & Krahn (1977) and the computed factors of safety using the SSP and KEM are summarized in Table 3-5.

Table 3-5. Computed and reference factors of safety (Fredlund & Krahn, 1977)

Case no.	Computed		Reference	
	SSP (M-P)	KEM	Spencer's	M-P
1	1.916	1.967	2.073	2.076
2	1.222	1.353	1.373	1.378
3	1.751	1.814	1.834	1.833

It is interesting to note that for all cases, the SSP gives factors of safety 4.7%-11% less than the reference values even though both methods employ the Morgenstern-Price method. The reference solutions correspond to circular failure surfaces, except for the case of the slope with a weak layer. This indicates that for limit equilibrium methods, there are variations in the solution when accommodating non-circular failure surfaces and applying different optimization algorithms.

3.3.1 Case 1: Homogeneous Slope

The stability of a homogeneous slope consisting entirely of Soil 1 is analyzed in this section. The critical slip surfaces are shown in Figure 3.5.

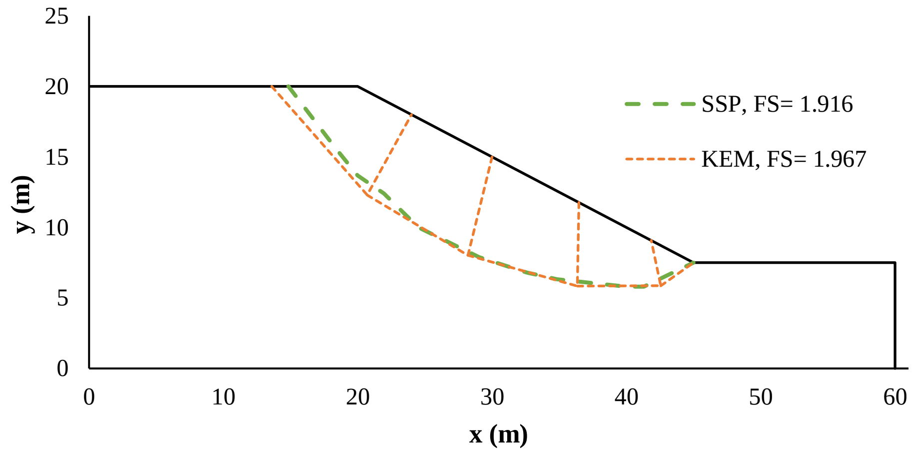

Figure 3.5. Critical slip surfaces, Case 1

The slope configuration and soil properties provide a $\lambda_{\phi c}$ of 3, indicating a toe failure. Both methods provide similar critical failure surfaces with the KEM predicting a greater factor of safety than predicted by SSP. The KEM solution gives a more conservative estimate for the FS than the reference value of 2.076. This deviation in the factor of safety is within the expected variation for rigorous limit equilibrium methods.

3.3.2 Case 2: Addition of a Weak Layer

The stability of the slope with the addition of a weak clay layer is examined in this section. The critical slip surfaces are shown in Figure 3.6. It demonstrates that if a weak layer exists in a slope, failure is likely to occur along it in a block sliding mechanism (Terzaghi et al., 1996).

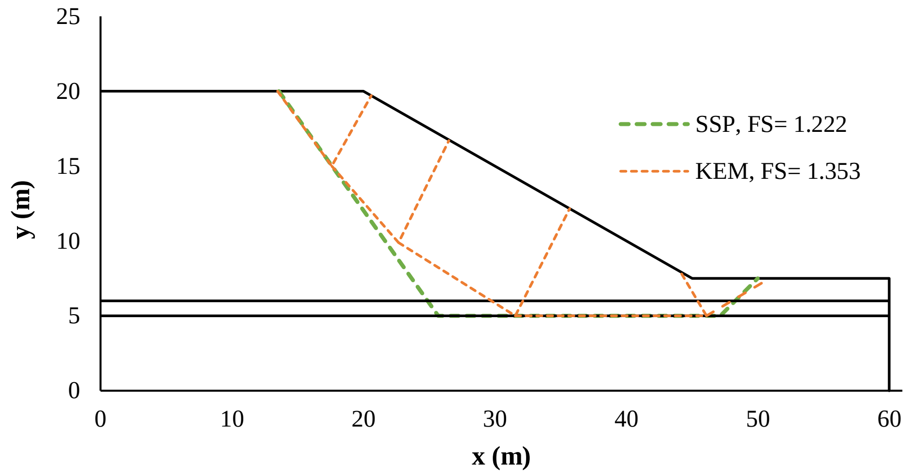

Figure 3.6. Critical slip surfaces, Case 2

With the addition of the weak layer, the factor of safety obtained using each method is reduced by approximately 30%. The objective of analyzing this slope was to determine whether the KEM is capable of locating the block sliding mechanism, which is assumed to be the correct failure mechanism for this slope. The KEM does in fact locate the block sliding mechanism and provides a critical failure surface similar to that predicted by the Morgenstern-Price method. However, the block sliding failure along the weak layer extends over a greater distance in the Morgenstern-Price method. The KEM provides a lower estimate of the FS (2.5% difference) when compared to the reference value of 1.378.

3.3.3 Case 3: Addition of a Piezometric Line

The stability of the slope with the addition of a piezometric line in an otherwise homogeneous slope is analyzed next. As expected, the addition of a water table reduces the effective stress in the soil, thereby reducing the factor of safety by approximately 10% for both methods as shown in Figure 3.7.

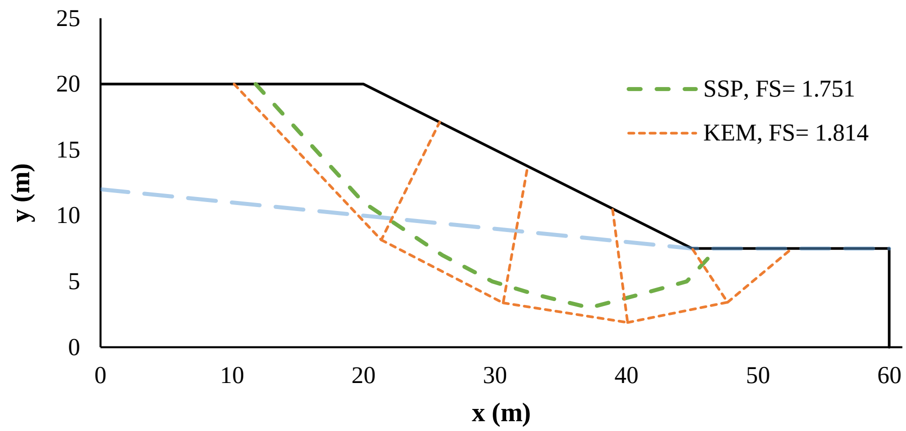

Figure 3.7. Critical slip surfaces, Case 3

The failure mechanism is altered from a toe failure to a deep-seated failure, with the critical failure surface obtained using the KEM being deeper. The factor of safety obtained by the KEM is nearly identical to the reference value with only 1% difference.

3.4 Cohesive Slope

In this example, the stability of a hypothetical cohesive slope with a height of 5 m and length of 10 m is analyzed. The clay has a cohesion of 25 kPa and a unit weight of 18 kN/m^3. As $\phi = 0$, this is essentially an undrained total stress analysis, with cohesion being equal to the undrained shear strength, s_u. A $\lambda_{\phi c}$ value of less than 1 indicates a deep-seated or base failure (Duncan & Wright, 1980). The soil has a friction angle $\phi = 0°$, thus $\lambda_{\phi c} = 0$. A deep-seated failure is to be expected as confirmed in Figure 3.8.

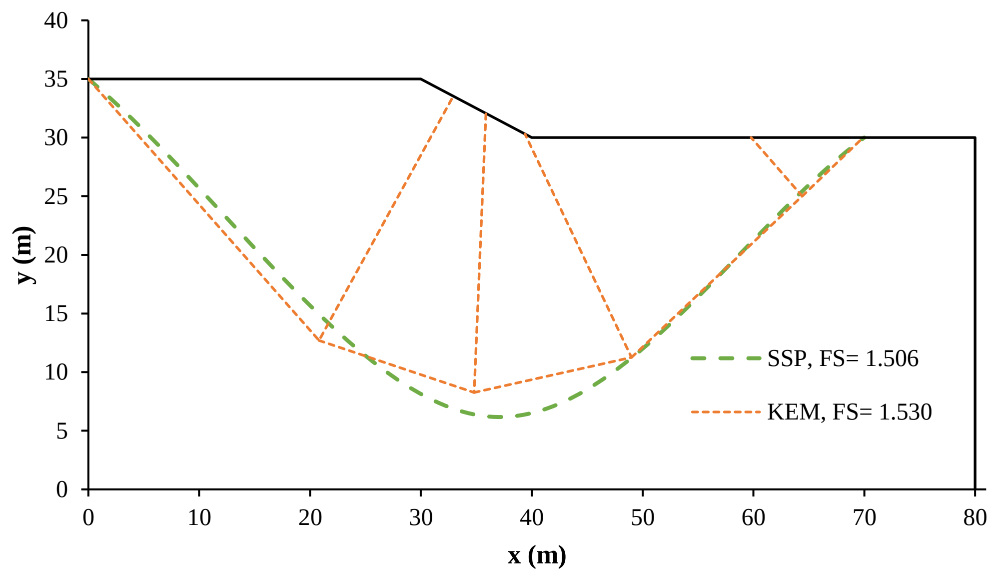

Figure 3.8. Critical failure surfaces of the cohesive slope

The KEM and the SSP provide nearly identical values for the factor of safety and similar slip surfaces, except near the toe. To verify the solution provided by the KEM, the stability charts developed by Janbu (1968) and Taylor (1948) were used to determine the factor of safety of the slope, both providing a value of 1.55. The difference in the factor of safety between the KEM and the stability charts is 1.3%, which is relatively small.

The mechanism shown in Figure 3.8 seems to resemble a bearing capacity failure. The ultimate bearing capacity of a foundation (q_{ult}) on a clay for $\phi = 0$ conditions is given by (Duncan et al., 2014):

$$q_{ult} = 5.53c \tag{3.2}$$

In the case of slope stability, the load causes failure (q) is the weight of soil above the toe of the slope (γH) (Duncan et al., 2014). Thus, the factor of safety is

$$FS = \frac{5.53c}{\gamma H} \tag{3.3}$$

Applying eq. (3.3) given the geometry of the slope and the soil properties, the factor of safety is 1.536. The factor of safety found from the bearing capacity equation is nearly identical to that obtained using the KEM. Thus, it appears that the slope failed through bearing capacity. It should be noted that lower and upper bound factors of safety are given by $\frac{4c}{\gamma H}$ and $\frac{6c}{\gamma H}$. These correspond to a mechanism consisting of 2 triangular elements, in which there is no shear interaction and shear interaction between the triangular elements, respectively. We should keep in mind that an undrained total stress analysis was completed here. If the slope were to develop over a long period of time, some consolidation could take place, thus increasing the factor of safety

3.5 Cohesionless Slope

In this example, the stability of a hypothetical cohesionless slope with a height of 5 m and length of 10 m is examined. The soil has a friction angle $\phi = 30°$ and a unit weight $\gamma = 18\ kN/m^3$. As stated in the previous example, Janbu's dimensionless parameter, $\lambda_{\phi c}$, can be utilized to predict the failure mechanism in a homogeneous slope. For slopes where cohesion $c = 0$, $\lambda_{\phi c}$ approaches infinity and the failure surface is parallel to the surface of the slope (Duncan & Wright, 1980). Translational failures occur where soil is displaced along a planar surface, such as a weak layer. For cohesionless slopes, this translational failure occurs parallel to the surface of the slope. The KEM locates the translational failure and provides the same factor of safety as the Morgenstern-Price method.

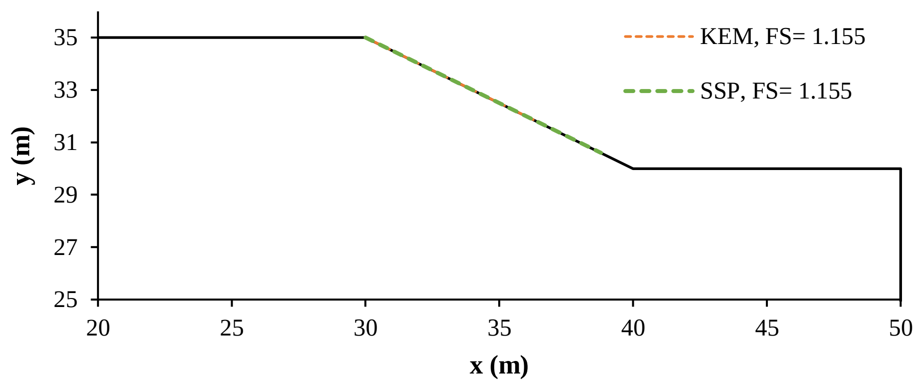

Figure 3.9. Critical failure surfaces of the cohesionless slope

For $c = 0$ where failure is parallel to the slope face, the factor of safety can be calculated using the friction angle of the slope and the slope angle (Duncan & Wright, 1980); i.e.

$$FS = \frac{\tan\phi}{\tan\beta} \tag{3.4}$$

For a slope where $\phi = 30°$ and $\beta = 26.5°$, a factor of safety of 1.155 is obtained, which agrees with the KEM and SSP solutions.

3.6 Foundation

In this example, the stability of a hypothetical embankment consisting of clay overlain by sand is analyzed (Duncan et al., 2014). The clay is assumed to consolidate over time, so only the short-term stability of the embankment is of concern (i.e. the clay's undrained shear strength is adopted as the appropriate failure parameter). The material properties of both soils are summarized in Table 3-6.

Table 3-6. Material properties (Duncan et al., 2014)

Material	φ (°)	s_u (kPa)	γ (kN/m^3)
Sand	40	0	22
Clay	0	119.7	22

The critical slip surfaces obtained using the KEM and M-P are shown below in Figure 3.10.

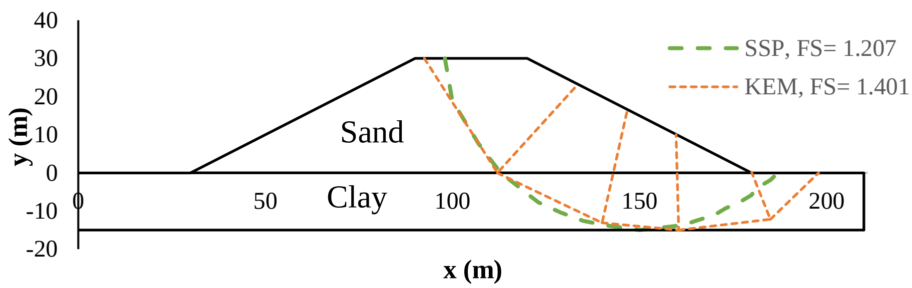

Figure 3.10. Critical failure surfaces of the foundation problem

The SSP solution indicates that the failure surface is a circular failure tangent to the base of the clay layer, which is typical for embankments. The KEM (5-element solution) provides a similar failure surface and tangential point, except the exit point of the failure surface is at a greater distance. Duncan et al. (2014) computed a FS of 1.20 for this problem utilizing Geo-Slope's SLOPE/W and Spencer's method. The SSP (Morgenstern-Price) solution agrees well with the reference factor of safety, while the KEM significantly overestimates it by 17%.

According to Duncan & Wright (1980), force equilibrium methods generally overestimate the factor of safety of embankment problems, often up to 30%. To determine whether a finer mesh was required for this problem, the analysis was repeated with a finer vertical mesh using 10 and 20 elements. Increasing the number of elements leads to higher factors of safety of 1.435 and 1.460 for the 10-element and 20-element solutions, respectively. The 5-element mesh was also subdivided horizontally and a reasonable factor of safety corresponding to an expected failure mechanism was found, as shown in Figure 3.11.

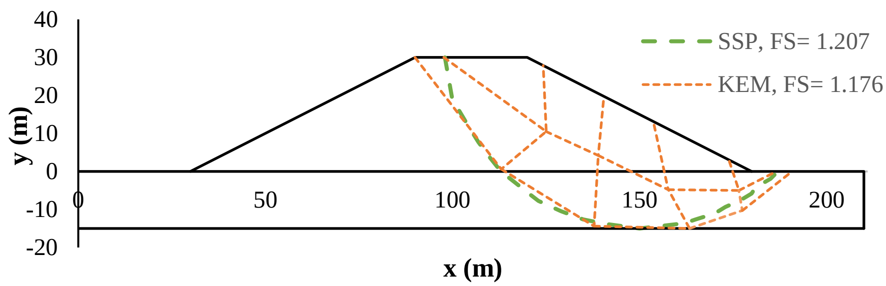

Figure 3.11. Critical failure surfaces of the foundation problem with 10 KEM elements (horizontal subdivision)

The horizontally subdivided mesh provides a FS of 1.17 which differs slightly from the reference factor of safety of 1.20. This example demonstrates that the KEM can sometimes requires horizontal mesh refinement. When carrying out analysis of more complex slopes, such as embankments, using the KEM, it is recommended to check the solution against robust limit equilibrium methods. For the case when similar solutions are not found, vertical and horizontal mesh refinement is recommended.

3.7 Retaining Wall

In this example, the stability of a hypothetical retaining wall structure created by Karchewski (2012) is studied. The retaining wall, which is made from concrete, lies on a clayey silt layer with the backfill being a sandy silt. The material properties are summarized in Table 3-7. The saturated unit weights are assumed to be equal to the dry unit weights.

Table 3-7. Soil material properties (Karchewski, 2012)

Material	φ’ (°)	c’ (kPa)	γ (kN/m^3)
Sandy silt	30	5	17
Concrete	50	1000	22
Clayey Silt	10	30	18

Typical analyses of retaining walls considers overturning, sliding and bearing capacity failures. However, these structures can also fail by global instability where the retaining wall itself is a part of the slope. The critical slip surfaces obtained using the SSP and KEM are shown below in Figure 3.12.

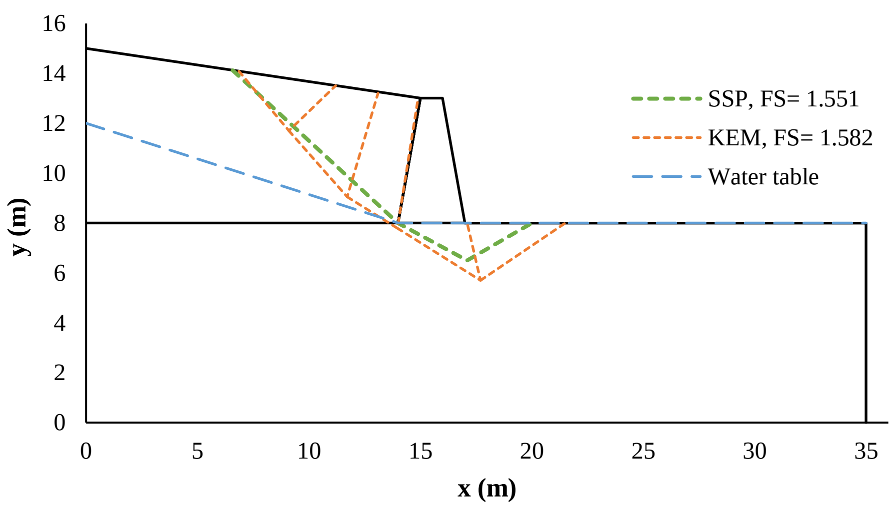

Figure 3.12. Critical failure surfaces of the retaining wall problem

The critical slip surfaces provided by the Morgenstern-Price method and the KEM are similar with the factor of safety differing by 2%. The effect of mesh refinement for this problem is discussed in Section 8.1.3.

Summary

- The kinematic element method is capable of locating the critical failure surface for a variety of conditions, ranging from homogeneous slopes to block sliding along a weak layer.
- The KEM generally provides FS similar to those obtained using rigorous limit equilibrium procedures that satisfy all conditions of equilibrium.
- The KEM was shown to be sensitive to mesh refinement for the embankment problem. The 5-element KEM solution overestimated the FS significantly. Vertical mesh refinement was carried out, but the factor of safety did not improve. Horizontal mesh refinement was carried out and factor of safety agreed well with rigorous limit equilibrium methods.

Chapter 4 Kinematics

One of the advantages of the kinematic element method is that virtual displacements of the rigid elements can be calculated, and the user is easily able to visualize the failure mechanism. The problem of slope stability can be thought of in terms of active and passive pressures (Berry & Reid, 1987). In the active condition, the soil fails by moving away from the failure surface and along the slope (Knappett & Craig, 2012). In the passive condition, the soil is compressed due to the displacement caused by the active earth pressure. A similar approach can be taken with regard to the methods of slices to identify which zone is active and which is passive.

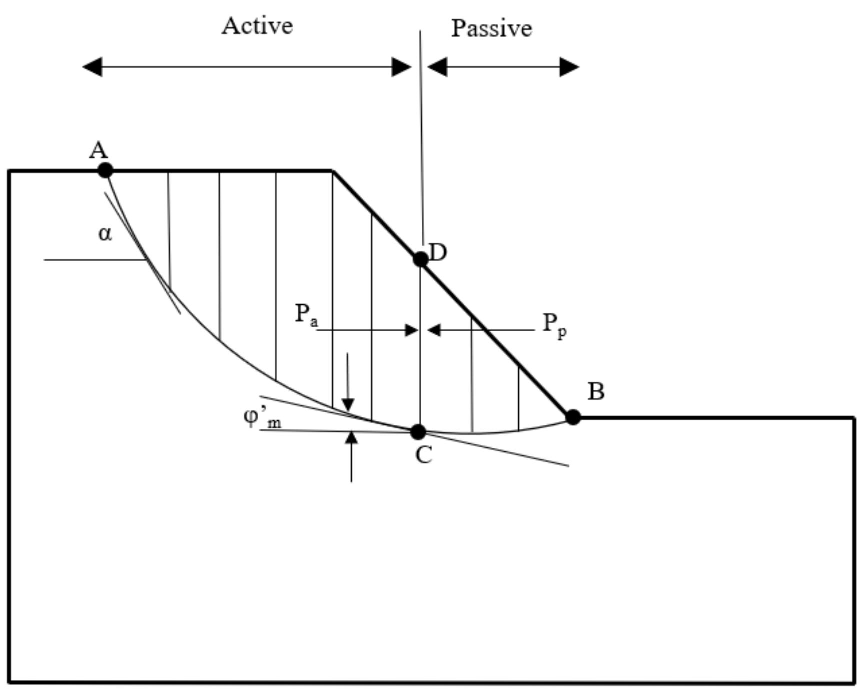

Figure 4.1. Active and passive pressures in slope stability. Adapted from Berry & Reid (1987)

Referring to Figure 4.1, for a failure surface with an entry Point A and exit Point B there exists a line along the slope, CD, where the failure in the slope transitions from the active condition to the passive. At the tangent of the failure plane at Point C that corresponds to the transition from active to passive, the angle of the base of the slice (α) is equal to the mobilized friction angle, ϕ_m. An alternative approach is to identify where the slope appears to move upwards; in other words where the gravity loading is doing negative work.

The observations made regarding the applications of earth pressure theory can be utilized to assist in interpreting the results for the kinematic analysis of slope failures. However, unlike the method of slices where 20 or more slices are used to model slope failures, the KEM often uses as few as 3 to 5 elements, so that the exact point of the transition from active to passive failure may be difficult to locate. In the figures presented in this section, the potential failure mechanism is given by the gray solid lines and the corresponding deformed elements following failure are given by the red, dotted lines.

4.1 Homogeneous Slope

The kinematics of the failure for the homogeneous slope from Section 3.3.1 is provided in Figure 4.2. As expected, the direction of soil movement is left to right and along the failure surface. As the soil from elements 1, 2, and 3 move downwards along the slope, the soil in elements 4 and 5 are forced to move upwards. This can be thought of in terms of pressure theory where elements 1 through 3 undergo active behavior with element 5 responding to passive pressure. Elements 1 and 5 display the greatest amount of movement. The lowest amount of movement in the vertical direction can be observed in element 4, which has a nearly horizontal base.

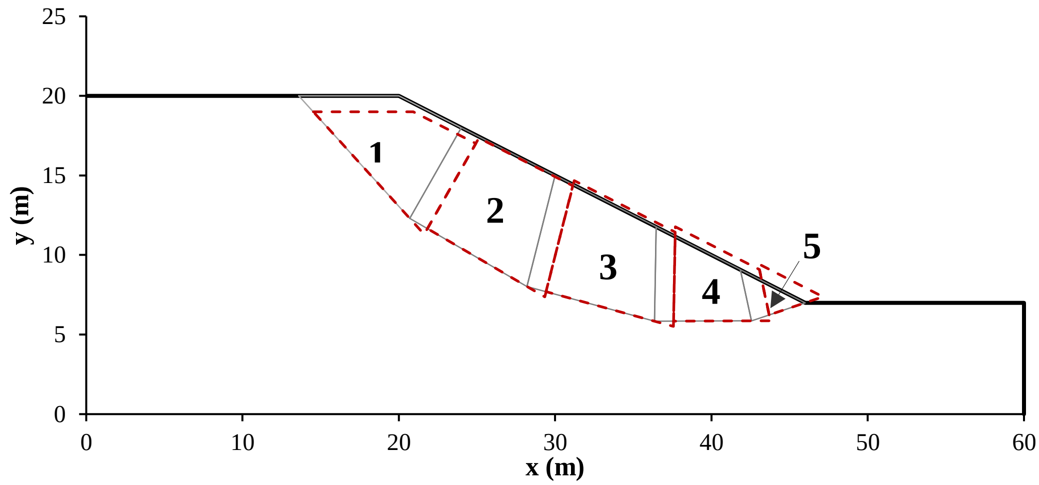

Figure 4.2. Kinematics of the homogeneous slope failure

Based on the stability analysis results of Section 3.3.1 ($\phi = 20°$ and $FS = 1.967$) the mobilized friction angle of the slope is 10.5°. The base inclination angle of element 3 is 15°, indicating that the soil is still in the active condition at that point along the slope. Element 4 has a nearly horizontal base inclination (much lower than the mobilized friction angle) indicating that it should be responding passively. This is confirmed by the minor positive displacement in the vertical direction relative to the slope surface observed in the element.

4.2 Slope with a Weak Layer

As discussed in Section 3.3.2, failure of slopes, which contain weak layers, is often governed by the block sliding mechanism. A diagram displaying the mechanism in terms of active and passive earth pressure is illustrated in Figure 4.3.

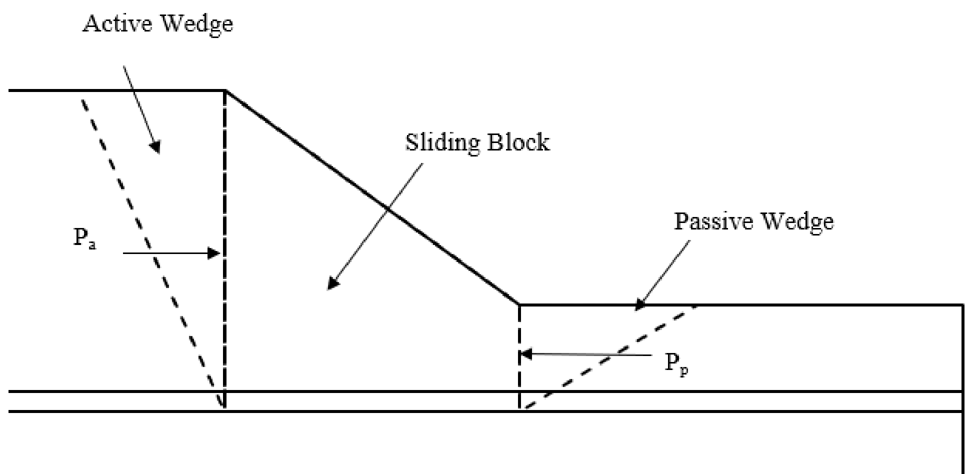

Figure 4.3. Block sliding mechanism. Adapted from Terzaghi et al. (1996)

Failure is initiated by the displacement of the soil along the active wedge forcing the block to slide horizontally along the weak layer. The strength along the weak layer in the block and the passive earth pressure to the right of the block resist the failure of the slope (Terzaghi et al., 1996). The kinematics of the sliding block failure shown in Section 3.3.2 are provided in Figure 4.4. The selected problem is that of the previous homogeneous slope with the addition of a weak layer. The factor of safety of the slope is 1.353 which is significantly lower than the previous case due to the presence of the weak layer.

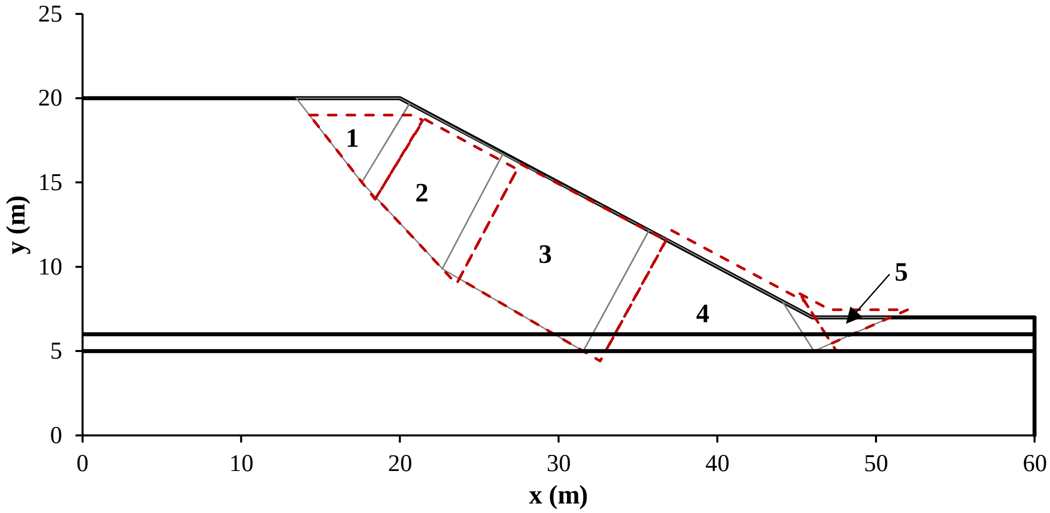

Figure 4.4. Kinematics of a block sliding failure

The mechanism defined in Figure 4.4 is similar to that displayed in Figure 4.3 with the active condition represented by elements 1, 2, and 3. Element 5 represents the passive wedge and element 4 is the sliding block which in addition to the passive pressure provided by element 5 resists failure. Elements 1 to 3 move downwards along the slope causing element 4 to slide along the weak layer. Element 5 is forced to translate towards the right and the soil in it is displaced and forced to move upwards due to the slip surface at the base.

4.3 Retaining Wall

The kinematics of the retaining wall from Section 3.7 is discussed next. The retaining wall potentially undergoing general shear failure is more complex than a simple homogeneous slope. The capability of the KEM in presenting the kinematics of this problem accurately is of interest. The retaining wall itself is much stronger than the soil, thus forcing failure to occur in the soil below. The kinematics of the global failure of the retaining wall is shown in Figure 4.5.

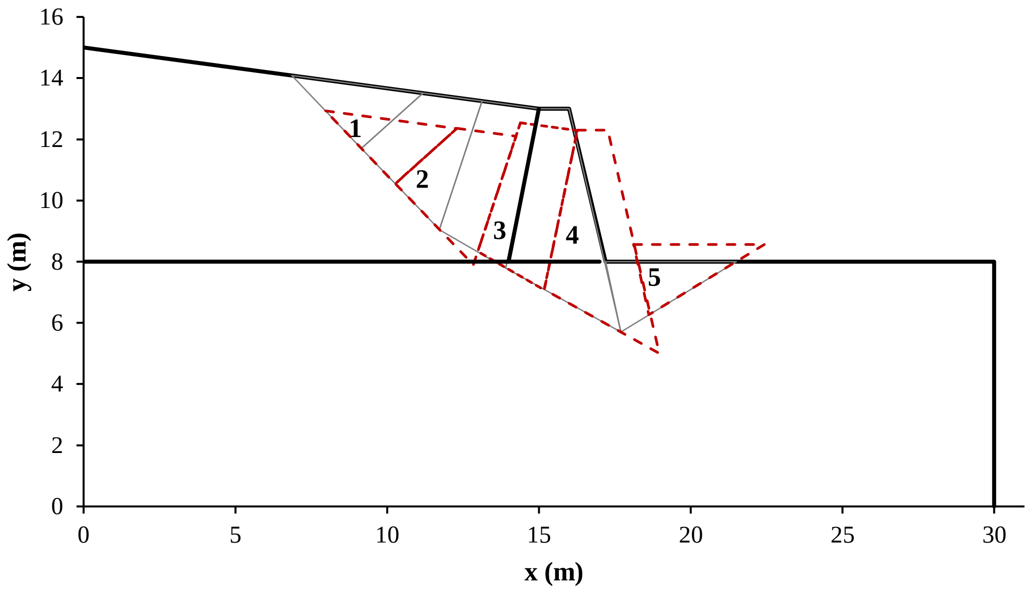

Figure 4.5. Kinematics of the retaining wall failure

Observations similar to the previous examples can be made regarding the active and passive earth pressure regions. Elements 1 through 4 move downwards along the slope, forcing element 4 to translate to the right and upwards. Elements 1 through 4 clearly represent the active condition of the slope failure and element 5 represents the passive condition. It is interesting to note that element 4 consists of the retaining wall and the active wedge below it.

Chapter 5 Derivation of a Kinematic Element Method Formulation with Vertical Interelement Boundaries

As previously discussed, in the kinematic element method, force equilibrium is solved for assumed failure mechanisms associated with rigid blocks. To introduce failure and determine the factor of safety, the actual failure parameters are reduced in magnitude until a failure mechanism can be attained. An important assumption is that moment equilibrium takes care of itself by having the resultant forces on each boundary shifting appropriately. The kinematics of the failure are required in order to ascertain the directions of the shear force along each boundary. In this section, we consider a KEM procedure similar to the method of slices where the interelement boundaries are vertical. This method will be referred to as Kinematic Element Method-Vertical (KEMv). A homogeneous, isotropic slope with a typical KEMv failure surface (given by the dotted lines) defined by three elements is illustrated in Figure 5.1. The KEMv for 3 and 5-element solutions were programmed in MATLAB. The MATLAB code for the 3-element solution is presented in the Appendix.

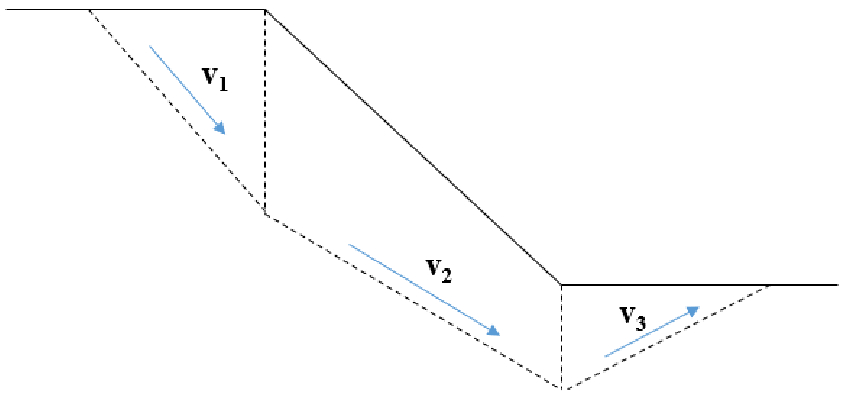

Figure 5.1. Sample KEMv slip surface with 3 elements

The interelement boundaries of the original KEM can be in any orientation. To simplify the mathematics and apply a procedure similar to the method of slices, the interelement boundaries in KEMv are vertical. In order to further simplify the derivation, the program was designed such that there must be interelement boundaries at the crest and toe of the slope. This restriction is not applied in the KEM developed by Gussmann (1982).

5.1 Statics

The forces acting on each element for the assumed deformation mechanism are shown in Figure 5.2, where W is the weight of an element, N and T denote the normal and shear force acting on the element along the failure plane, respectively, E and X represent the interelement normal and shear forces, respectively, and n and t are the unit vectors for the normal and tangent to the shear plane, respectively.

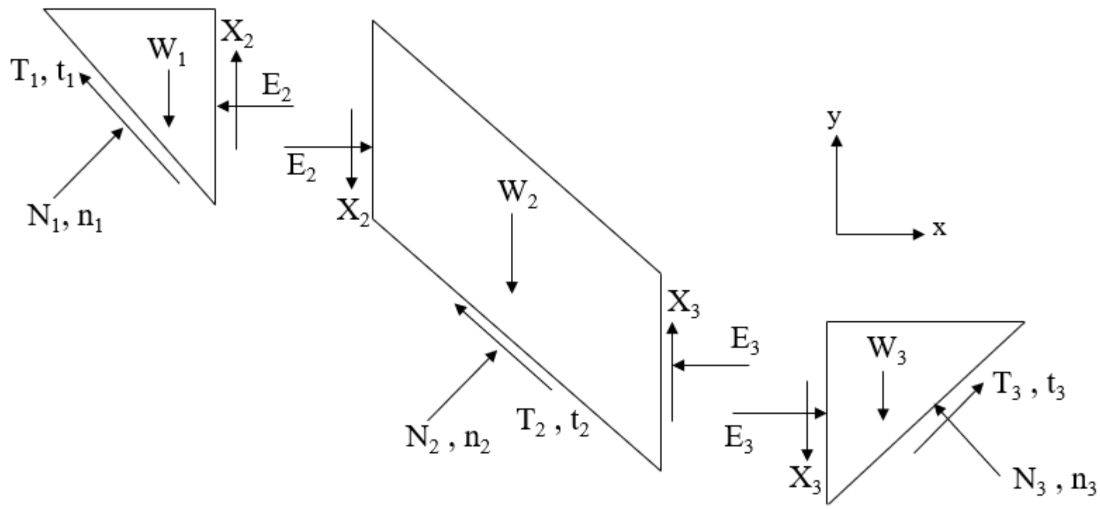

Figure 5.2. Forces acting on KEMv elements (3-element solution)

The directions of all forces, excluding the failure plane normal and shear forces have been predetermined graphically assuming that the movement of the slope is left right. For example, as Element 1 is assumed to move downwards and to the right, the interelement shear force (X_2), must act in the positive y-direction. Following this observation, the direction of the remaining interslice shear forces are readily determined. Since the geometry of each element is known, it is a straightforward task to determine the unit vectors. For example, if we consider surface AB, $\Delta x_2 = x_A - x_B$ and $\Delta y_2 = y_A - y_B$ yielding a length of $l_2 = \sqrt{\Delta x_2^2 + \Delta y_2^2}$ and direction cosines $\left(n_{2,x}, n_{,2,y}\right) = (\frac{\Delta x_2}{l_2}, \frac{\Delta y_2}{l_2})$. Noting that n and t are perpendicular, the following is a key observation that can be made: $n_{2,x} = t_{2,y}$ and $n_{2,y} = -t_{2,x}$. This simple observation allows for less quantities to be calculated and simplifies the equations.

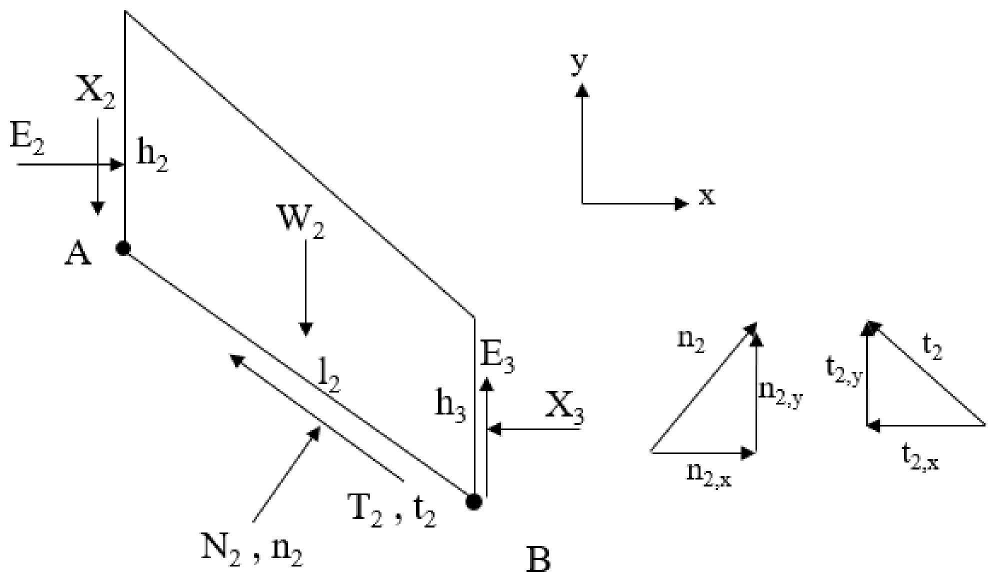

Figure 5.3. Forces and unit vectors for element 2

In the original KEM, the shear forces acting along the failure plane and between elements are described by the Mohr-Coulomb failure criterion and the same assumptions are made herein. The potential failure mechanism for a given geometry corresponds to a situation where the failure parameters are reduced via the factor of safety to the point where a sliding mechanism can develop:

$$FS = T/T_m \quad \rightarrow \quad T_m = T/FS \tag{5.1}$$

with T_m being the mobilized shear along the failure surface, FS denotes the value that reduces the shear strength (T). Utilizing the above relation, the equations for the mobilized shear force along the failure plane can be calculated where i is the element number.

$$T_{i,m} = \frac{N_i \tan\phi + cl_i}{FS} \ \rightarrow T_{i,m} = N_i \tan\phi_m + c_m l_i \tag{5.2}$$

The same procedure can be applied to derive the interelement shear force equation where h is the height of the interelement boundary and i is the interelement boundary number:

$$X_{i,m} = E_i \tan \phi_m + c_m h_i \tag{5.3}$$

Applying the failure condition reduces the number of unknown quantities. By beginning with Element 1, we can calculate N_1 and E_2. The corresponding shear components are obtained by applying eqs. (5.2) and (5.3). We can then move to element 3 and repeat the process. Application of these equations reduces the number of unknown quantities significantly. For each element, the two unknowns which need to be solved, are the interelement normal force and the failure plane normal force. To simplify the presentation of the derivation, the following terms are introduced:

$$t_m = \tan \phi_m \tag{5.4}$$

$$C_{i,m}^{l} = c_m l_i \tag{5.5}$$

$$C_{i,m}^{h} = c_m h_i \tag{5.6}$$

where $C_{i,m}^{l}$ and $C_{i,m}^{h}$ are the mobilized cohesive force along the failure plane and interelement boundary, respectively.

5.2 KEMv Solution for a 3-Element Failure Mechanism

The solution algorithm for the KEMv using 3 elements is presented in this section. The proposed methodology can be extended to solutions with larger number of elements. In the solution for KEMv, an initial factor of safety (FS_0) is assumed for all interelement boundaries and failure planes, except for the failure plane of the middle element (Element 2). At the failure plane of element 2, an updated factor of safety (FS') is calculated along with the associated error. If the absolute value of the error is greater than 0.0005, the solution iterates until convergence, i.e. $|Error| \leq 0.0005$.

$$Error = FS' - FS_o \tag{5.7}$$

The following steps are required to calculate the factor of safety for a 3-element failure mechanism:

1. Calculate the unknown forces acting on elements 1 and 3: N_1, E_2, N_3, E_3. The only remaining unknowns are N_2 and $T_{2,m}$ while two equations of equilibrium are available.
2. Calculate N_2 and the mobilized shear force $T_{2,m}$.
3. Calculate T_2 which is the shear force associated with a FS of 1 (eq. (5.8).
4. Recalling the Fellenius definition of the factor of safety, calculate the updated factor of safety (FS') using eq. (5.9).
5. Calculate the associated error using eq. (5.7).

$$T_2 = N_2 tan\phi + cl_2 \tag{5.8}$$

$$FS' = (\frac{T_2}{T_{2,m}}) \tag{5.9}$$

This solution is similar to the method presented by Engel & Lauer (2017). In the KEMv formulation, the fictitious driving force (ΔT) is not calculated but is readily determined where $\Delta T = T_2 - T_{2,m}$. In the proposed formulation, the values of the mobilized and required shear forces are computed and compared to determine the error associated with each assumed value of FS_0. In the following sections, the equations for determining the unknown forces are presented.

5.2.1 Element 1

The equations for horizontal and vertical force equilibrium can be written for element 1 and the unknown forces (N_1 and E_2) can be calculated.

$$\Sigma F_h = 0 \;\rightarrow\; N_1 n_{1,x} + T_1 t_{1,x} - E_2 = 0 \tag{5.10}$$

$$\Sigma F_v = 0 \;\rightarrow\; N_1 n_{1,y} + T_1 t_{1,y} + X_2 - W_1 = 0 \tag{5.11}$$

Substituting the known relations between the normal and tangential unit vectors and the normal and shear forces, N_1 and E_2 can be calculated

$$N_1 = \frac{-C^l_{1,m} t_m t_{1,x} - C^l_{1,m} t_{1,y} - C^h_{2,m} + W_1}{t_m^2 t_{1,x} + 2 t_m t_{1,y} - t_{1,x}} \tag{5.12}$$

$$E_2 = \frac{C^h_{2,m} t_m t_{1,x} - C^l_{1,m} t^2_{1,x} - C^l_{1,m} t^2_{1,y} + W_1 t_m t_{1,x} - C^h_{2,m} t_m t_{1,y} + W_1 t_{1,y}}{t_m^2 t_{1,x} + 2 t_m t_{1,y} - t_{1,x}} \tag{5.13}$$

5.2.2 Element 3

The procedure used to determine the unknown forces for element 1 can be applied to the element 3, as well.

$$\Sigma F_h = 0 \quad \rightarrow \quad N_3 n_{3,x} + T_3 t_{3,x} + E_3 = 0 \tag{5.14}$$

$$\Sigma F_v = 0 \quad \rightarrow \quad N_3 * n_{3,y} + T_3 t_{3,y} - X_3 - W_3 = 0 \tag{5.15}$$

$$N_3 = \frac{-C^l_{3,m} t_m * t_{3,x} - C^l_{3,m} t_{3,y} + C^h_{3,m} + W_3}{t_m^2 t_{3,x} + 2t_m t_{3,y} - t_{3,x}} \tag{5.16}$$

$$E_3 = \frac{-C^h_{3,m} t_m t_{3,x} - C^l_{3,m} t^2_{3,x} - C^l_{3,m} t^2_{3,y} + W_1 t_m t_{3,x} + C^h_{3,m} t_{1,y} + W_3 t_{3,y}}{t_m^2 t_{3,x} + 2t_m t_{3,y} - t_{3,x}} \tag{5.17}$$

5.2.3 Element 2

Following the calculation of the unknown forces acting on elements 1 and 3, N_2 and $T_{2,m}$, can be calculated. Once again, the equations for vertical and horizontal force equilibrium are written. It must be noted that in the calculation of the forces for the final element, the mobilized shear force is not a function of the normal force (i.e. the relation in eq. (5.2) is not applied).

$$\Sigma F_h = 0 \quad \rightarrow \quad N_2 n_{2,x} + T_2 t_{2,x} + E_2 - E_3 = 0 \tag{5.18}$$

$$\Sigma F_v = 0 \quad \rightarrow \quad N_2 n_{2,y} + T_2 t_{2,y} - X_2 + X_3 - W_2 = 0 \tag{5.19}$$

$$N_2 = -X_2 t_m t_{2,x} + X_3 t_m t_{2,x} - C^h_{2,m} t_{2,x} + C^h_{3,m} t_{2,x} - W_3 t_{2,x} - X_2 t_{2,y} + X_3 t_{2,y} \tag{5.20}$$

$$T_{2,m} = X_f t_m t_{2,y} - X_3 t_m t_{2,y} + C^h_{2,m} t_{2,y} - C^h_{3,m} t_{2,y} + W_2 t_{2,y} - X_2 t_{2,x} + X_3 t_{2,x} \tag{5.21}$$

Once N_2 is found, T_2 can be calculated using eq. (5.8). Following the calculation of $T_{2,m}$, the updated factor or safety (FS') and the associated error ($Error$) can be obtained using eqs. (5.9) and (5.7), respectively.

5.3 Proposed Iteration Scheme

The KEMv requires an iterative solution, thus a root-finding scheme is required. The bisection method, which is a relatively simple method, was applied to determine the factor of safety. The factor of safety was defined as a function of the error. The bisection method requires an upper and lower bound estimate (i.e. a range where the value of the error function changes from positive to negative or vice versa). In utilizing this algorithm, it must be noted that the updated factor safety (FS') is not explicitly part of the solution. The error is a function of the updated factor of safety, thus FS' is implicitly utilized (see Appendix). Initially, there were issues with this method as the applicable range for the method was unknown. To locate an appropriate search range, the factor of safety was increased incrementally, and the error was calculated. The error function and mobilized shear forces for the problem in Section 3.1 are presented in Figure 5.4(a) and Figure 5.4(b), respectively. The shear forces and error function shown in Figure 5.4 correspond to the 5-element solution.

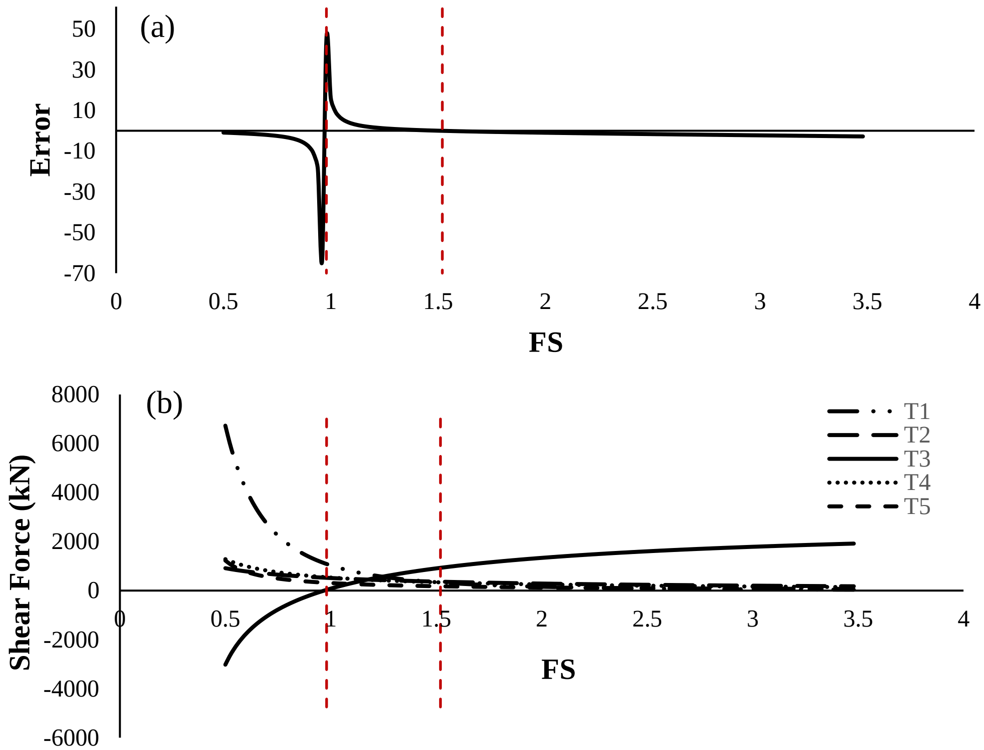

Figure 5.4. (a) Error function and (b) Mobilized shear forces for a sample slope stability problem

The error function indicates that there are two possible solutions to the problem at factors of safety of 0.970 and 1.520. This issue was found for all of the simulated problems. After analyzing the computed values for all forces from various analyses, we find that the value of the mobilized shear force along the failure plane of the middle element indicated the correct solution. The mobilized shear force of the middle element (T_3) is approximately 0 at a FS of 0.970. This is an unfeasible solution as it is impossible for the mobilized shear force to be zero during failure. Thus, the appropriate solution to this problem is 1.520. For all KEMv solutions, manual verification of the computed mobilized shear forces is required to select the correct root.

Chapter 6 Vertical Interelement Boundary Assumption

The interelement boundaries in KEM can take any orientation and in combination with the particle swarm optimization algorithm adopted by Gussmann (2017), the failure surface as well as the corresponding mesh associated with the minimum factor of safety can be obtained. In this section, the effect of restricting the elements to having vertical interelement boundaries is explored. This provides an opportunity to determine the effectiveness of the KEMv formulation derived in Chapter 5 as it is applicable for elements with vertical interelement boundaries. The location of some of the points along the failure surfaces are different as the KEMv program has the added requirement of interelement boundaries at the toe and crest of the slope. In Chapters 6 and 7, the KEM solution obtained using Gussmann's program with the vertical interelement boundary restriction will be referred to as Gussmann's Kinematic Element Method- Vertical (GKEMv) to avoid confusion with the formulation derived in Chapter 5. Also, the KEM solution determined using Gussmann's program without boundary restrictions will be referred to as GKEM for Chapters 6 and 7.

6.1 Homogeneous Slope

The effect of the vertical boundary restriction on homogeneous slopes with mixed soils is discussed using the example from Section 3.1. Figure 6.1 shows the slip surfaces obtained using the KEM for vertical and optimal interelement boundaries. Also, the slip surface from the GKEMv was entered into the KEMv program with the coordinates of the interelement boundary along the failure plane given by red diamonds. There is a minor difference in the failure surfaces given by KEMv and GKEMv caused by the KEMv requirement for an interelement boundary at the crest. Applying the vertical boundaries provided a higher FS (3.5%) and a shallower failure surface.

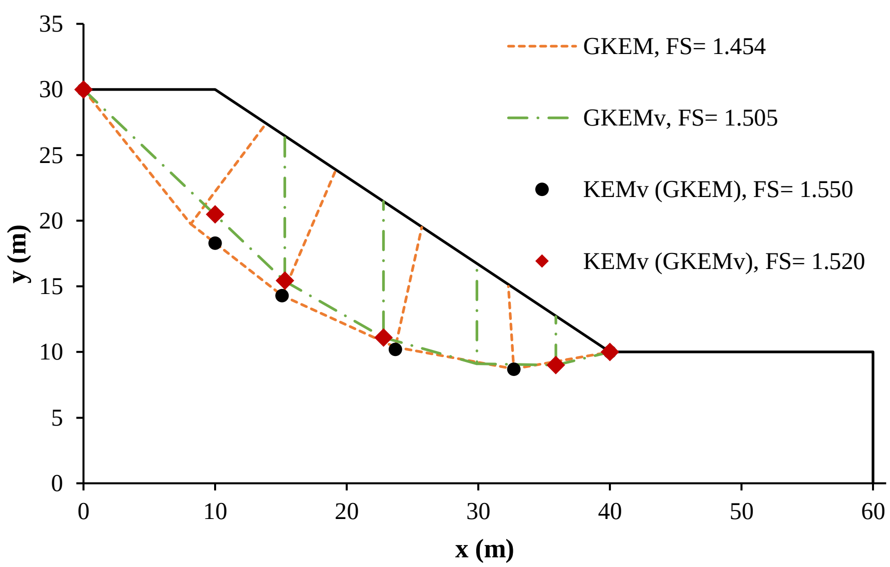

Figure 6.1. Critical slip surfaces of the homogeneous slope for different boundary orientations

For the homogeneous slope examined here, the KEMv program provides a factor of safety similar to that obtained by GKEMv. The difference in the computed values (1%) is likely caused by the minor difference in the slip surfaces. A check was made to determine if the difference in the FS between the optimal orientation and the vertical boundary case is due to the difference in the failure surface created by the PSO algorithm. This was accomplished by using the failure surface obtained using GKEM to determine the factor of safety with KEMv. The corresponding factor of safety was found to be 1.550 which leads us to conclude that the PSO algorithm did not have a significant impact on the FS and that the variance in the solutions was caused by the orientation of the boundaries. The factor of safety given by the SSP was 1.372 while the reference factor of safety was 1.429.

6.2 Cohesive Slope

The effect of vertical boundary restrictions on cohesive slopes is addressed using the problem from Section 3.4. The GKEM provides a larger failure surface than the restricted case as observed in Figure 6.2.

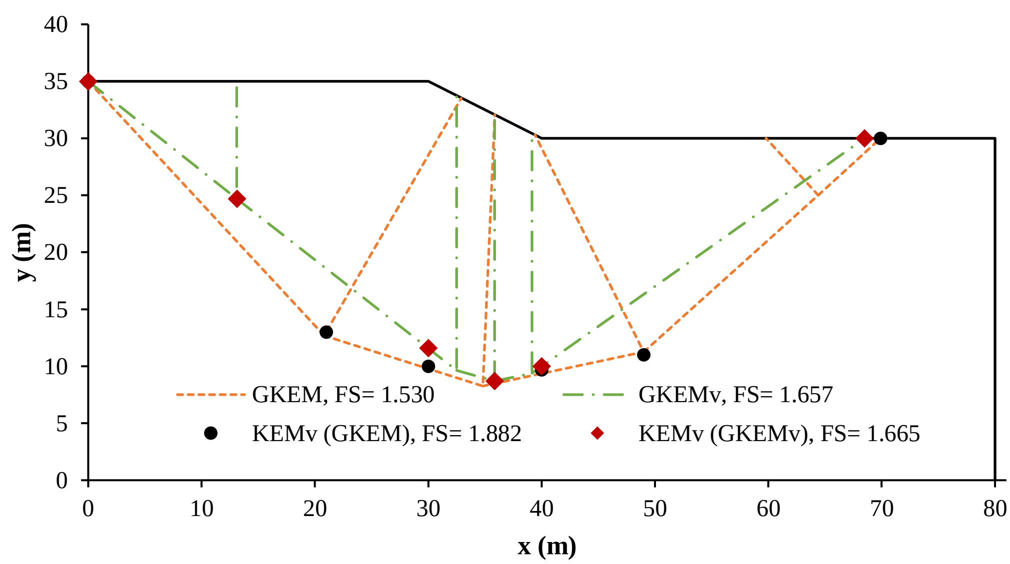

Figure 6.2. Critical failure surfaces of the cohesive slope for different boundary orientations

Applying vertical interelement boundaries changed the shape of the failure surface from a pseudo-circular shape to a triangle. This indicates that the GKEM (KEM without restrictions placed on element orientations) provides a more flexible and realistic failure surface. As observed for the case of the homogeneous slope in Section 6.1, the factor of safety is overestimated.

We also observe that the KEMv provides a similar factor of safety as the GKEMv. The 0.5% difference between the two values was likely caused by the minor difference in the failure surfaces. As for the homogeneous case, the domain corresponding to the minimum factor of safety for GKEM was used to determine the FS using the KEMv program. A factor of safety of 1.882 was obtained, which is 13% larger than the FS corresponding to the GKEMv and KEMv slip surfaces. This supports the conclusion made in Section 6.1 that the vertical boundary restriction leads to higher factors of safety and a modification of the failure surface.

6.3 Cohesionless Slope

Next, we address the effect of the vertical interelement boundary assumption on the cohesionless slope from Section 3.5. For this particular case, the internal boundaries are short, thus they have a limited impact on the failure surface. Regardless of interelement boundary orientations, the factor of safety was found to be 1.155.

The GKEM displays failure which extends farther down the slope, but the failure mechanism is identical. The lack of variance in the factor of safety was likely due to the shallow nature of the failure. As the lengths of the boundaries were so minute, the interelement surfaces were effectively points. The expression given for the factor of safety for translational failure in cohesionless slopes, eq. (3.4), is derived from a special case of the infinite slope failure mechanism, eq. (6.1), where $c = 0$.

$$FS = \frac{c + \gamma Z \cos^2\beta \tan\phi}{\gamma Z \cos\beta \sin\beta} \quad \xrightarrow{c=0} \quad \frac{\tan\phi}{\tan\beta} \tag{6.1}$$

The expression for factor of safety becomes independent of the height of the failure surface. Thus, it is not unexpected that the factor of safety of cohesionless slopes is independent of the orientation of the interelement boundaries.

Summary

- Restricting the interelement boundary orientation to be vertical overestimates the FS and provides a shallower failure surface.
- The KEMv formulation provides nearly identical values for FS as GKEMv. The KEM may not truly be an upper limit solution as thought by Gussmann (1982) as the GKEMv solutions are nearly identical to that of KEMv, which is based on limit equilibrium principles.
- With KEM, we determine, as part of the solution, an optimal discretization for a given number of elements, as well as the minimum factor of safety. The results of the analyses in this section indicates that the use of non-vertical boundaries provides a more flexible failure surface and a more accurate estimate for the factor of safety.

- It would be interesting to modify the KEMv program to be capable of analyzing surfaces with various interelement boundary orientations to see if it provided the same factors of safety as Gussmann's KEM.

Chapter 7 Examination of Interelement Forces

In this chapter, the interelement shear and normal forces along the failure surface obtained using KEMv and GKEMv are compared to the interslice forces from the Morgenstern-Price solution (SSP) developed by Karchewski (2012). The kinematic element method only preserves horizontal and vertical force equilibrium. It is assumed that moment equilibrium is satisfied implicitly, but the location where the shear forces act is not determined as part of the solution. As such, the variation of interelement shear and normal forces along the failure plane (i.e. in the horizontal direction) cannot be studied for the optimal orientation. However, when the interelement boundaries are restricted to vertical lines, the location of the shear and normal forces in the horizontal direction are known. Thus, the interelement forces can be compared to that obtained using the Morgenstern-Price method. For the purposes of this discussion, the interelement forces from GKEMv and KEMv and the interslice forces from the SSP will be referred to as "interelement forces".

In addition to comparing the values of the interslice and interelement forces, the ratio of the interelement interslice shear and normal forces are also compared. In the SSP, the ratio of the interslice shear and normal forces is a predetermined half-sine function multiplied by a scaling factor, λ. According to Morgenstern & Price (1965), the ratio of the interslice shear to normal force can be represented by any function, so long as it is reasonable. The most accurate functions can be found through measurements of in-situ stress or calculated using the finite element method (Morgenstern & Price, 1965). The

Mohr-Coulomb failure criterion utilized to represent the shear failure along the boundaries of the elements in KEMv can also be thought of as an interelement shear force function that relates the interelement shear and normal forces. In this discussion, the ratio of the interslice and interelement shear to normal forces (i.e. X/E) will be referred to as interelement force ratios.

7.1 Homogeneous Slope

In this section, the interelement forces for the homogeneous slope with the mixed soil presented in Section 3.1 is analyzed. The soil has a friction angle $\phi = 15°$, cohesion $c = 41.65\ kPa$ and unit weight $\gamma = 18.82\ kN/m^3$. The variations of the interelement forces and force ratios along the failure surface are shown in Figure 7.1.

Figure 7.1(b) shows that the interelement shear and normal forces for all methods increase to a maximum value near the middle of the failure surface and decrease to 0 at the end of the failure surface. The peak magnitude of the interelement normal forces are similar but the peak magnitude of the GKEMv and KEMv shear forces are approximately 200 kN greater than those of SSP. The interelement shear and normal forces for all methods are nonlinear. The SSP and KEMv display negative shear and normal forces in the upper part of the slope.

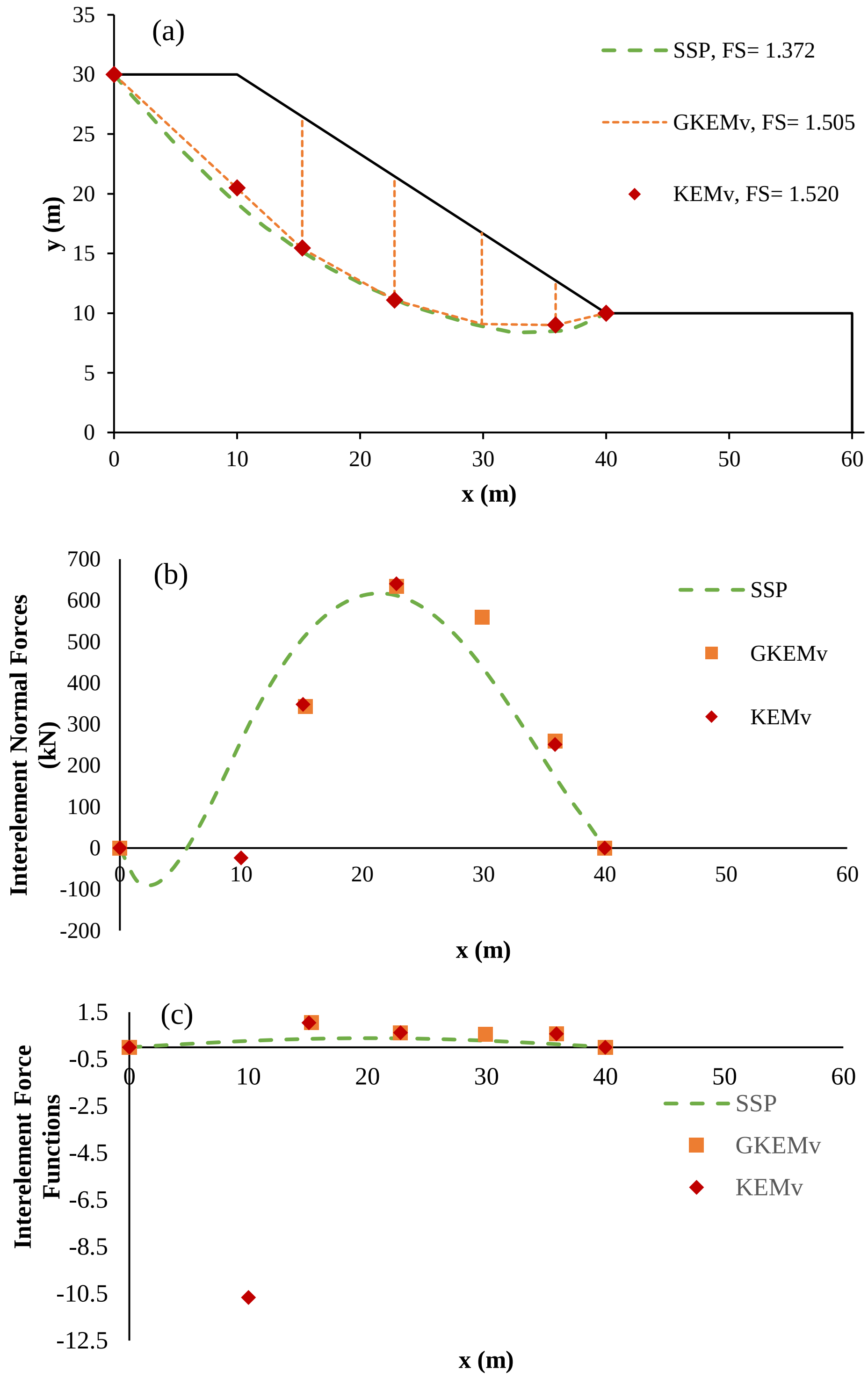

Figure 7.1. (a) Critical slip surfaces, (b) interelement normal forces and (c) interelement force ratios for the homogeneous slope

The variation of the interelement force ratios are shown in Figure 7.1(c). For KEMv, the ratio decreases to approximately -11 at the crest and increases to approximately 0.5 where it remains constant. The interelement force ratio for GKEMv increases to a maximum of 1.1 at its first boundary and similar to KEMv, decreases to approximately 0.5 where it remains constant. The value of the interelement shear force is generally lower than the normal force, so this was unexpected. It seems apparent that the interelement force ratio in the KEM and KEMv are largest in magnitude at the first interelement boundary. Stolle & Guo (2008) applied the RFEM to the method of slices and computed interslice normal and shear stresses. They also observed that the ratio between the interslice shear and normal stress was high at the upper end of the sliding surface for mixed and especially for cohesive soils. The cohesive component of the shear force term in KEMv and GKEMv is independent of the normal force and is dependent on the height of the interelement boundary and the value of cohesion. The computed normal force for KEMv is low (in magnitude) and negative at the first interelement boundary. Thus, the computed interelement force is a relatively large (in magnitude) negative number. The primary difference between the GKEMv and KEMv was the location of the first element. It is likely that for this slope geometry and material properties, the selection of the element at the crest results in the development of negative normal interslice forces. The algorithm developed by Gussmann (2017) properly accommodates potential mechanisms wherein tensile forces develop. This likely resulted in the mechanism predicted by the GKEMv in which the first interelement boundary was located 15 m from the beginning of the slope.

7.2 Cohesive Slope

In this section, the interelement forces for the 5 m high cohesive slope from Section 3.4 ($c = 25\ kPa$) are examined. The variations of the interelement and interslice forces along the failure surfaces are shown in Figure 7.2.

Similar trends are observed for the distribution of the interelement forces for the cohesive slope. This time, peak normal forces are nearly identical for all methods. The GKEMv and KEMv peak shear forces are greater than that predicted by SSP. In KEMv and GKEMv, the shear and normal forces are related by the Mohr-Coulomb failure criterion whereas the SSP assumes a half-sine function. The interelement shear forces are higher in KEMv and GKEMv because of the cohesive strength term (ch) where c and h are the cohesion of the soil and height of the interelement boundary, respectively. The normal forces for GKEMv and KEMv increase monotonically to the peak and decrease approximately linearly. The apparent linear decrease in the interelement normal force was likely due to the lack of elements.

The interelement shear and normal forces obtained using GKEMv and KEMv are nearly identical. This was not observed for the case of the homogeneous slope as there is a greater difference in the location of the interelement boundaries and thus the failure surface. High interslice force ratios found in the upper parts of the slope agreed well with the conclusions made by Stolle & Guo (2008). Given that the interelement shear forces are higher in the KEMv and GKEMv for the cohesive slope, interelement force ratios are higher than those of the SSP.

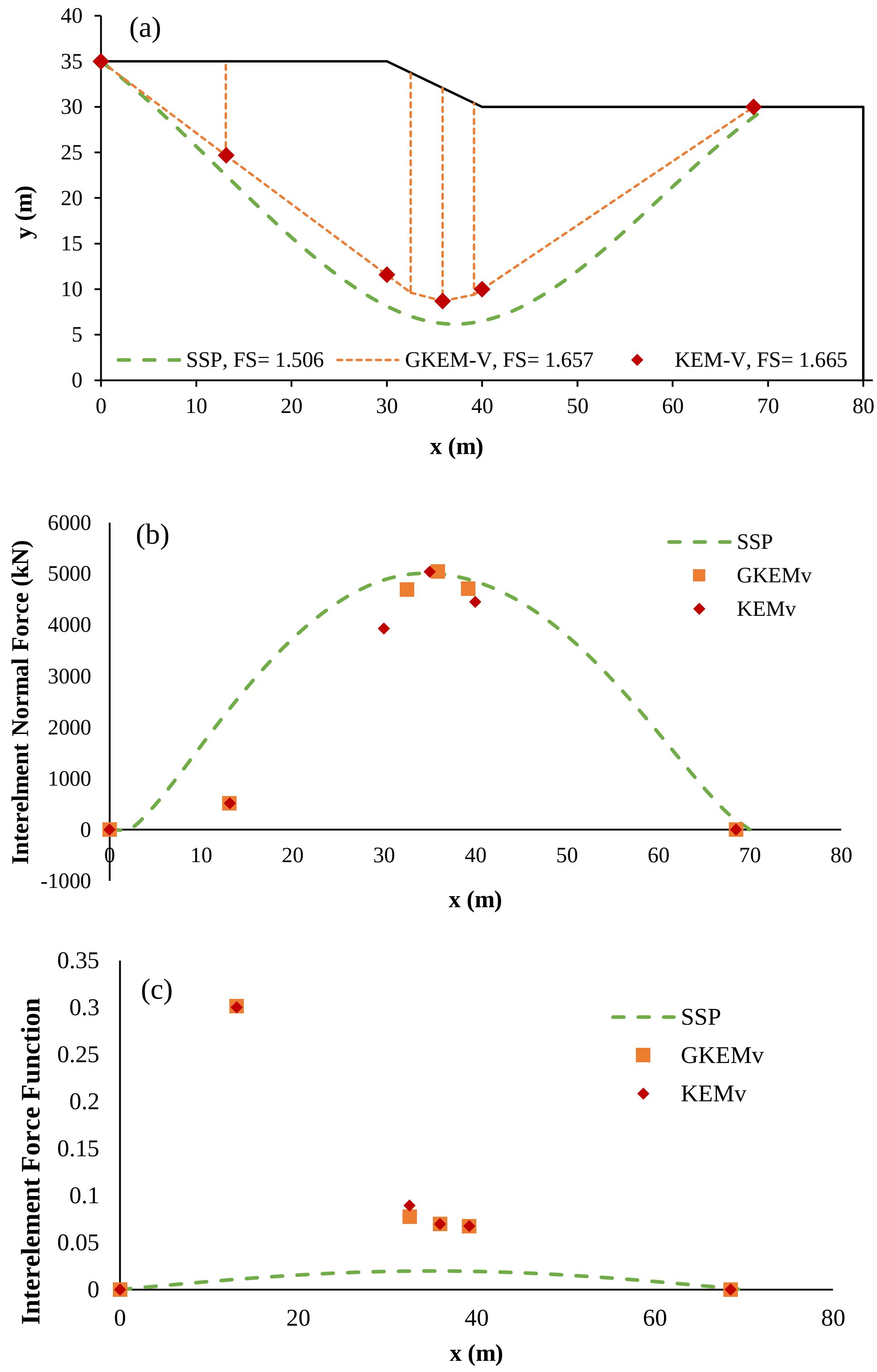

Figure 7.2. (a) Critical slip surfaces, (b) interelement normal forces and (c) interelement force ratios for the cohesive slope

The analysis was carried out with the cohesion of the soil being 15 kPa and 20 kPa. The critical failure surfaces for the different cohesion values are shown in Figure 7.3 and the interelement forces and force ratios are shown in Figure 7.4.

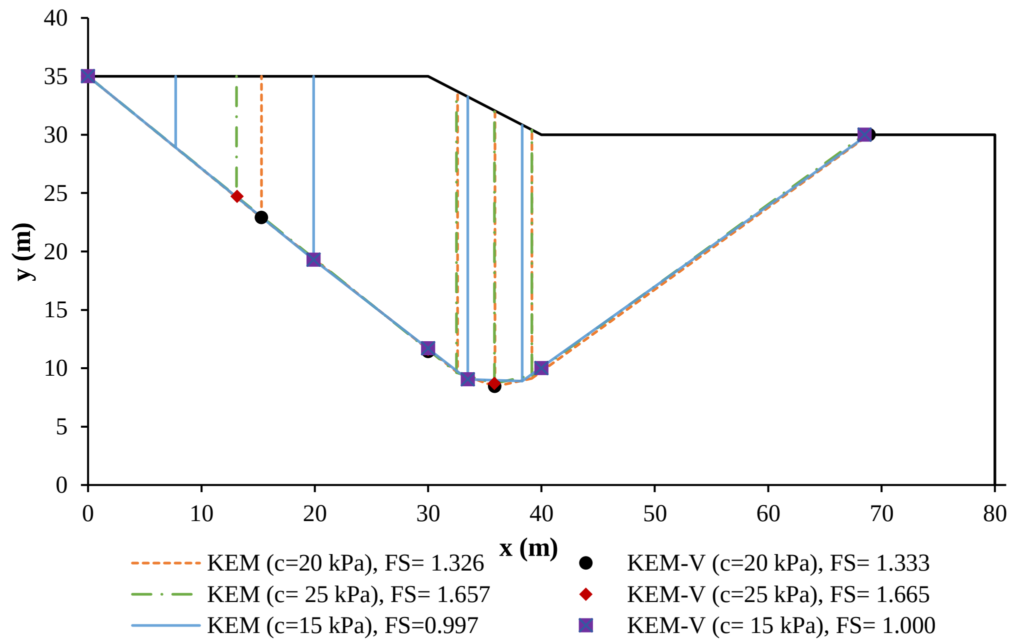

Figure 7.3. Critical slip surfaces for the cohesive slope with vertical boundaries and varying cohesion

The interelement forces have nearly identical distributions. The soil is cohesive ($\phi = 0$) so the shear resistance along the interelement boundaries is due to the mobilized cohesion ($C_m^h = c_m * h$). The mobilized cohesion ($c_m = \frac{c}{FS}$) values for the cases when cohesion is 15 kPa, 20 kPa and 25 kPa is approximately 15 kPa. As the critical slip surfaces and the mobilized cohesion are identical, the interelement shear forces are similar.

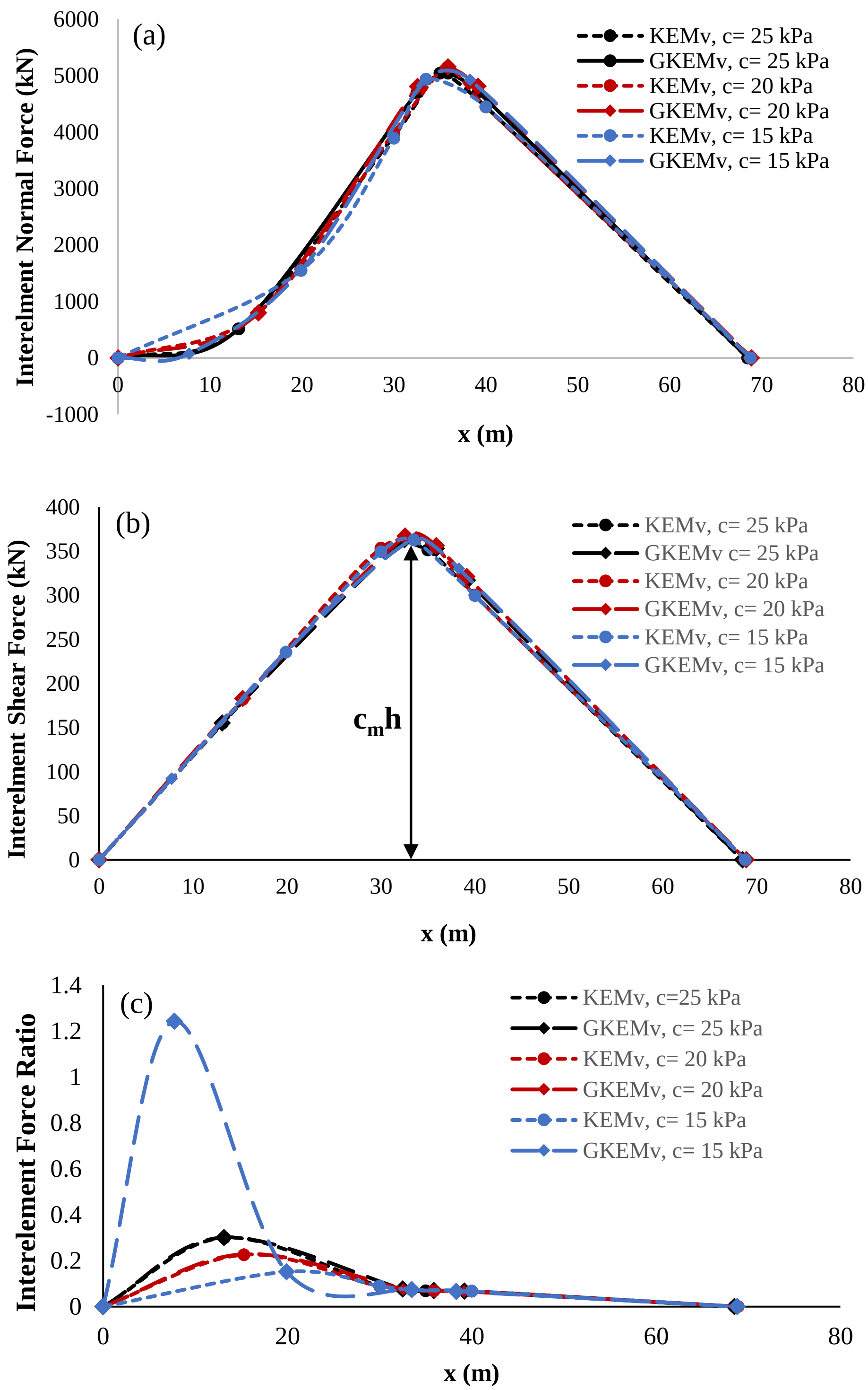

Figure 7.4. (a) Interelement normal forces, (b) interelement shear forces and (c) interelement force ratios for varying values of cohesion

The interelement force ratios in Figure 7.4(c) vary for the different values of cohesion, indicating that the greatest difference lies in the computed normal forces. The force ratios for all values of cohesion display a maximum at the first element followed by a decrease to a stable value. Generally, GKEMv and KEMv give similar values for interelement forces and force ratios, except for the case where $c = 15\ kPa$ as there is a significant difference in the element locations between GKEMv and KEMv. Based on the similarities in the computed interelement forces and factors of safety, we can conclude that the KEMv formulation derived in Chapter 5 provides solutions as accurate as Gussmann's KEM with vertical boundaries.

7.3 Cohesionless Slope

In this section, the interelement and interslice shear forces for the 5 m high cohesionless slope from Section 3.5 ($\phi = 30°$) is examined. The variations of the interelement and interslice forces along the failure surface are presented in Figure 7.5.

Unlike the cases of the mixed and cohesive slopes, the interelement forces from the SSP are greater than those of GKEMv and KEMv (by 6 orders of magnitude). While the absolute values of the interelement forces from the KEMv and GKEMV are lower, the force ratios are similar to that of the SSP. The force ratios for KEMv and GKEMv are identical and have a similar peak value as the SSP. The KEMv and GKEMv force ratios are somewhat parabolic whereas the SSP force function is a half-sine.

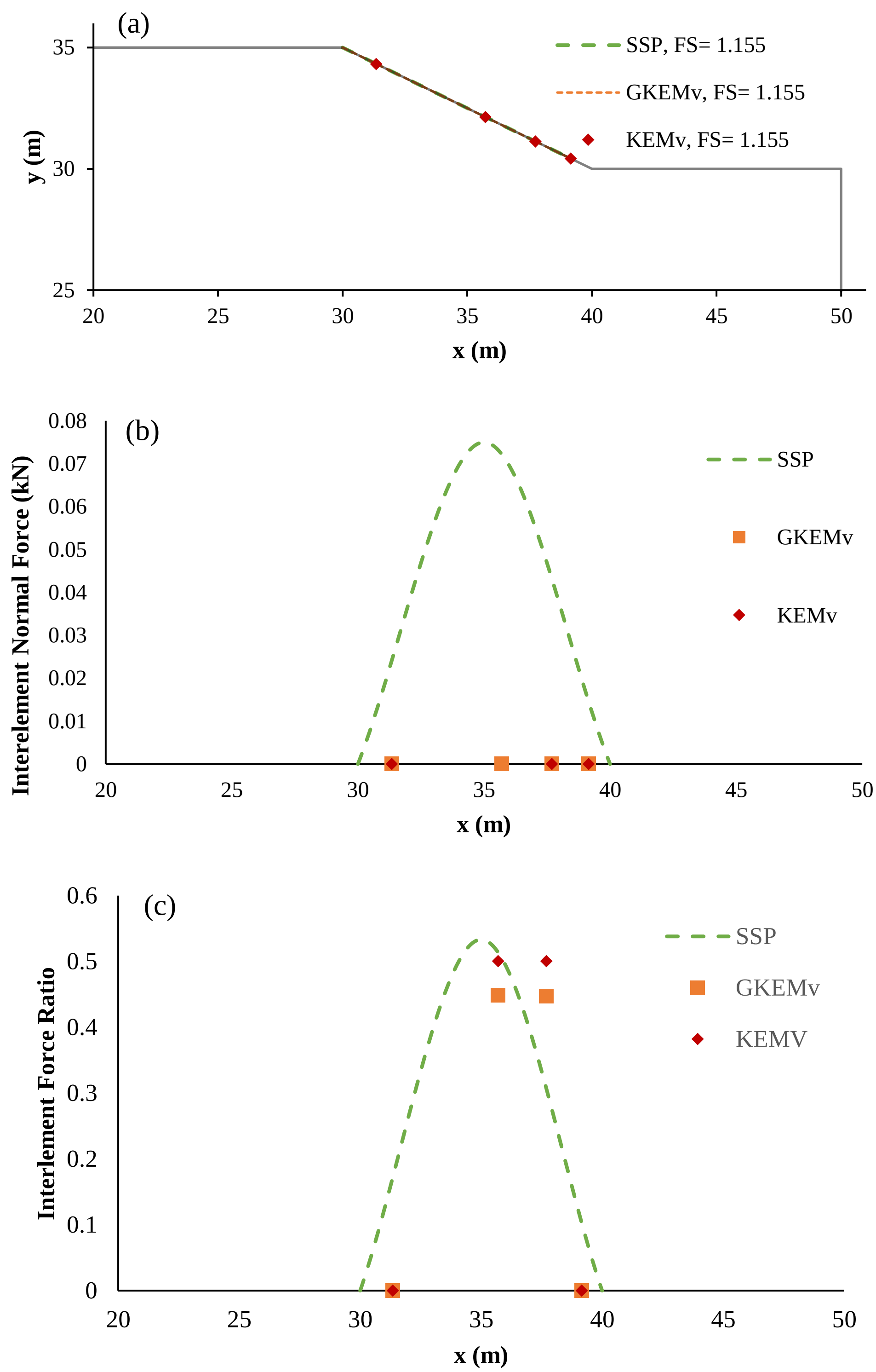

Figure 7.5. (a) Critical slip surfaces, (b) interelement normal forces and (c) interelement force ratios for the cohesionless slope

As discussed previously in Section 6.3, translational failure in cohesionless slopes is independent of the height of the failure. The average interslice height from the SSP program was $1x10^{-2}$ m while those of the KEMv and GKEMv were $4x10^{-8}$ m. Thus, the difference in the interelement forces between the methods was due to the discrepancy in heights.

Summary

- GKEMv and KEMv provide nearly identical values for interelement forces when slip surfaces are identical and the interelement boundary locations are similar.
- For the case when the interelement boundaries are different, GKEMv and KEMv generally give similar distributions for the interelement normal and shear forces, including the peak values. However, they may differ in the location and magnitude of the maximum of the interelement force ratio.
- In the case of the slope with the mixed soil, the peak values for KEMv and GKEMv were similar to that of SSP. However, that was not the case for the cohesive and cohesionless soil. Because shear resistance in interelement boundaries for KEMv and GKEMv is a function of cohesion, the computed interelement shear forces and thus, force ratio, were higher. All methods provided similar distributions and peak values for the interelement force ratio.
- The distribution of forces and force ratios in KEMv and GKEMv was shown to be sensitive to the location of the interelement boundaries. For mixed and especially cohesive soils, the interelement force ratio encounters a maximum in the upper part

of the slope (at the first interelement boundary) caused by low, possibly negative values for the normal force. Following the maximum, the force ratio decreases to a constant value. These observations were also made by Stolle & Guo (2008) for the RFEM.

Chapter 8 Sensitivity Analysis

Limited information is available in the English-speaking literature regarding the sensitivity of the kinematic element method to the selection of the number of elements required for the solution and changes in material properties. In this section, the solutions provided for the various slope problems utilizing different numbers of elements are compared. A simple parametric study was carried out to determine the change in the factor of safety and location of the critical failure surface with changes in material properties and slope orientations. The results of the parametric study will be compared to the predictions by the Morgenstern-Price method obtained using the Slope Stability Program developed by Karchewski (2012).

8.1 Number of Elements

The variation in the solution from the KEM due to the refinement of the mesh is explored in this section for 3 different problems: a simple homogeneous slope, a slope with a weak layer, and a retaining wall. The analyses were carried out using 3, 5 and 10 elements where the mesh was refined with more elements. Horizontal mesh refinement was carried out for all problems with the division of the 5-element solution into two rows of elements (i.e. 10 elements in total). Horizontal mesh refinement was found to have a marginal effect on the factors of safety with on average a 0.1% change, so it is not discussed in this section.

8.1.1 Homogeneous Slope

For the case of a simple homogeneous slope, the example presented in Section 3.1 is examined. The soil has cohesion $c = 41.65\ kPa$, friction angle $\phi = 15°$ and unit weight $\gamma = 18.82\ kN/m^3$. As observed in Figure 8.1, increasing the number of elements has a small effect on the critical slip surface. For the case of the 5-element and 10-element solutions, the critical slip surfaces are nearly identical.

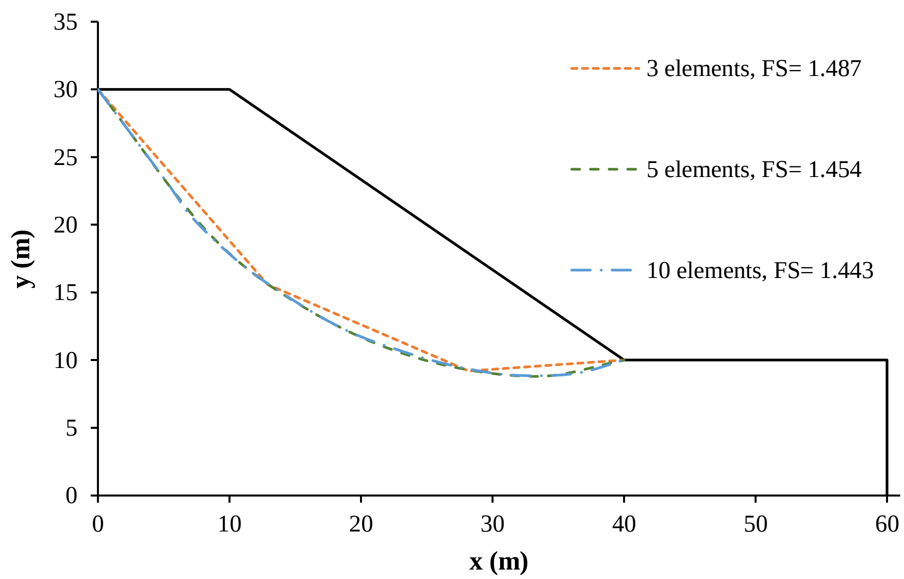

Figure 8.1. Variation of factor of safety and critical failure surface with increasing number of elements for the homogeneous slope

An increase in the number of elements corresponded to improved accuracy in the factor of safety. The factor of safety obtained using 3 elements had a 4% difference relative to the reference value (1.429) presented in Table 3-1 while less than 1% difference was found using 10 elements.

8.1.2 Slope with a Weak Layer

The effect of increasing the number of elements for a block sliding failure mechanism is discussed in this section using the example from Section 3.3.2 with the critical slip surfaces shown in Figure 8.2. The silt (Soil 1) has a cohesion $c = 28.7\ kPa$, friction angle $\phi = 20°$ and unit weight $\gamma = 18.85\ kN/m^3$. The weak layer (Soil 2) has a friction angle $\phi = 10°$ and the same unit weight as Soil 1.

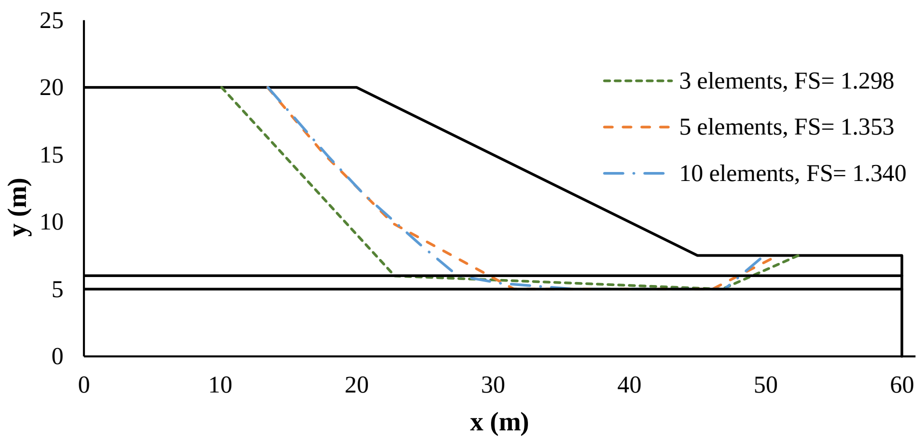

Figure 8.2. Variation of factor of safety and critical failure surface with increasing number of elements for the slope with a weak layer

Both the 5-element and 10-element solutions display the block sliding mechanism and have nearly identical failure surfaces while the 3-element solution provides a pseudo-circular failure as if the weak layer did not exist. Refining the mesh from 3 to 5 elements increases the factor of safety. However, further refinement of the mesh from 5 elements to 10 elements reduces the factor of safety. Unlike the previous problem, the solution does not converge with increasing number of elements. The problem was also solved with 10, 12 and 15 elements to determine if the solution converged with a higher number of elements, see Figure 8.3.

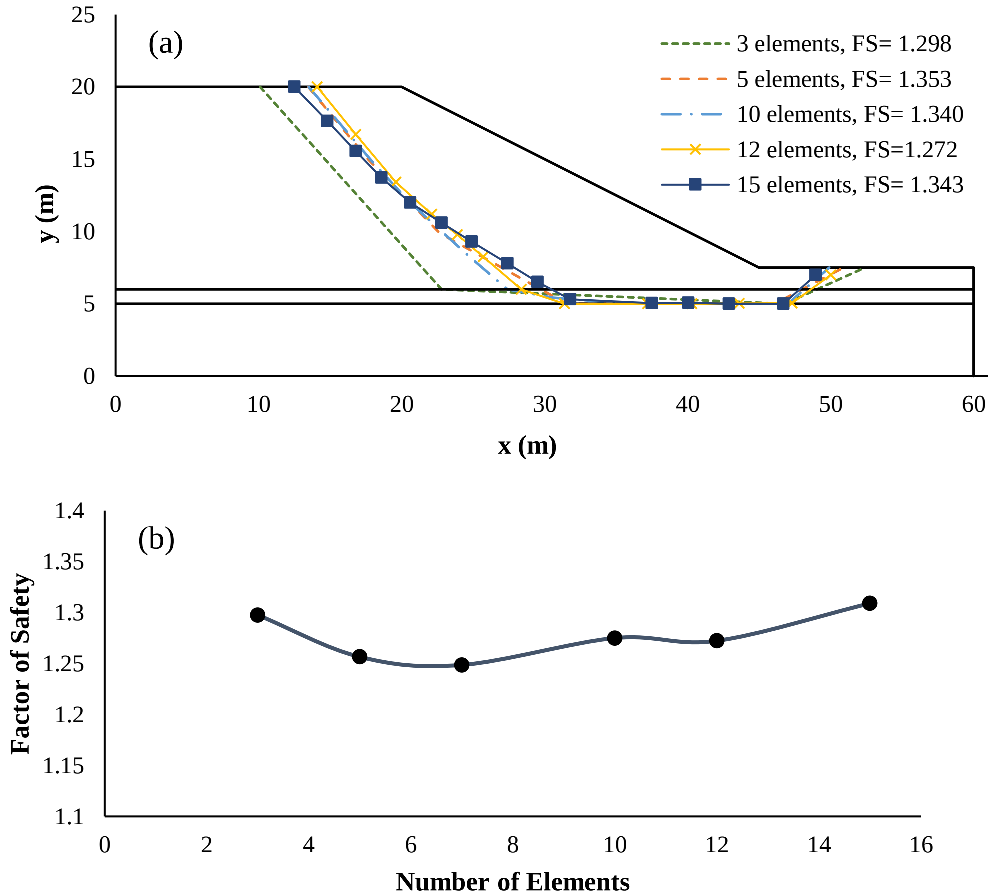

Figure 8.3. Variation of (a) critical failure surface and (b) factor of safety with further mesh refinement for the slope with a weak layer

There appears to be very little difference in the critical failure surface with the refinement of the mesh from 5 elements to 15 elements. Solutions with more than 15 elements were attempted but were not obtained. The addition of the weak layer to the slope increased the complexity of the problem and the maximum number of elements where the iterative scheme converged was 15. Furthermore, the factor of safety does not converge monotonically, which leads to the conclusion that KEM does not provide a bounding solution. It is possible that the factor of safety oscillates, in which case a reasonable estimate is approximately 1.3. The 5-element solution estimates a reasonably accurate factor of safety and an appropriate failure mechanism and surface. Fredlund & Krahn (1977) obtained a factor of safety of 1.378 for this problem using the Morgenstern-Price method, see Table 3-5. As stated previously in Section 3.3.2, the SSP provides a much lower factor of safety (1.207) for this problem even though it employs the Morgenstern-Price method with the discrepancy caused by differences in the optimization algorithm and assumptions regarding the interslice forces. The 5-element solution and estimate of 1.3 deviate from the reference value by approximately 2% and 5.6%, respectively. This margin of error is within the accepted range of the assumed rigorous limit equilibrium methods.

8.1.3 Retaining Wall

Next, we look at the influence of mesh refinement on the solution of the retaining wall problem from Section 3.7. The failure surfaces are shown below in Figure 8.4.

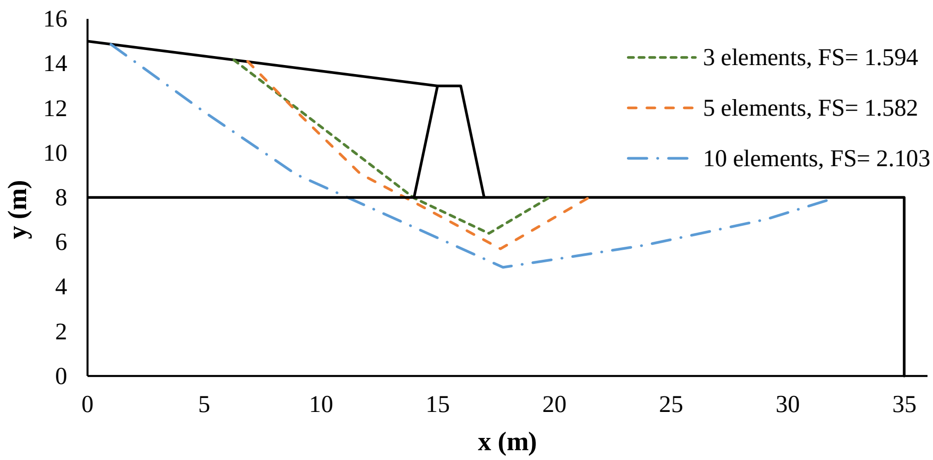

Figure 8.4. Variation of factor of safety and critical failure surface with mesh refinement for the retaining wall problem

The 3 and 5-element solutions located similar mechanisms that includes a wedge behind the retaining wall and another below it. Both provided nearly identical factors of safety. Meanwhile, the 10-element solution was unable to locate the correct critical slip surface. Instead, it predicts a significantly larger global failure of the slope. Multiple attempts were required to find a feasible solution for the 10-element mesh as other solutions displayed tensile forces. The side of the retaining wall is essentially the surface of the slope, which has an inclination of 79º (i.e. sub-vertical). The KEM algorithm appears to experience difficulties when encountering tensile forces. This behavior was observed for the case of the homogeneous slope in Section 7.1 as well. The refinement of the mesh from 5 to 10 elements likely made the analysis more sensitive to the presence of tension. There may not have been a configuration of the elements within the critical slip surface defined by the 3 and 5-element solutions for which tensile forces did not appear. An attempt was made to subdivide the 5-element solution vertically and horizontally to produce 10-element solutions in a roundabout manner. However, the solutions were found to be inadmissible due to tensile forces.

The problem was also solved with 7 and 12 elements to determine if the solution converged with a higher number of elements, see Figure 8.5. Owing to the complexity of the problem (multiple materials, inclined crest), the maximum number of elements in a solution where the iterative scheme converged was 12.

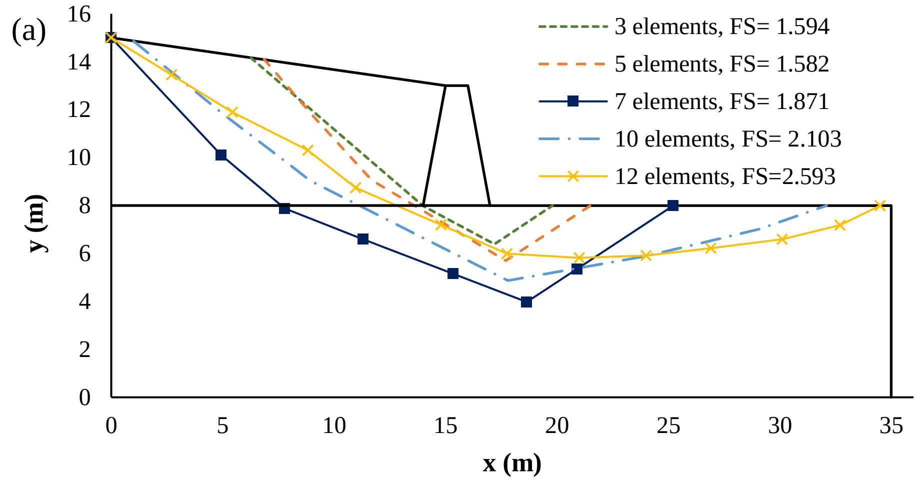

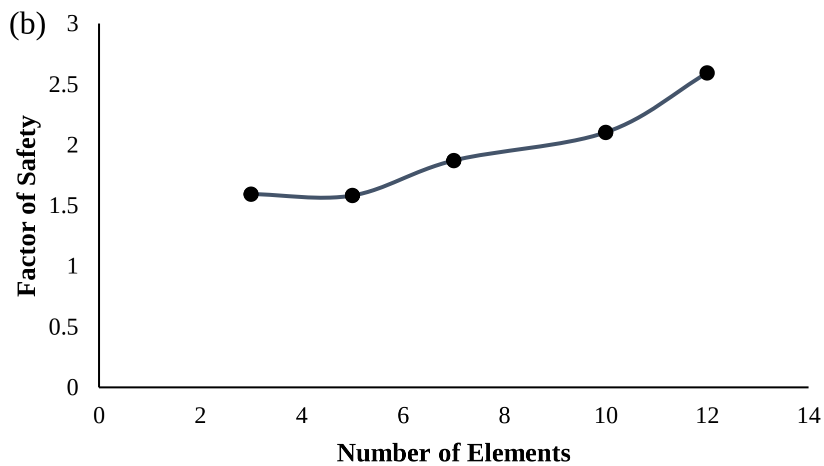

Figure 8.5. Variation of (a) critical failure surface and (b) factor of safety with further mesh refinement for the retaining wall problem

As observed in Figure 8.5, when the number of elements is greater than 7, the size of the critical failure surface and corresponding minimum factor of safety increases as the number of elements increases. As the number of elements increases, the interelement boundaries cannot be oriented in a manner such that tensile forces are not produced as part of the solution. As such, the algorithm assumes a larger critical failure surface such that tensile forces do not appear along the boundaries. The maximum extent of the problem in the KEM was 40 m and the exit point of the 12 element solution is at approximately 34.5 m, so the problem boundary likely has little influence on the solution. The solution clearly does not converge with further mesh refinement. However, it must be noted that increasing the number of elements from 3 to 5 decreased the factor of safety from 1.594 to 1.582 and had a marginal effect on the critical failure surface. The 5-element solution also compares well with the SSP (see Section 3.7), predicting a similar critical surface and a factor of safety within 2%. when refining the mesh from 3 elements to 5 elements. A 5-element solution for this retaining wall problem in terms of predicting an appropriate failure surface and factor of safety appears to be appropriate.

8.2 Parametric Study

As part of the sensitivity analysis, a parametric study was carried out to determine the change in the factor of safety and critical slip surface caused by varying soil properties (friction angle, cohesion, unit weight), as well as the slope geometry (slope height and angle). In this section, KEM solutions using 5 elements is presented. The slip surfaces in the SSP are automatically generated with the number of slices varying from 30 to 40. The base case for the study is a homogeneous slope with a height of 10 m and angle of 45º. The soil for the base case has a friction angle $\phi = 20°$, cohesion $c = 20\ kPa$ and unit weight $\gamma = 19\ kN/m^3$. In the parametric study, the results obtained using the KEM are compared to that obtained by the SSP.

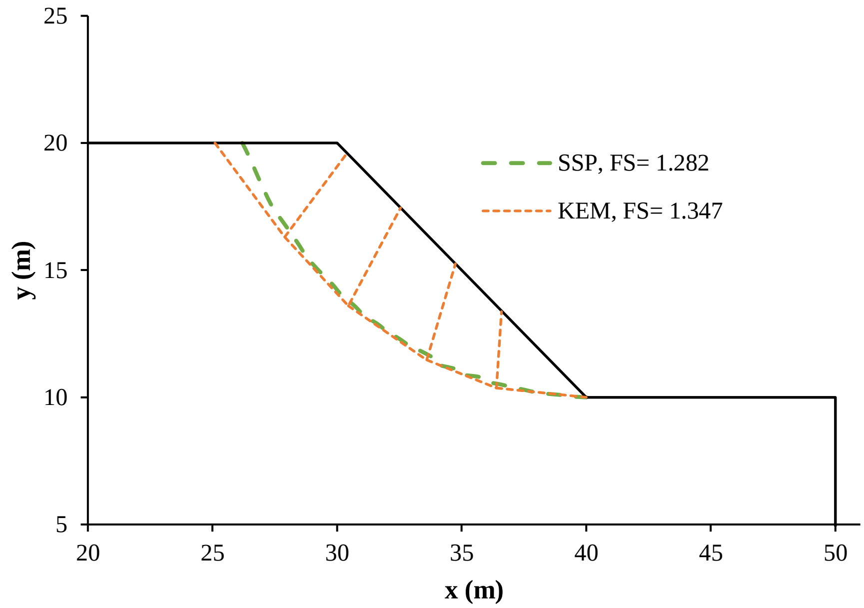

Figure 8.6. Critical slip surfaces for the base case of the parametric study

There is a slight difference (5%) in the FS between the two solutions. The factor of safety of the slope was also obtained using Janbu's slope stability charts. A factor of safety of 1.3 was obtained, indicating only a 3.6% difference compared to the KEM solution. As observed in Figure 8.6, the KEM and SSP provide similar critical slip surfaces. The critical failure surfaces and corresponding minimum factors of safety presented for KEM are for 5-element solutions as indicated previously. Table 8-1 summarizes the variation of the parameters.

Table 8-1. Summary of parametric study variables

Parameter	Variance	Increment
Cohesion, c (kPa)	±10	5
Friction Angle, φ (°)	±10	5
Unit Weight, γ (kN/m^3)	±2	1
Slope Height, H (m)	±5	5
Slope Angle, β (°)	±15	15

Janbu's dimensionless parameter ($\lambda_{\phi c} = \gamma H \tan\phi\, / c$) for this slope is 3.46, which indicates that a toe failure should develop as observed in Figure 8.6. As mentioned previously in Section 3.1, the value of $\lambda_{\phi c}$ can be used to predict the failure mechanism of the slope. It can also be used qualitatively to describe the change in the failure surface with soil properties. An increase in $\lambda_{\phi c}$ corresponds to the critical slip surface becoming shallower while a decrease corresponds to a deeper surface (Duncan & Wright, 1980).

8.2.1 Cohesion

The cohesion of the soil was varied from 10 kPa to 30 kPa while the unit weight, friction angle and geometry of the slope were held constant. The variation of the factor of safety and failure surface for some values is presented in Figure 8.7(a).

As the cohesion of the soil increases the failure surface of the soil becomes larger. Janbu's dimensionless parameter ($\lambda_{\phi c}$) is inversely related to cohesion and as it increases, the failure surface becomes shallower. This trend is observed in Figure 8.7(a), where the failure surface becomes deeper with a rise in cohesion and factor of safety.

The factor of safety obtained using both the KEM and SSP was found to increase linearly with cohesion as observed in Figure 8.7(b). Naderi (2013) carried out sensitivity analysis of the factor of safety for a general limit equilibrium formulation with a half-sine interslice force function using Geo-Slope's SLOPE/W software. In the sensitivity analysis, the soil properties and slope geometry are varied. He observed a similar trend for the factor of safety where it increased linearly with cohesion. In the equation for shear failure, eq. (2.25), the cohesive component varies linearly with cohesion. Given that the shear force varies linearly with cohesion, a linear variation in factor of safety with cohesion is not surprising.

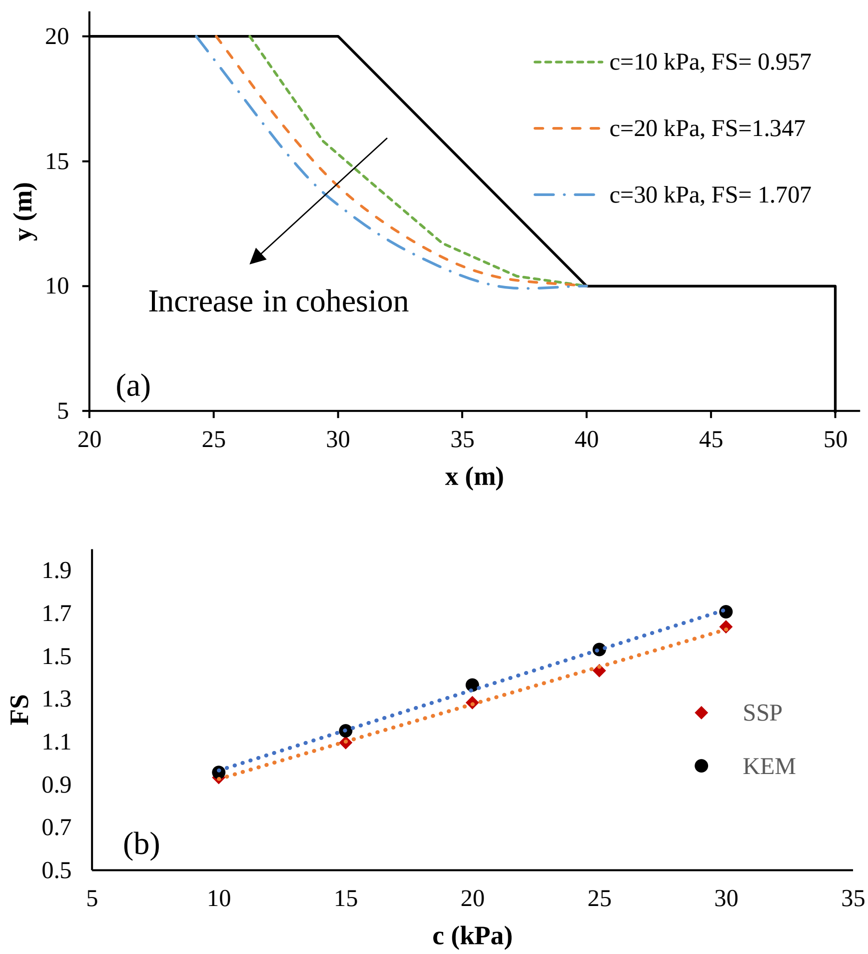

Figure 8.7. (a) Critical failure surfaces and (b) Factors of safety with variation in cohesion

8.2.2 Friction Angle

The friction angle of the soil was varied from 10° to 30 ° while the unit weight, cohesion and geometry of the slope were held constant. Figure 8.8 shows the failure surfaces corresponding to the selected values. The friction angle of the soil is positively correlated to $\lambda_{\phi c}$. Thus, an increase in ϕ should result in a shallower failure surface. This behavior is confirmed by examining Figure 8.8 with the failure surface becoming shallower as ϕ increases.

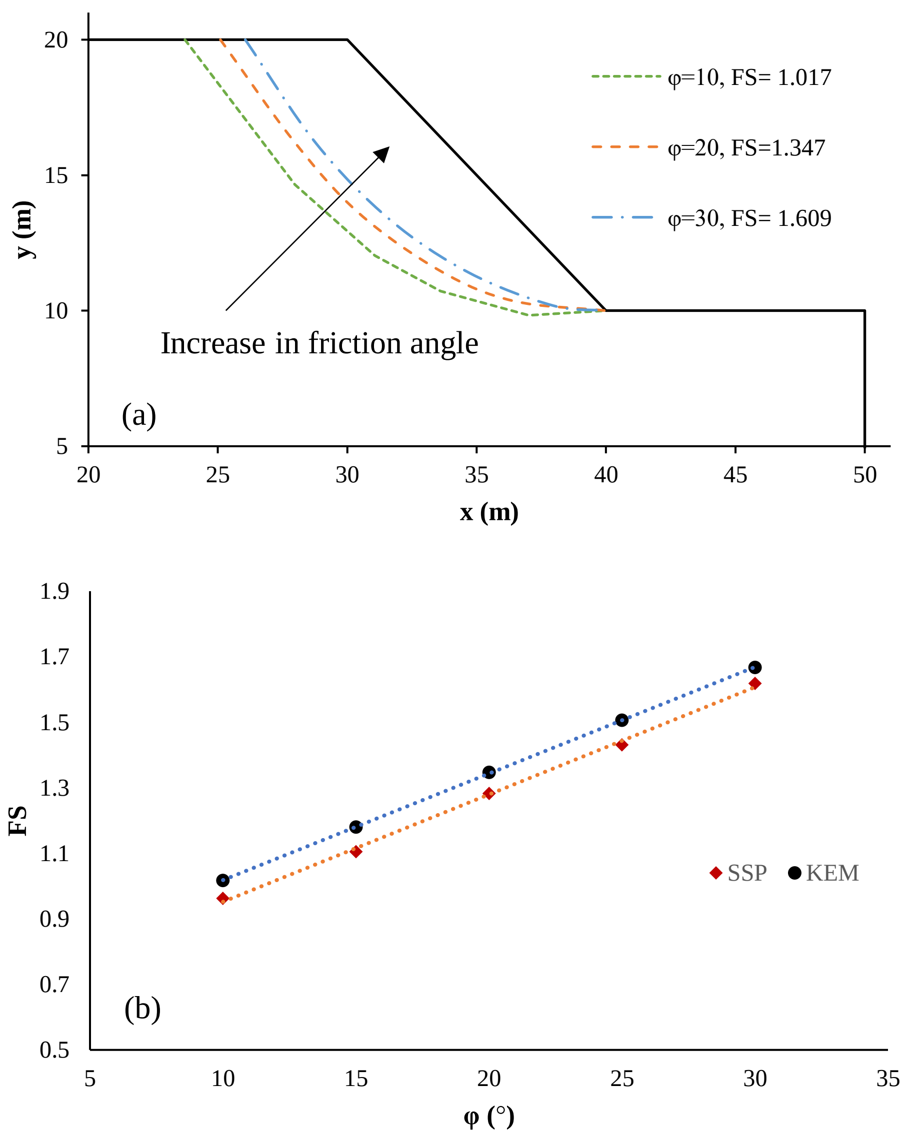

Figure 8.8. (a) Critical failure surfaces and (b) Factors of safety with variation in friction angle

Similar to the results for a variation in cohesion, the factor of safety increases linearly with friction angle as observed in Figure 8.8(b). Increasing the friction angle improves the shear resistance along the slip surface, thus causing an increase in the factor of safety. Naderi (2013) made similar observations regarding the variation in FS with friction angle. This was unexpected as the frictional component for shear failure in eq. (2.25) is given by $N \tan \phi$ which is a non-linear expression. To investigate this issue, the variation of $\tan \phi$ with ϕ was plotted in Figure 8.9.

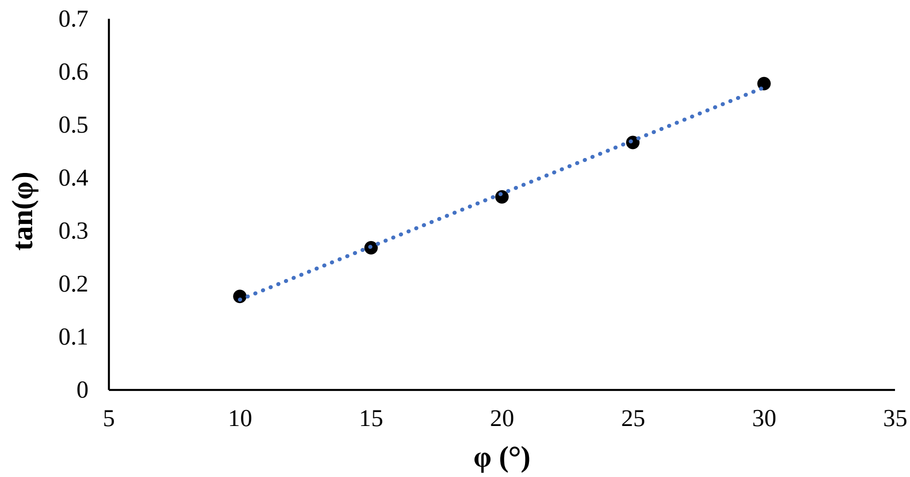

Figure 8.9. Variation of $\tan \phi$ with ϕ over the parametric study range

Figure 8.9 shows that while the tangent function is non-linear, it appears to be linear over the range of the study. Given this information, it is not unexpected that the factor of safety varies linearly with friction angle.

8.2.3 Unit Weight

In this section, the influence of unit weight on the factor of safety of the soil is addressed. The unit weight of the soil was varied from 17 to 21 kN/m^3 while the cohesion, friction angle and geometry of the slope were held constant. Given that the unit weight of a soil varies far less than the friction angle or cohesion, the range of values tested was smaller.

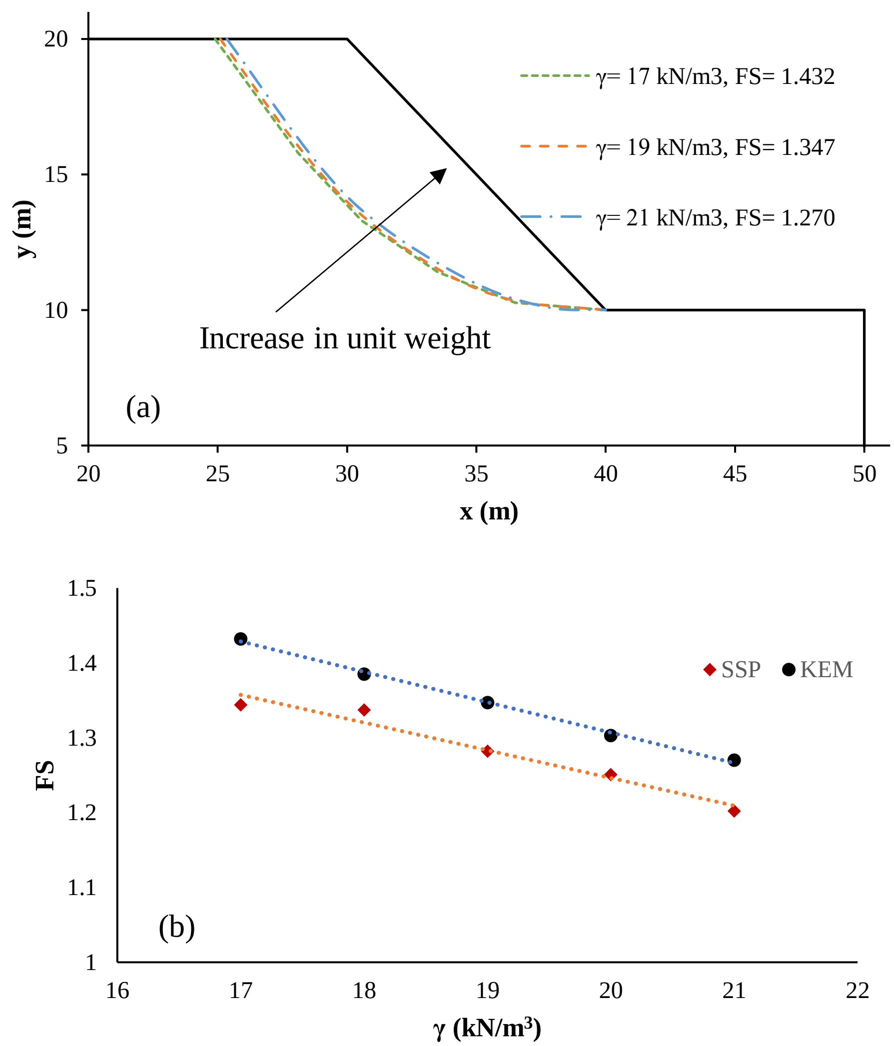

Figure 8.10. a) Critical failure surfaces and b) Factors of Safety with variation in unit weight

An increase in the unit weight of the soil causes the critical slip surface to become shallower as shown in Figure 8.10(a) although the change appears to be small. Similar to the friction angle, unit weight of the soil is positively correlated to $\lambda_{\phi c}$. Thus, an increase in γ results in a shallower failure surface, confirming the observations made previously.

Figure 8.10(b) shows that the factor of safety of the slope varies linearly with the unit weight of the soil with the two quantities being negatively correlated. Since the weight of the soil is the driving force, a reduction in the unit weight of the failed mass increases the factor of safety, assuming the shear resistance is held constant. The results presented by Naderi (2013) corroborate those of this study.

8.2.4 Slope Height

This section examines the variation of the factor of safety with slope height. The height of the slope was varied from 5 m to 15 m while the slope angle and material properties were held constant. The critical failure surfaces for the different cases are provided in Figure 8.11.

The KEM and SSP provide nearly identical critical slip surfaces and factors of safety for both slopes. With an increase in the slope height, the factor of safety decreases non-linearly as shown in Figure 8.12.

Both methods give nearly the identical values for the factor of safety. As the slope height rises, the effect of the increased volume of the failed mass has a greater effect on the stability of the slope than the larger failure surface and shear resistance. As the growth in the driving force is greater than the resisting force, the factor of safety decreases. Also, this is not unexpected given that the shear stress in the soil increases as the steepness of the slope increases.

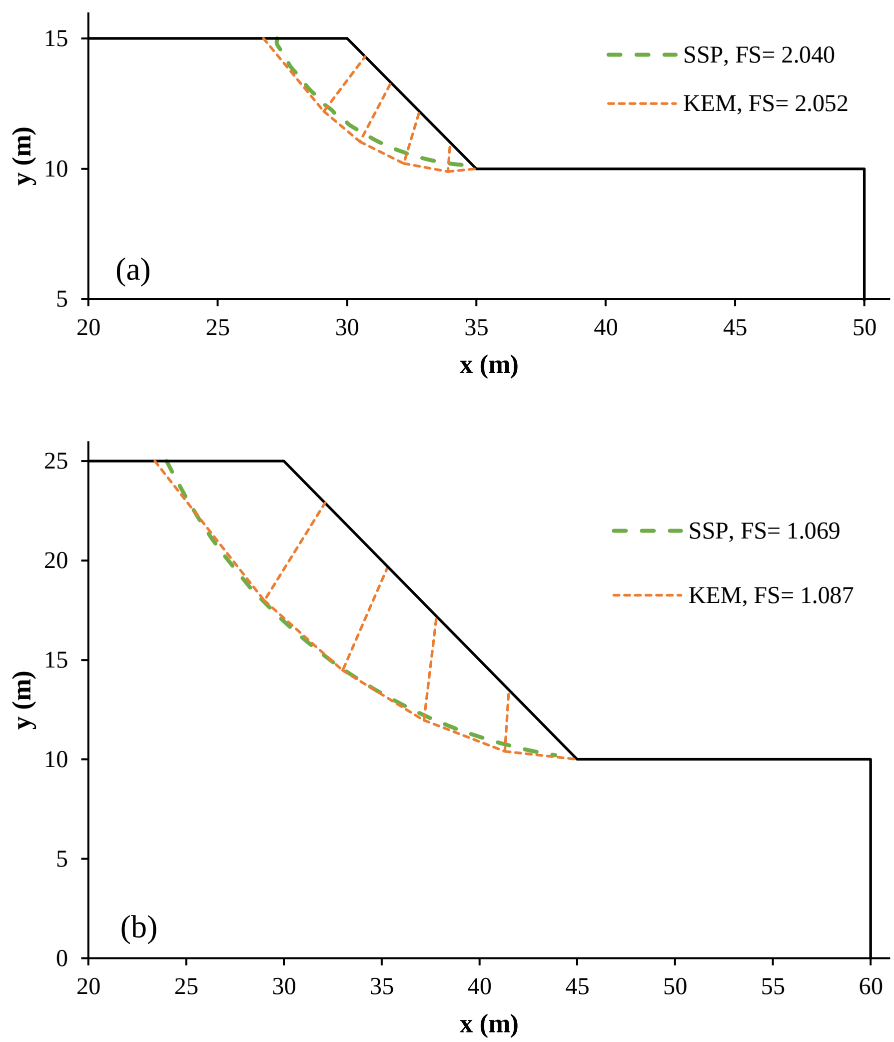

Figure 8.11. Critical slip surfaces with different slope heights: (a) H= 5 m, (b) H= 10 m

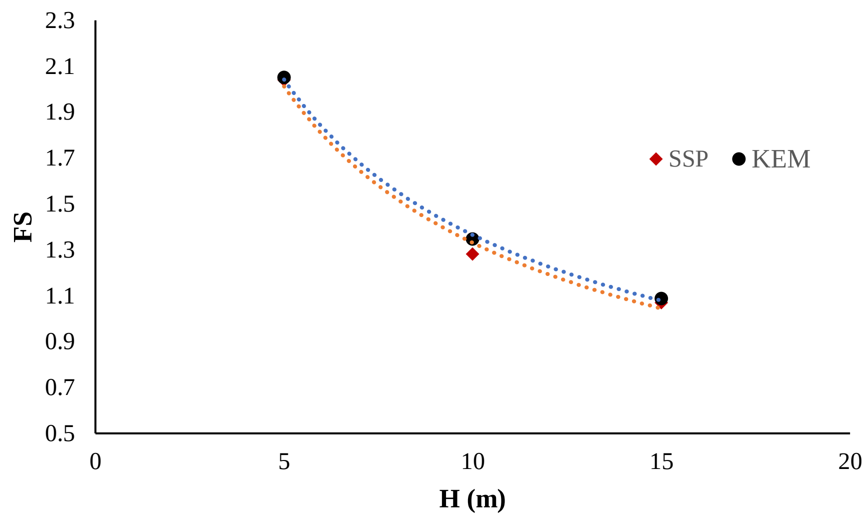

Figure 8.12. Variation of factor of safety with slope height

8.2.5 Slope Angle

To study the effect of slope angle on the factor of safety, it was varied from 30º to 60º while the slope height and material properties were held constant. The critical failure surfaces for the slope angles of 30º and 60º are shown in Figure 8.13.

The critical failure surfaces and factors of safety obtained using KEM and SSP are similar. With an increase in the slope angle, the factor of safety obtained using both methods decreases, as one might expect. The variation is approximately linear as shown in Figure 8.14.

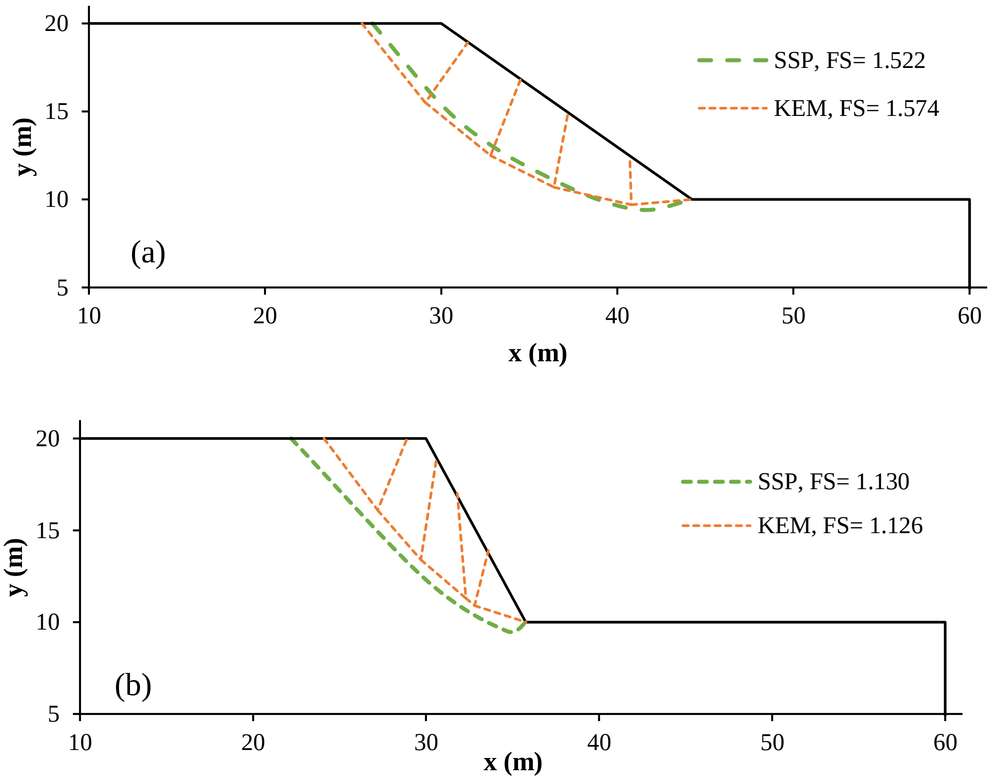

Figure 8.13. Critical failure surfaces with different slope angles: (a) β= 30º, (b) β= 60º

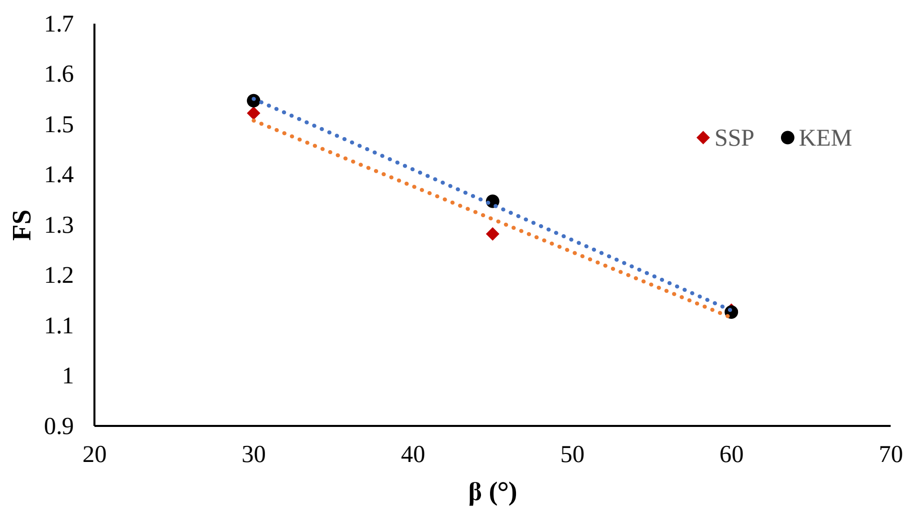

Figure 8.14. Variation of factor of safety with slope angle

If we consider one of the factor of safety equations for Spencer's method, eq. (2.18), we observe that the denominator consists of a $\sin\alpha$ term (component of the weight of the soil driving failure) while the numerator consists of a $\cos\alpha$ term (component of the weight of the soil resisting failure). As the slope angle (β) increases, there is a corresponding rise in the base slice angle (α) as well. As α increases, the $\cos\alpha$ term (the resisting force) decreases while the $\sin\alpha$ term (driving force) increases. Thus, an increase in slope angle corresponds to a decrease in the factor of safety.

8.3 Compilation of Slope Stability Analysis Results

It was of interest to know how the KEM compares to the Morgenstern-Price method for various conditions. Thus, the factors of safety from the example problems in Chapter 3 and the parametric study in Section 8.2 were plotted in Figure 8.15.

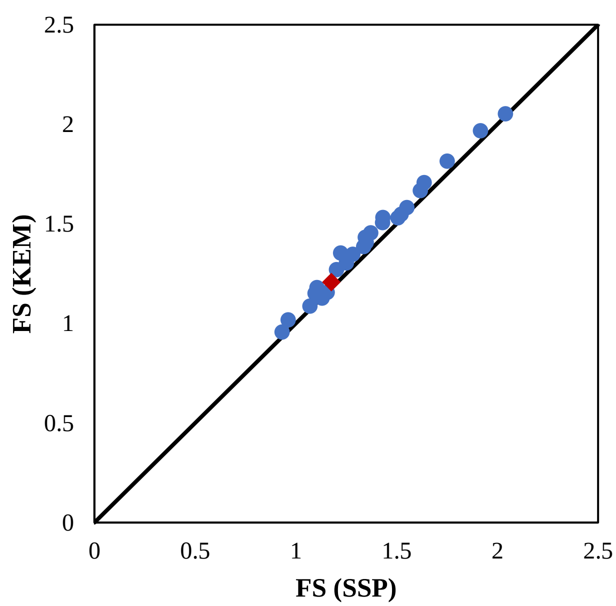

Figure 8.15. Compilation of factors of safety from analyses

The factors of safety in the blue dots correspond to the 5-element KEM solution. The red diamond corresponds to the 10-element solution (5-element solution with a horizontal subdivision) for the foundation problem in Section 3.6. Generally, the KEM predicts higher values for factor of safety than SSP. The average differences in the computed factors of safety is approximately 4%. As mentioned previously, the SSP provides lower values for the factor of safety compared to other limit equilibrium formulations, including other Morgenstern-Price method solutions. This difference is caused by the application of non-circular critical slip surfaces along with different optimization algorithms. In some examples, such as the slope with a weak layer in Section 3.3.2, the KEM predicted a lower value for the factor of safety than the reference Morgenstern-Price solution. Thus, we can conclude that the KEM generally provides solutions as accurate as rigorous limit equilibrium formulations.

Summary

- For homogeneous slopes, a 3-element solution is sufficient to delineate the critical failure surface and obtain a reasonably accurate factor of safety.
- Convergence issues were observed for more complex problems, such as the retaining wall. It is possible for the KEM algorithm to overestimate the factor of safety and critical failure surface for more complex problems when tensile forces appear in the solution. For more complex failures, the use of 5 elements is recommended to locate a reasonable failure mechanism and a reasonably accurate factor of safety.

- The kinematic element method provided results similar to those of the Morgenstern-Price method. The KEM displayed the expected trends in the variation of factor of safety with the parameters, such as linear relation between FS and cohesion, unit weight and friction angle. The change in failure surface with material properties displayed by KEM agrees with the empirical relations suggested by Janbu (1954).
- These observations along with the results of Chapter 3, indicate that the KEM is a useful and accurate tool in slope stability analysis. The KEM seems to provide the same critical failure surface as the Morgenstern-Price method with the only difference being the use of vertical interslice boundaries. When used simply to locate the critical failure surface and corresponding minimum factor of safety, the kinematic element method is on par with the limit equilibrium method.

Chapter 9 Case Study: Embankment Failure Mitigation

Thompson & Emery (1977) presented a case study of a bridge embankment where cracks were observed along with movement at the toe of the slope. The cracks and movement in the embankment were observed once its height was 9.8 m. This was a significant issue as the original planned height of the embankment was 14.3 m. The embankment was located in an area consisting of layers of lake clays overlain by glacial till with bedrock consisting of Queenston shale. The fill material was obtained from another construction site and consisted of a mixture of silt, clay, sand, silty sand, and clayey silt. In the original design of the embankment, slope stability analysis had been carried out, in which the critical failure surface was expected to be circular. The inclination of the slope was designed such that the factor of safety during construction (i.e. short-term stability) was 1.8. Based on the initial stability analysis, the slope should not have shown signs of potential failure. A site investigation was carried out and a weak layer, likely inadvertently created during construction, was located below the fill. Finite element analyses were subsequently performed, which predicted that high shear stresses should develop in the weak layer below the fill, indicating that the slope could potentially fail along the weak layer. Various mitigation measures were considered, and the final decision was to construct a berm consisting of the same material as the fill with a width of 12.2 m and height of 5.5 m. The material properties of the embankment layers are summarized in Table 9-1.

Table 9-1. Embankment material properties (Thompson & Emery, 1977)

Material	s_u (kPa)	γ (kN/m^3)
Fill	143.7	21.36
Weak Layer	38.32	21.36
Clayey Silt (very stiff)	143.7	19.95
Clayey Silt (firm)	35.95	20.42
Silt Till	431.1	21.84

The cross-section of the embankment at its final height along with the berm is shown in Figure 9.1.

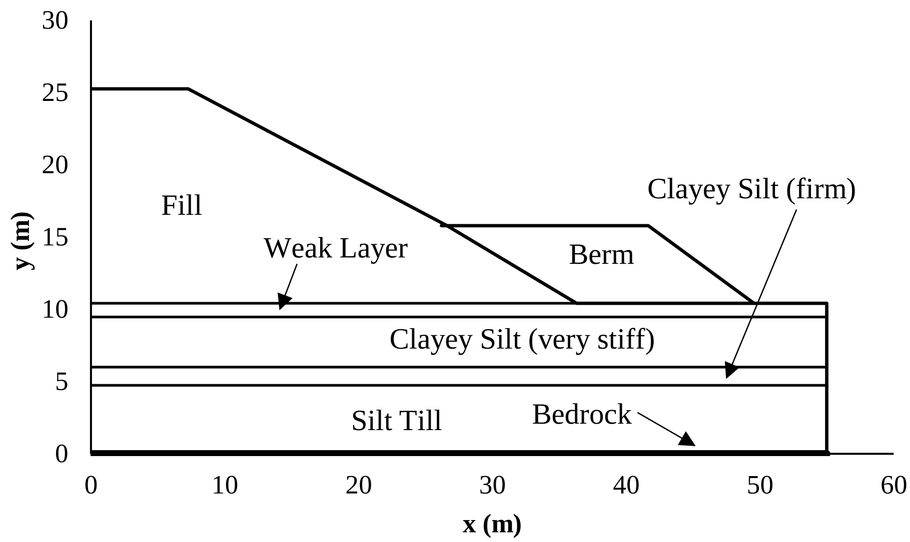

Figure 9.1. Cross-section of the bridge embankment; adapted from Thompson & Emery (1977)

The critical failure surfaces obtained using the SSP and the KEM are presented in Figure 9.2. The critical failure surface provided by the KEM shows a block sliding mechanism along the weak layer below the fill.

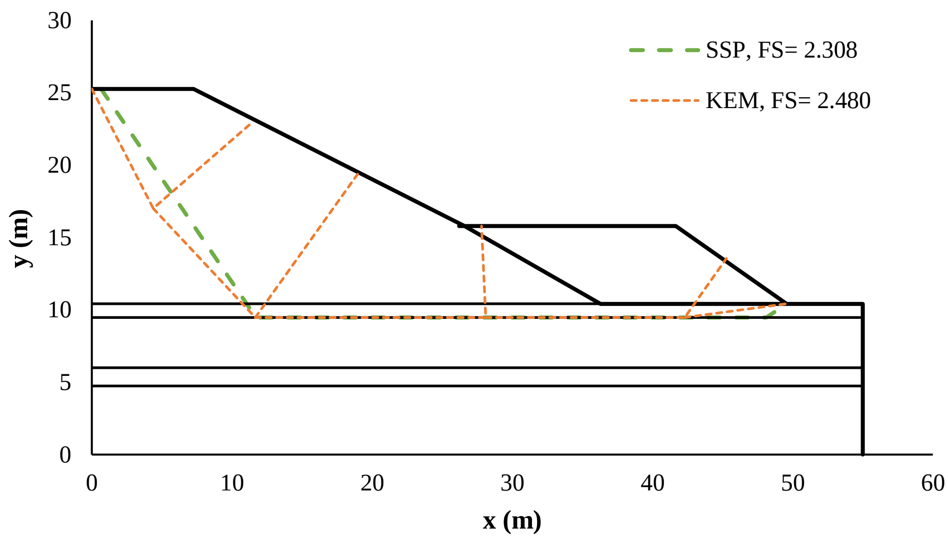

Figure 9.2. Critical failure surfaces of the bridge embankment

The function of the berm was to decrease the shear stresses in the slope and to provide additional weight to resist the failure (Duncan, et al., 2014). The SSP displays the same mechanism with a similar critical failure surface. The results of the KEM agree with those of the FEM carried out by the authors and confirms their suspicions. The KEM provides a factor of safety of 2.480 for the slope which is slightly higher than what was obtained using the SSP. As observed previously in Section 3.1 and 3.3.2, the SSP underestimates the factor of safety for failure in slopes with mixed soils and especially in the case of the block sliding mechanism. Thus, the factor of safety of 2.48 provided by the KEM is reasonable and significantly larger than the preferred FS of 1.8. This indicates that the slope was safe during construction and the objective of the designers was clearly met.

The kinematics of the slope movement are presented in Figure 9.3. The active condition is represented in elements 1 and 2 with element 5 representing the passive wedge.

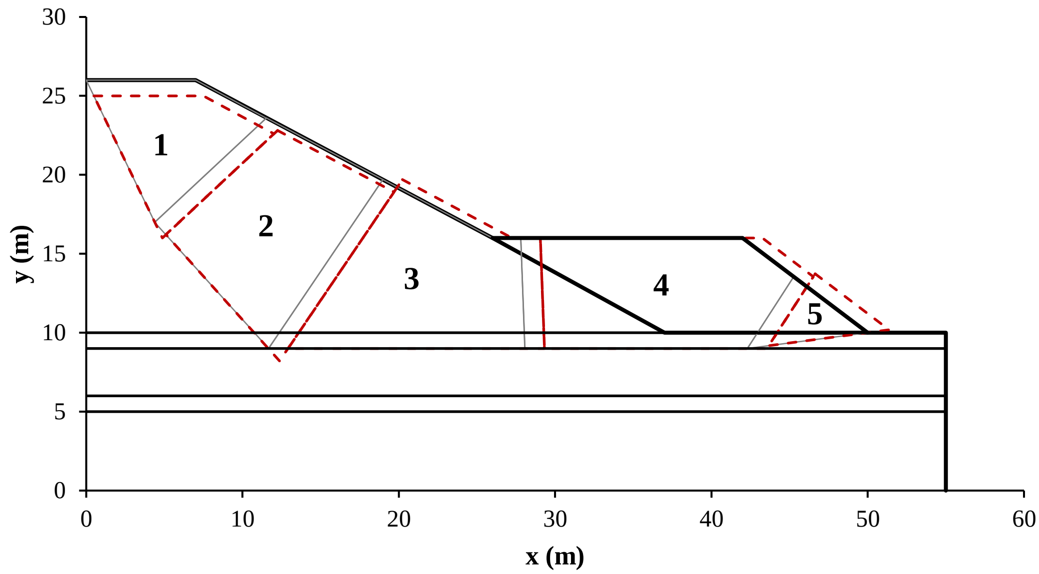

Figure 9.3. Kinematics of the embankment failure

Elements 1 to 2 move downwards along the slope causing elements 3 and 4 to slide along the weak layer. Element 5 is forced to translate towards the right and the soil in it is displaced and forced to move upwards. One of the benefits of the KEM is that the potential failure mechanisms can be clearly observed. It is interesting to observe that the entire berm is incorporated into the sliding block. It is quite clear that with the addition of the berm, the active wedge pushes against a significantly larger block, leading to a higher factor of safety.

Chapter 10 Concluding Remarks and Recommendations

The kinematic element method was shown to be effective for a wide range of slope stability problems. KEM is a powerful technique for experienced engineers that requires some, a priori, insight with regard to the most likely failure mechanism. It is more versatile but does not lend itself to simple automation that LEMs based on the method of slices enjoys. The kinematic element method generally located the appropriate failure mechanism, whether it be a circular failure for an embankment or a block sling mechanism for a slope with a weak layer. Generally, the KEM provided similar critical failure surfaces as the Morgenstern-Price method. The differences in the computed factors of safety between the two methods were within the range expected for limit equilibrium methods that satisfy all conditions of equilibrium. The KEM had difficulties with the foundation problem, where it located the appropriate failure mechanism and provided a similar critical slip surface as the Morgenstern-Price method, but significantly overestimated the factor of safety. Horizontal mesh refinement of the 5-element KEM critical slip surface provided a factor of safety which was similar to that of the Morgenstern-Price method solution and the reference Spencer's method solution.

The sensitivity of the KEM solution (critical slip surfaces and minimum factor of safety) to the number of elements was investigated. A 5-element solution was found to be ideal in terms of locating the appropriate failure mechanism and providing a reasonably accurate estimate of the factor of safety. For more complex problems, the KEM algorithm had convergence issues. In the retaining wall problem, the factor of safety and critical failure surface continued to increase. This was attributed to tensile forces being produced. For a lower number of elements, the location and values of tensile forces were not identified due to the procedure calculating "best" average values. The option of inserting a tension crack should be included in the KEM program to relieve tensile forces in the solution and to ensure the appropriate critical failure surface and corresponding minimum factor of safety is obtained. In the sensitivity analysis, for the given problems, horizontal mesh refinement had little impact on the factor of safety. However, this was not the case for the foundation problem where it reduced the factor of safety by 16%. It is recommended that more embankment problems should be analyzed using KEM to find if the factor of safety is overestimated. For the cases where the factor of safety is overestimated, horizontal and vertical mesh refinement should be carried out to determine their impact. It is further recommended to carry out horizontal mesh refinement for a variety of slope problems, similar to those in Chapter 3.

In Chapter 4, the KEM appeared to accurately display potential failure kinematics. Slope failure was also discussed in terms of earth pressure theory and related to the KEM solution. Elements in the KEM which are in active pressure display downward movement, while elements in passive pressure move upwards. The transition from active to passive pressure in a 5-element solution is abrupt. For further study, it would be interesting to produce a 20-element solution to delineate a smoother slip surface and better determine where the transition from active to passive pressure occurs.

In Chapter 5, the derivation of the KEMv showed a simplified version of how the KEM mechanism. In Chapter 6, the effect of restricting the interelement boundaries to vertical lines was explored. This restriction generally overestimated the factors of safety and resulted in more rigid failure surfaces. The KEMv solution was compared to GKEMv and was found to predict similar values for the factor of safety for a given slip. Generally, the interelement forces and force ratios for KEMv and GKEMv were similar. For the cases where the interelement boundaries were identical, nearly identical values were computed. The KEM was originally defined by Gussmann (1982) to be an upper bound solution while the KEMv was based on limit equilibrium principles. Given the similarities between the computed factors of safety and interelement forces, the KEM may be a limit equilibrium solution. To confirm this, the KEMv should be extended for inclined interelement boundaries and the factors of safety for similar slip surfaces should be compared. The extension of KEMv for inclined boundaries may help better define the KEM solution. The KEMv should also be modified to include multiple soil layers, remove requirements of interelement boundaries at the toe and crest, and add the option for effective stress analysis with pore water pressures (i.e. a piezometric line).

In Chapter 7, the interelement forces in KEMv and GKEMv were shown to be sensitive to the location of the elements. For mixed and cohesive soils, smaller normal forces were computed in the upper parts of the slope while shear forces were relatively high due to the cohesive strength. Thus, large interelement force ratios are computed in the upper parts of the slope. To further investigate the sensitivity of the interelement forces, the boundary locations should be varied. The locations of interelement boundaries cannot be specified in GKEMv, but it is possible in KEMv. The location of the interelement boundaries for a given slip surface should be varied in KEMv to compare interelement forces and force ratios.

In Chapter 8, a parametric study was carried out to determine the effect of varying soil parameters and slope geometry on the critical slip surfaces and minimum factors of safety. The change in critical slip surfaces predicted by KEM was consistent with empirical relations suggested by Janbu' dimensionless parameters. The trends in factors of safety paralleled that of the Morgenstern-Price method. The factors of safety computed by KEM were approximately 4% higher than those of the Morgenstern-Price method. As stated previously, this variance is within the tolerance for rigorous limit equilibrium methods.

References

Ahmed, S. (2017). *MATLAB script for slope stability calculations with COMSOL Multiphysics*. (Unpublished master's thesis). Université Du Québec, Montréal, Canada.

Arai, K., & Tagyo, K. (1985). Determination of noncircular slip surface giving the minimum factor of safety in slope stability analysis. *Soils and Foundations, 25(1),* 43-51.

Berry, P. L., & Reid, D. (1987). An Introduction to Soil Mechanics. Maidenhead: McGraw-Hill Book Company (UK) Limited.

Bishop, A. W. (1955). The Use of the Slip Circle in the Stability Analysis of Slopes. *Géotechnique, 5(1),* 7-17.

Cheng, L. Y., Li, J., Chen, S. X., & Chu, X. J. (2013). An Application of the Maximum Shear Strain Increment in Searching Sliding Surfaces. *Applied Mechanics and Materials, 423-426,* 1618-1622. doi:10.4028/www.scientific.net/AMM.423-426.1618

Cheng, Y. M., Lansivaara, T., & Wei, W. B. (2007). Two-dimensional slope stability analysis by limit equilibrium and strength reduction methods. *Computers and Geotechnics, 34,* 137-150. doi:10.1016/j.compgeo.2006.10.011

Cheng, Y. M., Li , L., Chi, S.-c., & Wei, W. B. (2007). Particle swarm optimization algorithm for the location of the critical non-circular failure surface in two-dimensional slope stability analysis. *Computers and Geotechnics, 34,* 92-103. doi:10.1016/j.compgeo.2006.10.012

Cruden, D. M., & Krahn, J. (1973). A reexamination of the Frank Slide. *Canadian Geotechnical Journal, 10,* 581-591.

Deng, D.-p., Zhao, L.-h., & Li, L. (2014). Limit equilibrium slope stability analysis using the nonlinear strength failure criterion. *Canadian Geotechnical Journal, 52,* 536-576. doi:10.1139/cgj-2014-0111

Donald, I. B., & Giam, P. S. (1989). *Example problems for testing soil slope stability programs*. Civil Engineering Research Report No. 8/1989. Melbourne: Monash University.

Duncan, J. M. (1996). State of the Art: Limit Equilibrium and Finite-Element Analysis of Slopes. *Journal of Geotechnical Engineering, 122(7),* 577-596.

Duncan, J. M., & Wright, S. G. (1980). The Accuracy of Equilibrium Methods of Slope Stability Analysis. *Engineering Geology, 16*, 5-17.

Duncan, M. J., Wright, S. G., & Brandon, T. L. (2014). *Soil Strength and Slope Stability* (2nd ed.). Hoboken: John Wiley and Sons, Inc.

Emery, J. (1978). Simulation of Slope Creep. *In Developments in Geotechnical Engineering* (Vol. 14, pp. 669-691). Elsevier.

Engel, J., & Lauer, C. (2017). *Einführung in die Boden- und Felsmechanik: Grundlagen und Berechnungen*. Munich: Carl Hanser Verlag GmbH & Co. KG.

Fan, K., Fredlund, D. G., & Wilson, G. W. (1986). An interslice force function for limit equilibrium slope stability analysis. *Canadian Geotechnical Journal, 23*, 287-296.

Fang, H.-Y., & Mikroudis, G. K. (1991). Stability of Earth Slopes. In H.-Y. Fang (Ed.), *Foundation Engineering Handbook* (2 ed., pp. 379-409). New York: Van Nostrand Reinhold.

Fredlund, D. G., & Krahn, J. (1977). Comparison of slope stability methods of analysis. *Canadian Geotechnical Journal, 14*, 429-439.

Fredlund, D. G., Krahn, J., & Pufahl, D. E. (1981). The Relationship between Limit Equilibrium Slope Stability Methods. *10th Conference of the International Society for Soil Mechanics and Foundation Engineering, 3*, pp. 409-416. Stockholm.

Griffiths, D. V., & Lane, P. A. (1999). Slope stability analysis by finite elements. *Géotechnique, 49(3)*, 387-403.

Gussmann, P. (2000). Effective KEM solutions for limit load and slope stability problems. *International Journal for Numerical and Analytical Methods in Geomechanics, 24(14)*, 1061-1077. doi:10.1002/1096-9853(20001210)24:143.0.CO;2-8

Gussmann, P. (1982). Kinematical Elements for Soils and Rocks. In Z. Eisenstein (Ed.), *Fourth International Conference on Numerical Methods in Geomechanics. 1*, pp. 47-52. Edmonton: University of Alberta Printing Services.

Gussmann, P. (1988). KEM in Geomechanics. In G. Swoboda (Ed.), *Sixth International Conference of Numerical Methods in Geomechanics. 2*, pp. 823-828. Innsbruck: A.A. Balkema.

Gussmann, P. (2017). *KEM Manual*. Unpublished: Ruhr-University Bochum, Bochum, Germany.

Hungr, O., Salgado, F. M., & Byrne, P. M. (1989). Evaluation of a three-dimensional method of slope stability analysis. *Canadian Geotechnical Journal, 26,* 679-686.

Janbu, N. (1954). Stability Analysis of Slopes with Dimensionless Parameters. *Harvard Soil Mechanics Series No. 46*. Cambridge: Harvard University Press.

Janbu, N. (1968). Slope stability computations. *Soil Mechanics and Foundation Engineering Report*. Trondheim: Technical University of Norway.

Janbu, N., Bjerrum, L., & Kjaernsli, B. (1956). Veiledning ved Løsning av Fundamenteringsoppgaver. *Norwegian Geotechnical Institute Publication No. 16*. Oslo: Norwegian Geotechnical Institute.

Karchewski, B. (2012). *Slope Stability Program (SSP) User's Guide 1.0*. Unpublished: McMaster University, Hamilton, Canada.

Karchewski, B., Stolle, D., & Guo, P. (2011). Determination of minimum factor of safety using a genetic algorithm and limit equilibrium analysis. *2011 Pan-Am CGS Geotechnical Conference: 64th Canadian Geotechnical Conference and 14th Pan-American Conference on Soil Mechanics and Geotechnical Engineering. 4*. Toronto: Canadian Geotechnical Society.

Kassim, K. A., Nazir, R., Ghafooripour, A., & Far, S. Y. (2012, September). Investigation of Slope Failures in Soil Mechanics. *Electronic Journal of Geotechnical Engineering, 17*, 2703-2718.

Knappett, J. A., & Craig, R. F. (2012). *Craig's Soil Mechanics* (8th ed.). New York: Spon Press.

Krahn, J. (2003). The 2001 R.M. Hardy Lecture: The limits of limit equilibrium analyses. *Canadian Geotechnical Journal, 40,* 643-660. doi:10.1139/T03-024

La Rochelle, P., Chagnon, J. Y., & Lefebvre, G. (1970). Regional geology and landslides in the marine clay deposits of Eastern Canada. *Canadian Geotechnical Journal, 7(2)*, 145-156.

Law, K. T., & Lumb, P. (1978). A limit equilibrium analysis of progressive failure in the stability of slopes. *Canadian Geotechnical Journal, 15,* 113-122.

Lei, G. H., Chiu, A. C., & Zheng, Q. (2011). Understanding the limitations of the Swedish method of slices from the stress perspective. *2011 Pan-Am CGS Geotechnical Conference: 64th Canadian Geotechnical Conference and 14th Pan-American Conference on Soil Mechanics and Geotechnical Engineering. 4*. Toronto: Canadian Geotechnical Society.

Linnweber, D., Niemunis, A., & Triantafyllidis, T. (2002). Neue Erfahrungen mit der KEM. *Bautechnik, 79*, 632-640. doi:10.1002/bate.200204250

Logan, D. L. (2012). *A First Course in the Finite Element Method* (5th ed.). Stamford: Cengage Learning.

Lui, S. Y., Shao, L. T., & Li, H. J. (2015). Slope stability analysis using the limit equilibrium method and two finite element methods. *Computers and Geotechnics, 63*, 291-298. doi:10.1016/j.compgeo.2014.10.008

Matsui, T., & San, K.-C. (1992, March). Finite Element Slope Stability Analysis by Shear Strength Reduction Technique. *Soils and Foundations, 32(1)*, 59-70.

McCarthy, D. F. (1982). *Essentials of Soil Mechanics and Foundations* (2nd ed.). Reston, Virginia: Reston Publishing Company.

Morgenstern, N. R., & Price, V. E. (1965). The Analysis of the Stability of General Slip Surfaces. *Géotechnique, 15(1)*, 79-93.

Naderi, M. A. (2013). *Determination of the Critical Slip Surface in Slope Stability Analysis*. (Unpublished master’s thesis). Eastern Mediterranean University, Gazimagusa, North Cyprus.

Nguyen, V. U. (1984). Determination of Critical Slope Failure Surfaces. *Journal of Geotechnical and Geoenvironmental Engineering, 111(2)*, 238-250.

Panthi, K. K., & Nilsen, B. (2006). Numerical analysis of stresses and displacements for the Tafjord slide, Norway. *Bulletin of Engineering Geology and the Environment, 65(1)*, 57-63.

Spencer, E. (1967). A Method of Analysis of the Stability of Embankments Assuming Parallel Inter-Slice Forces. *Géotechnique, 17*, 11-26.

Stolle, D. F., Guo, P., & Ng., K. (2004). Finite element analysis of slope stability. In S. Pietruszczak, & G. N. Pande (Ed.), *9th Symposium on Numerical Models in Geomechanics- NUMOG IX* (pp. 623-630). Ottawa: A.A. Balkema.

Stolle, D., & Guo, P. (2008). Limit equilibrium slope stability analysis using rigid finite elements. *Canadian Geotechnical Journal, 45*, 653-662. doi:10.1139/T08-010

Taylor, D. W. (1948). *Fundamentals of Soil Mechanics*. New York: Wiley.

Terzaghi, K., Peck, R. B., & Mesri, G. (1996). *Soil Mechanics in Engineering Practice* (3rd ed.). New York: John Wiley and Sons.

Thompson, C. D., & Emery, J. J. (1977). Influence of localized plastic layer on embankment stability. *Canadian Geotechnical Journal, 14(4)*, 524-530. doi: https://doi.org/10.1139/t77-053

Toprak, B., & Korkmaz, E. (2017). Comparison of Efficient (Effective) Stress Analysis Methods on Highway Fill Construction on Clay Ground. *Academics World 58th International Conference*, (pp. 8-10). Oslo.

Uzielli, M., Nadim, F., Lacasse, S., & Phoon, K.-K. (2006). Soil Variability Analysis for Geotechnical Practice. *2nd International Workshop on Characterisation and Engineering Properties of Natural Soils*. Singapore: ResearchGate. doi:10.1201/NOE0415426916.ch3

Vermeer, P. A., Stolle, D. F., & Bonnier, P. G. (1997). From the classical theory of secondary compression to modern creep. *9th International Conference on Computer Methods and Geomechanics. 4*, pp. 2469-2478. Wuhan: Balkema.

Xing, Z. (1988). Three-Dimensional Stability Analysis of Concave Slopes in Plan View. *Journal of Geotechnical and Geoenvironmental Engineering, 114(6)*, 658-671. doi:10.1061/(ASCE)0733-9410(1988)114:6(658)

Zhu, D. Y., Lee, C. F., & Jiang, H. D. (2003). Generalized framework for limit equilibrium methods for slope stability analysis. *Géotechnique, 53(4)*, 377-395.

Zienkiewicz, O. C., & Taylor, R. L. (2000). *The Finite Element Method. Volume 1: The Basis* (5th ed.). Oxford: Butterworth-Heinemann.

Zolfaghari, A. R., Heath, A. C., & McCombie, P. F. (2005). Simple genetic algorithm search for critical non-circular failure surface in slope stability analysis. *Computers and Geotechnics, 32, 139-152*. doi:10.1016/j.compgeo.2005.02.001

Appendix: MATLAB Code for a 3-Element KEMv Solution

The KEMv solution requires the use of two driver programs. As discussed in Section 5.3, the factors of safety and error function are determined by incrementally increasing the factor of safety. The driver program associated with this is *kem2.m*. Once the factors of safety, error function and mobilized shear forces are computed, the appropriate range for application of the bisection method is determined. The driver program which executes the bisection program is *kem.m*.

Driver Program for *kem2*

```
%  kem2.m
%-----------------------------------------------------------------
------------

%   xg,yg  = global coordinate values of each node
%   ico = nodal connectivity of each element

%-----------------------------------------------------------------
------------

clear;
idata;
ER = [];
F0 = 0.28;
Forces= [];

for iter = 1:101
  F0 = 0.02 + F0;
  [err,N1,N2,N3,E2,E3,X2,X3,T1,T2,T3] =
solver(F0,phif,cf,tx(1),ty(1),tx(2),ty(2),tx(3),ty(3),l(1),l(2),l
(3),h(2),h(3),W(1),W(2),W(3));
```

```
  ER = [ER; F0, err];
  Forces= [Forces; F0,N1,N2,N3,E2,E3,X2,X3,T1,T2,T3];
end

plot(ER(:,1),ER(:,2));

fileID = [fname, '.out'];
fileIDx = fopen(fileID,'w');
fprintf(fileIDx,'%6s %6s\r\n','FS','Error');
fprintf(fileIDx,'%6.3f %6.2f\r\n',ER');

fprintf(fileIDx,' \r\n','FS','Error');
fprintf(fileIDx,' \r\n','FS','Error');

fprintf(fileIDx,'%6s %6s %6s %6s %6s %6s %6s %6s %6s %6s
%6s\r\n','FS','N1','N2','N3','E2','E3','X2','X3','T1','T2','T3');
fprintf(fileIDx,'%6.3f %6.1f %6.1f %6.1f %6.1f %6.1f %6.1f %6.1f
%6.1f %6.1f %6.1f \r\n',Forces');
fclose(fileIDx);

file_id= [fname, '.xlsx'];
xlswrite(file_id,'FS','Error','B1');
xlswrite(file_id,ER,'Error','B2');
xlswrite(file_id,Forces,'Forces','B2');
warning('off','MATLAB:xlswrite:AddSheet');
```

Driver Program for *kem*

```
%  kem.m
%-----------------------------------------------------------------
------------

%   xg,yg  = global coordinate values of each node
%   ico = nodal connectivity of each element

%-----------------------------------------------------------------
------------

clear;
idata;
ER = [];
Forces= [];

a= input('Enter lower bound of FS: ');
b= input('Enter upper bound of FS: ');
```

```
%for iter = 1:100
% a = 0.02*iter+0.5;
 [fa,N1a,N2a,N3a,E2a,E3a,X2a,X3a,T1a,T2a,T3a] =
solver(a,phif,cf,tx(1),ty(1),tx(2),ty(2),tx(3),ty(3),l(1),l(2),l(
3),h(2),h(3),W(1),W(2),W(3));
 [fb,N1b,N2b,N3b,E2b,E3b,X2b,X3b,T1b,T2b,T3] =
solver(b,phif,cf,tx(1),ty(1),tx(2),ty(2),tx(3),ty(3),l(1),l(2),l(
3),h(2),h(3),W(1),W(2),W(3));
 ER = [ER; a, fa; b fb];
 Forces= [Forces; a,N1a,N2a,N3a,E2a,E3a,X2a,X3a,T1a,T2a,T3a];
 Forces= [Forces; b,N1b,N2b,N3b,E2b,E3b,X2b,X3b,T1b,T2b,T3b];
%end

if fa*fb > 0
  disp('Wrong choice')
else
  p = (a + b)/2;
  [fp,N1,N2,N3,E2,E3,X2,X3,T1,T2,T3] =
solver(p,phif,cf,tx(1),ty(1),tx(2),ty(2),tx(3),ty(3),l(1),l(2),l(
3),h(2),h(3),W(1),W(2),W(3));
   ER = [ER; p, fp];
  err = abs(fp);
  Forces= [Forces; p,N1,N2,N3,E2,E3,X2,X3,T1,T2,T3];
  while err > 0.00005
  if fa*fp<0
    b = p;
  else
    a = p;
  end
    p = (a + b)/2;
   [fp,N1,N2,N3,E2,E3,X2,X3,T1,T2,T3,F_v,F_h] =
solver(p,phif,cf,tx(1),ty(1),tx(2),ty(2),tx(3),ty(3),l(1),l(2),l(
3),h(2),h(3),W(1),W(2),W(3));
    ER = [ER; p, fp];
    err = abs(fp);
    Forces= [Forces; p,N1,N2,N3,E2,E3,X2,X3,T1,T2,T3];
  end
end

plot(ER(:,1),ER(:,2));

fileID = [fname, '.out'];
fileIDx = fopen(fileID,'w');
fprintf(fileIDx,'%6s %6s\r\n','FS','Error');
fprintf(fileIDx,'%6.3f %6.2f\r\n',ER');

fprintf(fileIDx,' \r\n','FS','Error');
fprintf(fileIDx,' \r\n','FS','Error');
```

```
fprintf(fileIDx,'%6s %6s %6s %6s %6s %6s %6s %6s %6s %6s
%6s\r\n','FS','N1','N2','N3','E2','E3','X2','X3','T1','T2','T3');
fprintf(fileIDx,'%6.3f %6.1f %6.1f %6.1f %6.1f %6.1f %6.1f %6.1f
%6.1f %6.1f %6.1f \r\n',Forces');
fclose(fileIDx);

file_id= [fname, '.xlsx'];
xlswrite(file_id,'FS','Error','B1');
xlswrite(file_id,ER,'Error','B2');
xlswrite(file_id,Forces,'Forces','B2');
warning('off','MATLAB:xlswrite:AddSheet');
```

Function for Storing Geometry and Element Information

The *idata.m* function reads the nodal information from the input file to determine the geometry of the elements and the unit vectors for the shear forces. Also, the soil material properties (unit weight, cohesion and friction angle) are read from the command window following prompts. Given the geometry of the elements and the unit weight, the weight of each element is calculated.

```
%  idata.m
%  Input data

nnodel=4;                    % number of nodes per element
nnodlb=2;                    % number of nodes per element on
boundary
nvar=2;                      % number of dofs per element

fname = input(' Enter the name of file .... ','s');
file1 = [ fname '.nnd'];

gama= input('Enter Unit Weight: '); % unit weight of material
phif= input('Enter Friction Angle: ');%% friction angle of
material
cf= input('Enter Cohesion: ');     % cohesion of material

%----------------------------------------------
%  input data for nodal coordinate values
%  xg,yg - global coordinates
```

```
%-----------------------------------------------

innodes = fopen(file1,'r');
[a] = fscanf(innodes,'%g %g',[2,inf]);
a = a';
nnod = size(a,1);       % total number of nodes in system
fclose(innodes);
xg(:,1) = a(:,1);
yg(:,1) = a(:,2);
a = [];

nel = nnod/2-1;

%  determine the element numbering and
%  the geometric characteristics of the elements,
%  and weights of the elements

h(1) = 0.0; v = 1.0;

for i = 1:nel
  i0 = 2*i-1;
 ico(i,1) =  i0; ico(i,2) =  i0+2; ico(i,3) =  i0+3; ico(i,4) =
i0+1;
 nd = ico(i,:); x = xg(nd(:));  y = yg(nd(:));
 h(i+1) = y(3)-y(2);
 dx(i) = x(1) - x(2); dy(i) = y(1) - y(2);
 l(i) = sqrt(dx(i)^2+dy(i)^2);
 tx(i) = dx(i)/l(i); ty(i) = dy(i)/l(i);
 area(i) = abs(dx(i)*(h(i+1)+h(i))/2);
 W(i) = gama*area(i);
end
```

Solver Function

The main driver programs *kem.m* and *kem2.m* call the same solver program, *solver.m*. The primary value of interest to the driver programs from the solver function is the $Error$. The $Error$ values from kem2.m are utilized to determine the appropriate range for the solution. In the kem.m program, the bisection method algorithm is a function of $Error$.

```
%solver.m


function [ErrorF,N1,N2,N3,E2,E3,X2,X3,T1,T2,T3] =
solver(F0,phif,cf,tx1,ty1,tx2,ty2,tx3,ty3,l1,l2,l3,h2,h3,W1,W2,W3
)
% solver determines that factor of safety for a given failure
mechanism
% Must enter with an initial guess for the factor of safety F

tm = tand(phif)/F0; cm = cf/F0;
det1 = tm^2*tx1+2*tm*ty1-tx1;
det3 = tm^2*tx3+2*tm*ty3-tx3;
%det2 = tx2^2+ty2^2=1;

% slice 1 (first)
N1 = (-cm*l1*tm*tx1-cm*l1*ty1-cm*h2+W1)/det1;
E2 = (-cm*h2*tm*tx1-cm*l1*tx1^2-cm*l1*ty1^2+W1*tm*tx1-
cm*h2*ty1+W1*ty1)/det1;
T1= N1*tm+ cm*l1;
X2= E2*tm+ cm*h2;

% slice 3 (last)
N3 = (-cm*l3*tm*tx3-cm*l3*ty3+cm*h3+W3)/det3;
E3 = -(cm*h3*tm*tx3-cm*l3*tx3^2-
cm*l3*ty3^2+W3*tm*tx3+cm*h3*ty3+W3*ty3)/det3;
T3= N3*tm+ cm*l3;
X3= E3*tm+ cm*h3;

% slice 2  (middle)
% det2 = (tx2^2+ty2^2)
N2 =  -(E2*tm*tx2-E3*tm*tx2+cm*h2*tx2-cm*h3*tx2+W2*tx2+E2*ty2-
E3*ty2);  %/det2;
T2 = (E2*tm*ty2-E3*tm*ty2+cm*h2*ty2-cm*h3*ty2+W2*ty2-
E2*tx2+X3*tx2);  %/det2;


% in the MATLAB code, FS' is not explicitly calculated as only
% the Error value is required for the bisection method algorithm

ErrorF = (N2*tand(phif) + cf*l2)/T2 - F0;
end
```